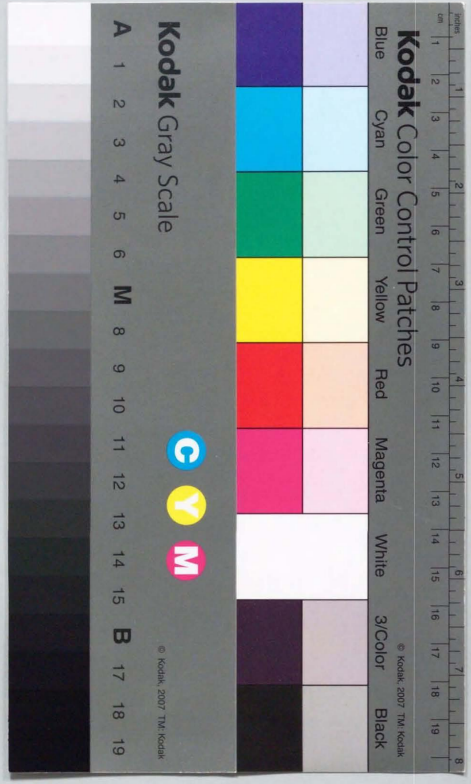

STUDY ON FEMTOSECOND OPTICAL SOLITON AMPLIFICATION AND TRANSMISSION IN AN ERBIUM-DOPED OPTICAL FIBER AMPLIFIER

(エルビウム添加光ファイバ増幅器におけるフェムト秒光ソリトンの増幅伝搬特性に関する研究)

黒 河 賢 二
Kenji Kurokawa

To
Michiyo

ACKNOWLEDGMENTS

I have many people to thank for their help in the completion of this thesis. First of all, I thank Professor Takayoshi Kobayashi of the department of Physics, the University of Tokyo, for his guidance, invaluable advice and encouragement throughout this work. I also thank the following people for their invaluable advice to this work:

All of this work was performed at NTT Laboratories. I express my sincere thanks to Professor H. Kimura, Professor H. Ishio, Dr. M. Kawase, Dr. Y. Koyamada, Dr. S. Shimada, Dr. Y. Wakui, Dr. K. Ishihara, and Dr. K. Nishimura. It was under their tenures as managers of NTT Laboratories that I had the opportunity to perform this research. I thank them all for their guidance and encouragement. In particular, I thank Dr. Yahei Koyamada, who recommended the thesis presentation, for his encouragement and guidance. I also thank Dr. T. Yabuta, Dr. T. Haibara, and Dr. M. Shimizu for their kind encouragement and guidance.

Very special thanks go to Dr. Masataka Nakazawa who was my group leader at NTT Laboratory when I was engaged in the research in this thesis. I was indebted to him for his continuous support and inspiration. Special thanks are due to Dr. Hirokazu Kubota for his corporation and fruitful discussions in completing the research in this thesis. Especially, most of the numerical analysis in this thesis was done by Dr. H. Kubota.

Many thanks go to my present group leader Y. Miyajima and my colleagues Y. Kimura, K. Suzuki, E. Yamada, T. Sugawa at NTT for their valuable suggestions and discussions. I also thank my many other colleagues at NTT. Finally, I thank my wife, Michiyo, for her understanding, encouragement, and help in many details that gave me strength.

CONTENTS

CHAPTER I. INTRODUCTION

1.1 Background

The optical soliton, which was first proposed by Hasegawa and Tappert in 1973[1.1.1], propagates stably over long distances in an optical fiber without waveform distortion, by balancing the group velocity dispersion (GVD) of the fiber with the third-order nonlinearity of the fiber, the so-called self phase modulation (SPM). In general, it can be said that the GVD in a transmission fiber is one of the main factors which limits communication speed. However, optical solitons can make it possible to construct a dispersion-free high speed optical communication system using fiber nonlinearity. Recent progress in optical soliton communication has been very rapid since it offers a great potential for opening a new field in high speed communication.

Ideal optical solitons propagate without distortion over long distances in a lossless transmission line. In practice, however, it is very important to compensate for the optical fiber loss of about 0.2 dB/km. Thus far, stimulated Raman scattering in fiber, which is a third-order nonlinear effect, has been used as optical gain, but this is far from the breakthrough needed for the realization of a practical soliton communication system because of a large optical pump source.

Recently, most of the difficult problems which prevented the realization of soliton communication have been solved by using new optical amplifiers, the so-called erbium-doped optical fiber amplifiers (EDFAs). Progress on research and development of EDFAs has been very rapid since they offer a real possibility of advancing high-speed optical communication[1.1.2-8]. The rapid progress started with a study which reported that 1.48 μm band InGaAsP laser diodes are an excellent pump

source for EDFAs[1.1.6]. This pumping scheme makes it possible for EDFAs to be applied practically, and a compact optical amplifier has been realized using laser diode pumping.

EDFAs' typical advantages are a high gain of more than 30 dB, low noise, wide bandwidth, polarization insensitive gain, and high saturation output power. They are also advantageous because they operate in the 1.5 μm region where fiber loss is minimized in ordinary silica-based single-mode optical fibers. Because of these excellent characteristics, EDFAs are very useful not only for high speed communication such as IM/DD (Intensity Modulation/Direct Detection), but also for optical soliton communication[1.1.9-11]. These amplifiers can provide a larger gain with a smaller pumping power than the Raman process.

Now, soliton technology has matured sufficiently with the aid of EDFAs. Experimental soliton transmissions exceed 100 Gbit/s in bit-rate, or, thousands of kilometers in distance using EDFAs[1.1.12-16].

1. 2 Optical Soliton

1. 2. 1 Historical Overview

The term "soliton" refers to special kinds of waves that can propagate undistorted over long distances and remain unaffected after collision with each other. Solitons have been studied extensively in many fields of physics, for example, water wave solitons[1.2.1-2], ion-plasma-wave solitons[1.2.3-4], hydrodynamic solitons[1.2.5], bimolecular polaron solitons[1.2.6], and nonlinear optical solitons[1.2.7-8]. In 1838 Russel first observed solitary waves in a narrow barge canal[1.2.1]. Korteweg and De Vries derived in 1895 the hydrodynamic equations of waves that move with velocities proportional to their amplitudes and found agreement with the observations[1.2.2].

In 1965 Zabusky and Kruskal[1.2.9] discovered that when two or more Korteweg - De Vries solitary waves collide they do not break-up and disperse, and they first used the term "soliton" to refer to these particle-like solitary waves. Then, in 1971 Zhakharov and Shabat[1.2.10] solved the nonlinear Schrödinger equation (NLSE) using the inverse scattering method and showed that the solutions were solitons. Hasegawa and Tappert[1.2.7] in 1973 pointed out that the Zhakharov and Shabat work applied to optical fibers, showed theoretically that an optical pulse in the fiber forms an envelope soliton. In 1980 Mollenauer, et al.[1.2.8], first experimentally demonstrated optical soliton propagation in fibers by using a high power color center laser. After that, there have been many numerical and theoretical investigations of soliton propagation in connection with the transmission capacity of optical fiber communication systems[1.2.11-13]. Many studies have been also undertaken to extend transmission distances in parallel with high speed communication research[1.2.14-18].

In 1989 it has been shown that solitons can be amplified and transmitted with Er^{3+}-doped fiber amplifier which is used to compensate for fiber loss[1.2.19]. High gain in the 1.5 μm region can be easily obtained by using Erbium doped fiber amplifier (EDFA) pumped by a compact laser diode. After that, Erbium doped fiber amplifier has been extensively used for optical communication systems in various ways. By using EDFAs, a lot of soliton transmission experiments have been succeeded. The existence of a stable soliton in a lumped amplifier system has been shown theoretically[1.2.20-22]. Today, experimental soliton transmissions exceed 100 Gbit/s in bit-rate, or, thousands of kilometers in distance using EDFAs[1.2.23-26].

1.2.2 Optical Soliton Propagation in Fibers

In a nonlinear medium, the refractive index is given by

$$n(t) = n_0 + n_2 |E(t)|^2 , \qquad (1.2.1)$$

where n_0 and n_2 are the linear and nonlinear index of refraction, respectively, and E(t) is an electric field. The second term represents the optical Kerr effect. When the intensity of the electric field changes, its phase $\phi(t)$ is modulated through the Kerr effect, namely self-phase modulation. The frequency change ($\Delta\omega$) of the pulse is given by

$$\Delta\omega = -\frac{\partial\phi(t)}{\partial t} = -\frac{2\pi n_2 l}{\lambda}\frac{\partial |E(t)|^2}{\partial t}, \qquad (1.2.2)$$

so that the frequency of the leading edge of the pulse becomes lower than the carrier frequency ω_0, and that of the trailing edge of the pulse becomes higher. This frequency swept pulse is called a chirped pulse.

When the chirped pulse propagates through a medium characterized by anomalous group velocity dispersion (GVD), the leading edge of the pulse propagates more slowly than its trailing edge, resulting in optical pulse compression. The temporal broadening due to the absolute value of GVD can be compensated for by the compression due to self-phase modulation (SPM) with anomalous GVD, making a stable optical soliton. In a silica optical fiber, anomalous dispersion exists in the wavelength region longer than 1.3 μm. It is quite advantageous for optical solitons that the loss minimum wavelength of silica fiber is around 1.5 μm at which the optical soliton can be generated. This characteristic is beneficial for long distance, high bit rate communication systems.

Nonlinear Schrödinger Equation

Consider the propagation of a pulse in a single-mode optical fiber without loss in which z corresponds to distance along the fiber. The electric field can be written as

$$\vec{E}(\vec{r},t) = \vec{x}\ 1/2\ \{ E(\vec{r}, t) \exp(-i\omega_0 t) + c.c. \} ,$$

$$E(\vec{r},t) = R(x, y)\ A(z, t) \exp(i\beta_0 z) , \qquad (1.2.3)$$

where R(x, y) is the modal distribution, A(z, t) is the envelope function, and β_0 is the propagation constant without the nonlinear effect (Kerr effect). From Maxwell's equation, the slowly varying amplitude A(z, t) satisfies

$$(\beta - \beta_0)A + i\frac{\partial A}{\partial z} + \delta\beta A = 0 , \qquad (1.2.4)$$

where $\delta\beta$ is a perturbation due to the nonlinearity of the fiber,

$$\delta\beta = (\omega_0 / c)\, n_2 \psi\, |A|^2 , \qquad (1.2.5)$$

with

$$\psi = \frac{\int dxdy |R(x,y)|^4}{\int dxdy |R(x,y)|^2} . \qquad (1.2.6)$$

The propagation constant β can be expanded in a Taylor series about the carrier frequency ω_0 as,

$$\beta = \beta_0 + \frac{d\beta}{d\omega}(\omega - \omega_0) + \frac{1}{2}\frac{d^2\beta}{d\omega^2}(\omega - \omega_0)^2 + \dots . \qquad (1.2.7)$$

By substituting Eq. (1.2.7) in Eq. (1.2.4),

$$i\frac{\partial A}{\partial z} + (\omega - \omega_0)\frac{d\beta}{d\omega}A + \frac{1}{2}(\omega - \omega_0)^2\frac{d^2\beta}{d\omega^2}A + \delta\beta A = 0 . \qquad (1.2.8)$$

By taking account of the following relation on the Fourier-transform,

$$\int_{-\infty}^{\infty}\frac{\partial A}{\partial t}e^{i(\omega-\omega_0)t}dt = Ae^{i(\omega-\omega_0)t}\Big]_{-\infty}^{\infty} - \int_{-\infty}^{\infty} i(\omega-\omega_0)Ae^{i(\omega-\omega_0)t}dt$$

$$= -\int_{-\infty}^{\infty} i(\omega-\omega_0)Ae^{i(\omega-\omega_0)t}dt , \qquad (1.2.9)$$

operation $\omega - \omega_0$ can be replaced by the differential operator $i\frac{\partial}{\partial t}$, and Eq. (1.2.8) becomes

$$(-i)\left(\frac{\partial A}{\partial z} + \frac{d\beta}{d\omega}\frac{\partial A}{\partial t}\right) + \frac{1}{2}\frac{d^2\beta}{d\omega^2}\frac{\partial^2 A}{\partial t^2} - \delta\beta A = 0. \qquad (1.2.10)$$

Here we employ a frame of reference moving with the pulse at the group velocity v_g (the so-called retarded frame). By making the transformation of $\tau = t - z/v_g = t - (d\beta/d\omega)z$, Eq. (1.2.10) becomes

$$-i\frac{\partial A}{\partial z}+\frac{1}{2}\frac{d^2\beta}{d\omega^2}\frac{\partial^2 A}{\partial t^2}-\delta\beta A=0 \quad . \tag{1.2.11}$$

Defining k by $\kappa = (\omega_0/c)\, n_2\psi$, Eq. (1.2.11) is

$$-i\frac{\partial A}{\partial z}+\frac{1}{2}\frac{d^2\beta}{d\omega^2}\frac{\partial^2 A}{\partial t^2}-\kappa|A|^2 A=0 \tag{1.2.12}$$

Normalization of Eq. (1.2.12) by defining $\frac{A}{\sqrt{P_0}}\equiv u$ gives in the anomalous group velocity dispersion region ($d^2\beta/d\omega^2 < 0$)

$$(-i)\frac{\partial u}{\partial q}=\frac{1}{2}\frac{\partial^2 u}{\partial s^2}+|u|^2 u \quad , \tag{1.2.13}$$

with

$$\kappa P_0 \equiv 1/z_0 \, , \tag{1.2.14}$$

$$s \equiv \tau/\tau_0 \, , \tag{1.2.15}$$

where

$$\tau_0=\sqrt{\left|\frac{d^2\beta}{d\omega^2}\right|z_0} \quad , \tag{1.2.16}$$

and

$$q \equiv z/z_0 . \tag{1.2.17}$$

Equation (1.2.13) is the standard form of the nonlinear Schrödinger equation (NLSE). An important scaling relation holds for Eq. (1.2.13). If u(q, s) is a solution of this equation, then $\varepsilon u(\varepsilon^2 q, \varepsilon s)$ is also a solution, where ε is an arbitrary scaling factor.

Soliton Solutions

Zakharov and Shabat[1.2.10] have shown how the nonlinear Schrödinger equation can be solved by the inverse-scattering method. According to the Zakharov and Shabat results, the general form for the fundamental soliton (N=1 soliton) is given by

$$u(q, s) = 2\eta\, \mathrm{sech}(2\eta s)\exp(2i\eta^2 q) \tag{1.2.18}$$

The energy W of the N=1 soliton is

$$\begin{aligned} W &= n\varepsilon_0 c\int|R(x,y)|^2 dxdy\cdot\int|A|^2 d\tau \\ &= n\varepsilon_0 c\int|R(x,y)|^2 dxdy\cdot P_0\tau_0\int|u|^2 ds \\ &= n\varepsilon_0 c\psi\alpha_{eff}\frac{\sqrt{|d^2\beta/d\omega^2|}}{\kappa\sqrt{z_0}}\int|u|^2 ds \\ &= n\varepsilon_0 c\psi\alpha_{eff}\, 4\eta\frac{\sqrt{|d^2\beta/d\omega^2|}}{\kappa\sqrt{z_0}} \quad , \end{aligned} \tag{1.2.19}$$

where α_{eff} is an effective core area,

$$\alpha_{eff}=\frac{\left(\int|R(x,y)|^2 dxdy\right)^2}{\int|R(x,y)|^4 dxdy} \quad . \tag{1.2.20}$$

The energy is proportional to η.

We shall choose the soliton with η=1/2 as the standard, along with its energy and its full width at half-maximum (FWHM). With this choice, Eq. (1.2.18) becomes

$$u(q, s) = \mathrm{sech}(s)\exp(iq/2) \quad . \tag{1.2.18}'$$

The FWHM s_1 of the intensity of this lowest-order soliton is

$$s_1 = 2\cosh^{-1}\sqrt{2} = 1.76 \quad . \tag{1.2.21}$$

The normalization distance z_0 corresponding to this value of s_1 is, according to Eqs. (1.2.15) and (1.2.16),

$$z_0=\frac{\tau_1^2}{(1.76)^2|d^2\beta/d\omega^2|} \quad , \tag{1.2.22}$$

where τ_1 is the FWHM of the soliton. This distance can be rewritten in terms of dispersion parameter D. Since $D = -2\pi c/\lambda^2(d^2\beta/d\omega^2)$, the normalization distance z_0 in terms of D is

$$z_0=\frac{2\pi c\tau_1^2}{(1.76)^2|D|\lambda^2}=0.322\frac{2\pi c}{\lambda^2}\frac{\tau_1^2}{|D|} \quad . \tag{1.2.23}$$

The peak power P_1 required to support the fundamental soliton is

$$\begin{aligned} P_1 &= n\varepsilon_0 c\int|R(x,y)|^2 dxdy\; P_0 \\ &= n\varepsilon_0 c\,\psi\,\alpha_{eff}\,(\kappa z_0)^{-1} \end{aligned}$$

$$= 0.777 \frac{\lambda^3}{\pi^2 c n_2^* \tau_1^2} \frac{|D|}{} \alpha_{eff} , \qquad (1.2.24)$$

where we used Eq. (1.2.22), $|D| = 2\pi c/\lambda^2 \ |d^2\beta/d\omega^2|$, and the relation $n_2[m^2/V^2] = n_2^*[m^2/W]\ n\varepsilon_0 c$. $n_2^* = 3.18 \times 10^{-20}\ m^2/W$.

Higher-order Solitons

In addition to the fundamental soliton (N=1), there are also a continuum of higher-order soliton solutions that obey the NLSE[1.2.27]. Among these, a special role is played by the solitons whose initial form at q=0 is given by

$$u(0, s) = N\,\mathrm{sech}(s) , \qquad (1.2.25)$$

where the soliton order N is an integer. The peak power necessary to launch the Nth-order soliton is N^2 times of that required for the fundamental soliton. Unlike the fundamental soliton that behaves as a unit and represents a balance between dispersion and nonlinearity, the higher-order solitons change shape as they propagate down the fiber since the two counteracting forces overshoot and undershoot. For example, a higher-order soliton tends to compress at first because self-phase modulation outweighs the group-velocity dispersion. However, the pulse narrows, the bandwidth of the pulse increases and the dispersive effects become stronger. The bound multi-solitons evolve periodically and the patterns corresponds to constructive and destructive interference between the pulses. $|u(q, s)|^2$ for all higher-order solitons is periodic with the period $q = \pi/2$[1.2.10]. Using the definition $q = z/z_0$ from Eq. (1.2.17), the soliton period z_{sp} is given by

$$z_{sp} = \frac{\pi}{2} z_0 = 0.322 \frac{\pi^2 c}{\lambda^2} \frac{\tau_1^2}{|D|} , \qquad (1.2.26)$$

where τ_1 is the FWHM of the soliton. Periodic evolution of the higher-order solitons is illustrated in Fig. 1.2.1 for the specific case N=3 by showing the

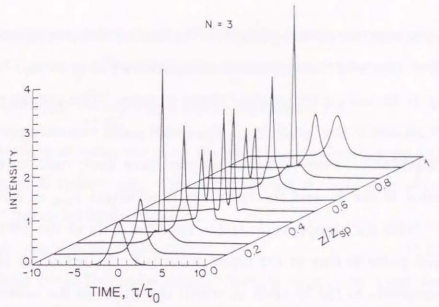

Fig. 1.2. 1 Temporal evolution over one soliton period for the third-order soliton. Note pulse splitting near $z/z_{sp}=0.5$ and soliton recovery beyond that (after Ref. 1.2.28).

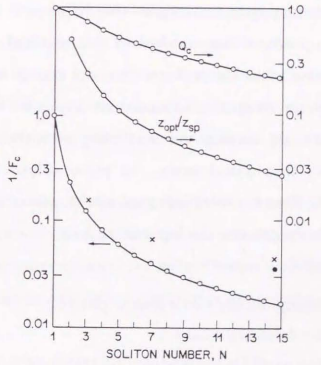

Fig. 1.2.2 Variation of compression factor F_c, optimum fiber length z_{opt}, soliton period z_{sp}, and quality factor Q_c with the parameter N. Open circles correspond to the integer values of N. Data points correspond to the experiments performed with a 320-m fiber (crosses) and a 100-m fiber (solid circle) (after Ref. 1.2.29).

pulse shapes over one soliton period[1.2.28]. As the pulse propagates along the fiber, it first narrows, then splits into two distinct pulses at $z_{sp}/2$, and then merges again to recover the original shape at $z=z_{sp}$. This pattern is repeated over each section of the length z_{sp}. The initial pulse narrowing is useful for pulse compression. Numerical techniques have been used to obtain the compression factor F_c and the optimum fiber length z_{opt} as a function of N[1.2.29]. Here the compression factor F_c is the ratio of the FWHM of the compressed pulse to that of the input pulse and the optimum fiber length z_{opt} corresponds to the location at which the width of the central spike is minimum. Figure 1.2.2 shows the variation of F_c^{-1} and z_{opt}/z_{sp} with N for values of N in the range 1-15, where z_{sp} is the soliton period.

Asymptotic Soliton Solution

It is very interesting to investigate what happens if the initial pulse shape or the peak power is not matched to that required by Eq. (1.2.25). Consider first the case when the peak power is not exactly matched and the value of N is not an integer. Satsuma and Yajima[1.2.30] have used perturbation theory for solving the scattering problem in the inverse scattering method. In physical terms, the pulse adjusts its width as it propagates along the fiber to evolve into a soliton. A part of the pulse energy is dispersed away in the process. An input of the form

$$u_i = (1+a)\,\mathrm{sech}(s) \quad (-\frac{1}{2} \le a \le \frac{1}{2}) \,, \tag{1.2.27}$$

at z=0 will evolve asymptotically into a soliton given by

$$|u_s(z \to \infty)| \equiv (1+2a)\,\mathrm{sech}\{(1+2a)s\} \,. \tag{1.2.28}$$

The pulse width associated with Eq. (1.2.28) is

$$\tau' = \frac{\tau_{input}}{1+2a} \,. \tag{1.2.29}$$

For a>0 the pulse narrows, and for a<0 the pulse broadens. No soliton is formed for $(1+a) \le \frac{1}{2}$. The input pulse evolves into a soliton by stripping off a fraction of energy $\frac{a^2}{(1+a)^2}$ that is lost to a dispersive field.

The effect of pulse shape on the soliton formation can be investigated by solving NLSE numerically. Figure 1.2.3 shows the evolution of a Gaussian pulse with the initial field given by

$$u(0,\tau) = \exp(-\tau^2/2) \,. \tag{1.2.30}$$

Even though N=1, the pulse shape changes along the fiber because of deviation from the hyperbolic secant shape required for the fundamental soliton. The interesting feature of Fig. 1.2.3 is that the pulse adjusts its width to evolve asymptotically into a fundamental soliton. In fact, the evolution appears to be complete by $z/z_0=5$, a distance that corresponds to about three soliton periods. An essentially similar evolution pattern occurs for other pulse shapes such as a super-Gaussian shape. The final width of the soliton and the distance needed to evolve into a fundamental soliton depend on the exact shape, but the qualitative behavior remains the same. Clearly, solitons can be excited easily if the initial peak power of the pulse exceeds a threshold value.

The characteristics of the optical soliton in optical fiber is summarized as follows: dispersion free, robust for perturbations, and self formation. Because of these property, the N=1 soliton seems promising as carriers for long distance, high bit rate optical communication systems.

1.2.3 Higher-Order Nonlinear Effects (Soliton Self-Frequency Shift effect)

The properties of optical solitons considered so far are based on the simple, unperturbed NLSE of Eq. (1.2.18). However, when the pulses widths

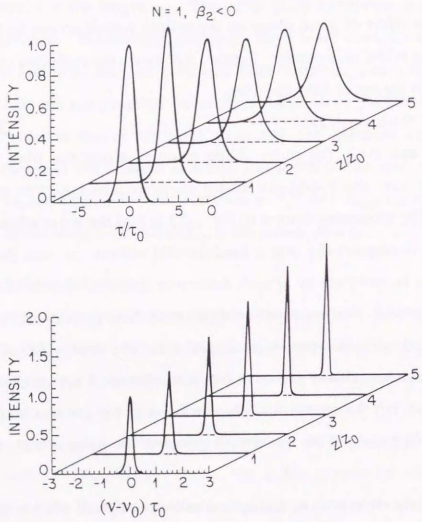

Fig. 1.2.3 Evolution of the pulse shape (upper plot) and the pulse spectrum (lower plot) over a distance $z=5z_0$ for an initially unchirped Gaussian pulse propagating in the anomalous-dispersion regime of the fiber ($\beta_2<0$) with parameters such that N=1 (after Ref. 1.2.28).

are so short and in the femtosecond region, it is necessary to include the higher-order nonlinear and dispersive effects. With these effects NLSE becomes

$$i\frac{\partial u}{\partial q}+\frac{1}{2}\frac{\partial^2 u}{\partial s^2}+|u|^2u=i\frac{k'''}{6k''\tau_0}\frac{\partial^3 u}{\partial s^3}-i\frac{2}{\omega_0\tau_0}\frac{\partial}{\partial s}\left(|u|^2u\right)+\frac{\tau_n}{\tau_0}u\frac{\partial}{\partial s}|u|^2 \quad . \qquad (1.2.31)$$

The first, second, and the third terms on the right-hand side correspond to the third order dispersion, the self-steeping effect, and the self Raman effect or the effect of a finite response time of the nonlinearity, respectively. The third order dispersion is originated from wavelength dependence of the GVD[1.2.31]. The self-steeping of the light pulse results from the intensity dependence of the group velocity[1.2.32].

The major perturbation is the Raman effects or so-called soliton self-frequency shift (SSFS)[1.2.33-34]. Raman effects cause a continuous downshift of the mean frequency of pulses propagating in optical fibers. This is particularly important for short pulses because the effect varies roughly with the inverse fourth power of the pulse width. To understand intuitively the SSFS, consider the Raman gain spectrum[1.2.35] in fused silica fibers. Because of the finite slope down to zero frequency, the soliton can self-induce gain for the lower-frequency part of its spectrum at the expense of the higher-frequency part. Therefore, the mean soliton frequency shifts because of a frequency-dependent gain or loss.

The nonresonant Raman effect in fibers is equivalent to a time-dependent nonlinearity, and there are two components to the Kerr nonlinearity n_2. About four-fifth of the n_2 is an electronic, instantaneous nonlinearity caused by ultraviolet resonances, while about one-fifth of n_2 arises from Raman-active vibrations. The imaginary part of this latter

contribution corresponds to the Raman gain spectrum and is time dependent with an average delay of ~3 to 6 fs in fused silica[1.2.36]. The simplest way to introduce Raman effects into the NLSE is to modify the nonlinear term to describe a delayed response of the form[1.2.33]

$$|u|^2 u \rightarrow u(t)\int ds f(s)|u(t-s)|^2 \cdot \qquad (1.2.32)$$

The function f(s) is real if there are no losses other than the Raman type, and to ensure causality f(-|s|)=0 while $\int ds f(s) = 1$ to recover Eq. (1.2.18) for sufficiently short delays (or long pulses). An exponential decay of the nonlinear response is assumed and f(s) = τ_n exp(-s/τ_n). Here τ_n is the response time and we use an estimated value of 5.9 fs[1.2.37]. For pulses much longer than the response time (i.e. $\tau >$ 100 fs) it is generally adequate to expand $|u(t-s)|^2$ in a Taylor series around t and keeping only the first-derivative term. Then Eq. (1.2.32) is expanded as

$$u(t)\int ds f(s)|u(t-s)|^2 \rightarrow u(t)\left\{|u(t)|^2 - \tau_n \frac{d}{dt}|u(t)|^2\right\} \cdot \qquad (1.2.33)$$

Gordon[1.2.33] has derived analytic formulas to describe the shift of the soliton center frequency as a function of distance in the fiber. He finds for fused silica fibers that

$$\frac{d\nu_0}{dz}[Thz/km] = -\frac{10^5 \lambda^2 D}{16\pi c \tau_0^3}\int d\Omega \frac{\Omega^3 R(\Omega/2\pi c)}{\sinh^2(\pi\Omega/2)} , \qquad (1.2.34)$$

where λ, D, c, and τ_0 are in units of centimeters and picoseconds. The function R is the Raman loss spectrum normalized to the peak value of 0.492 at 13.2 THz, and it can be approximated by a straight line R(ν)≅0.492 (ν/13.2), where ν is in THz. For example, if we use τ_0=τ/1.763, λ=1.5 μm and D=15 ps/(km nm), then with the linear approximation Eq. (1.2.34) reduces to

$$d\nu_0/dz\ [THz/km] = 0.0436/\tau^4 . \qquad (1.2.35)$$

The fourth power of pulse width results since the soliton's peak power scales as τ^{-2}, the spectral width of the soliton is proportional to τ^{-1}, and the Raman

gain coefficient increases linearly with increased frequency separation, which also scales as the spectral width. The SSFS becomes very important for high bit rate optical communication because the frequency shift due to the SSFS is inversely proportional to the fourth power of the pulse width.

1.2.4 Soliton Interactions

The times interval T_B between the neighboring pulses determines the bit rate B of a communication system (B=1/T_B). It is thus necessary to determine how close two solitons can come without interacting with each other. The same nonlinearity that bounds a single soliton also introduces an interaction force between the neighboring solitons.

First we describe qualitative behavior of the nonlinear interactions. The nonlinear term in the nonlinear Schrödinger equation (NLSE), $|U|^2U$, is important in terms of qualitative behavior. Let U be a pulse pair, u+v, expand the nonlinear term, and extract the term relating u. This gives

$$u(|u|^2+2|v|^2+uv^*) . \qquad (1.2.36)$$

The first and second terms are self and cross phase modulation (SPM and XPM), respectively. The last term is a phase-sensitive interference term. When we ignore the dispersive term, the nonlinear phase rotation on pulse u is proportional to $|u|^2+2|v|^2+uv^*$. Since the SPM term cancels out the GVD term of the NLSE, the frequency shift is proportional to

$$\frac{\partial}{\partial t}\left(2|v|^2 + uv^*\right) . \qquad (1.2.37)$$

Let u=sech(t) and v=sech(t+Δt)$e^{i\phi}$ which means that pulse v advances by Δt and has phase of φ relative to pulse u. When Δt is large, we disregard the term $|v|^2$ because its effect on the pulse u is small compared to the uv* term. The frequency shift at the center of the pulse u is

$$\Delta\omega \propto -\frac{\partial}{\partial t}(uv^*)\Big|_{\tau=0} \cong 2e^{-\Delta t}e^{-i\phi} \quad . \tag{1.2.38}$$

For an in-phase case, $\phi=0$, $\Delta\omega$ is greater than 0, which means u becomes faster than its original speed because the carrier frequency is in the anomalous dispersion region. This result in the generation of the attraction force. While $\phi=\pi$, $\Delta\omega$ becomes less than 0, which means u becomes slower than its original speed. This result in the generation of the repulsive force.

Quantitative behavior of the nonlinear interactions is described as follows. The amplitude of a soliton pair at the fiber input can be written in the following normalized form,

$$u(0, \tau) = \text{sech}(\tau - q_0) + r\,\text{sech}[r(\tau + q_0)]\,e^{i\theta} \quad , \tag{1.2.39}$$

where r is relative amplitude, θ is the relative phase, and q_0 is the initial separation. q_0 is related to the bit rate by

$$B = 1/(2q_0\tau_0) \cong 0.88/(q_0\tau) \quad . \tag{1.2.40}$$

Soliton interaction can be studied by solving NLSE numerically with input from Eq. (1.2.39). However, considerable physical insight is gained by using the inverse scattering method with u given by Eq. (1.2.39). Such studies[1.2.38-39] show that interaction depends not only on the soliton separation q_0 but also on the relative phase θ and the relative amplitude r. In the specific case of $\theta=0$, r=1, and $q_0 \gg 1$ the separation q at any distance (normalized distance) ξ is given by[1.2.38]

$$\exp(q - q_0) = |\cos(2\xi e^{-q_0})| \quad . \tag{1.2.41}$$

This relation shows that $q(\xi)$ varies periodically along the fiber with oscillation period

$$\xi_p = (\pi/2)\exp(q_0) \quad . \tag{1.2.42}$$

Perturbation theory yields the same result[1.2.40]. A more accurate expression, valid for arbitrary values of q_0, is given by[1.2.39]

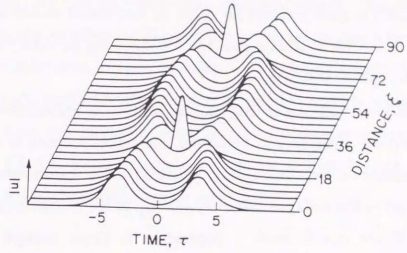

Fig. 1.2.4 Evolution of a soliton pair along the fiber showing periodic collapse due to mutual interaction. The parameters are N=1, θ=0, r=1, and q_0=3.5 (after Ref. 1.2.39).

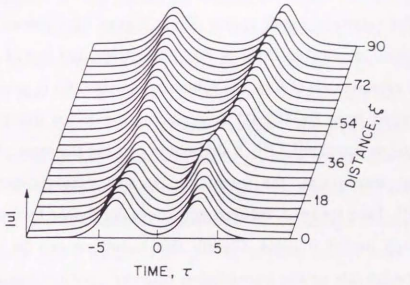

Fig. 1.2.5 Evolution of a soliton pair under conditions identical to those of Fig. 1.2.4 except that $\theta=\pi/4$ so that solitons are not in phase at ξ=0 (after Ref. 1.2.39).

$$\xi_p = \frac{\pi \sinh(2q_0)\cosh(q_0)}{2q_0 + \sinh(2q_0)} \quad . \tag{1.2.43}$$

Equation (1.2.41) is quite accurate for $q_0 \geqq 3$, as also found numerically[1.2.41]. Figure 1.2.4 shows the evolution pattern[1.2.42] showing periodic collapse of a soliton pair for $q_0=3.5$, $\theta=0$, and $r=1$.

The periodic collapse of neighboring solitons is undesirable from the system standpoint. One way to avoid the interaction problem is to increase the soliton separation such that $z_p \gg L_T$, where L_T is the transmission distance, $z_p = z_{sp} \exp(q_0)$ is the collapse distance, and z_{sp} is the soliton period. Since $z_p/z_{sp} \cong 22{,}000$ for $q_0=10$, such a separation is large enough for most communication systems. The bit rate is then limited by Eq. (1.2.40), but can approach 45 Gbit/s if we use 2-ps solitons for data transmission.

There are several schemes through which the soliton separation can be considerably reduced. It turn out that the attractive force between the soliton is very sensitive to their relative phase θ and the relative amplitude r. In fact, it turns into a repulsive force for $\theta \neq 0$ so that the solitons eventually separate apart even for relatively small values of θ. Figure 1.2.5 shows evolution under conditions identical to those of Fig. 1.2.4 except that $\theta=\pi/4$ instead of $\theta=0$. For the extreme case of $\theta=\pi$, the soliton separation $q(\xi)$ is governed by a relation obtained from Eq. (1.2.41) by replacing the cosine function by the hyperbolic cosine function[1.2.38]. If the soliton pair has the same phase ($\theta=0$) but different amplitudes, the interaction is still periodic but without collapse[1.2.39]. Even for r=1.1, the separation does not change by more than 10 % during each period if $q_0 \geqq 4$. Clearly this technique can be useful for increasing the bit rate or the transmission capacity. Soliton interaction can also be modified by many other factors such as initial chirp[1.2.42-43], higher-order dispersion[1.2.44], and higher-order nonlinear effects[1.2.45-46]. When the

pulse width is in a femto ~ picosecond region, soliton interaction is significantly modified by higher-order nonlinear effects. The attractive force becomes repulsive when the pulses begin to merge, because a bound 2-soliton splits into individual solitons traveling with different speeds due to soliton self-frequency shift[1.2.45-46]. Another factor that must be considered is the effect of loss and periodic amplification on soliton interaction. It is found[1.2.42] that stable transmission can be achieved when neighboring solitons are launched with unequal amplitudes.

1.3 General features of the Erbium-doped Optical Fiber Amplifier (EDFA)

1.3.1 Historical Background

Since the first observation of room-temperature laser action of Er^{3+}:glass in 1965 by Snitzer and Woodcock[1.3.1], and the early investigation of Nd^{3+}-doped fiber amplifiers[1.3.2] and diode-pumped lasers[1.3.3], recent improvements of the modified chemical vapor deposition (MCVD) process[1.3.4-5] offered the possibility of incorporating a large variety of rare-earth ions in low-loss silica glass fibers[1.3.6-7]. Interest in Er^{3+} was stimulated by the fact that its main laser transition near 1.5 μm falls into the low-loss window of the optical fiber communications. The first room-temperature CW laser action of Er^{3+}:glass was made possible by the low-pump power thresholds achievable in single-mode fibers[1.3.6]. Figure 1.3.1 shows the laser tuning range and fluorescence spectrum[1.3.6]. By using a Ti:sapphire laser at 980 nm for a pump source, high-power, tunable output near 1.5 μm was obtained with more than 250 mW from 1.52 μm to 1.57 μm[1.3.8].

Traveling-wave erbium-doped fiber amplifiers (EDFAs) were soon investigated, and high gains (30-35 dB) were reported using pumps at 665

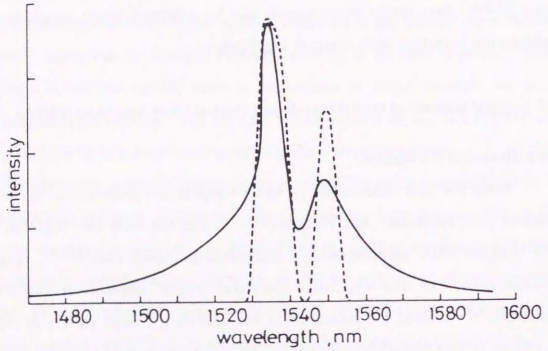

Fig. 1.3.1 Lasing tuning range (broken line) and fluorescence spectrum (solid line) of an Er^{3+}-doped fiber laser (after Ref. 1.3.6).

nm[1.3.7] and 514 nm[1.3.9]. Amplification of high-bit-rate (2 Gb/s) optical signals in single or multiple channels[1.3.10-11] showed that EDFAs can be used in broad-band optical communication systems and, because of slow gain-recovery dynamics, are also immune to crosstalk effects[1.3.11]. Another advantage is the insensitivity of the gain to signal polarization[1.3.10]. As fiber amplifiers can be designed to have negligible coupling loss to standard communication fibers, high fiber-to-fiber gains ($G \geqq 30$ dB) can be achieved, which makes the EDFA attractive for a variety of system applications, i.e., as preamplifiers, in-line repeaters, or power amplifiers.

Practical implementations of the EDFA require that semiconductor laser diode (LD) sources be used for the pump. The first LD-pumped fiber amplifier was achieved with a GaAlAs laser diode at 807 nm and net gains of +6 dB using 15 mW were achieved[1.3.12]. The 807-nm pump band is unfortunately inefficient, because of the concurrent effect of pump excited-state absorption (ESA)[1.3.13]. For comparison, the use of 980-nm ESA-free pump band was shown to yield gains up to +15 dB for the same pump power[1.3.14]. The 980-nm wavelength can be generated with strained-layer InGaAs LDs[1.3.15]. The pump band near 1.48 μm which is also free from ESA was investigated by Snitzer et al.[1.3.16]. Using a 1.48-μm InGaAsP laser diode, a gain of +12.5 dB with a 16-mW pump was reported[1.3.17], which represents the first practical and efficient LD-pumped EDFA.

After that, intensive study of EDFAs was made for practical applications and now EDFA is used for commercial telecommunication systems in the world[1.3.18-21].

1.3.2 Basic Properties of EDFAs

Physical Properties

The conventional optical fiber has a low-loss window between 1.5 and 1.6 μm, where the optical loss can be as low as 0.2 dB/km. The 1.52 - 1.57 μm gain band of erbium coincides with this low loss window. The energy level diagram of erbium-doped silica glass is shown in Fig. 1.3.2 and the emission and absorption cross-sections for transitions between the $^4I_{15/2}$ and $^4I_{13/2}$ states are shown in Fig. 1.3.3[1.3.22]. Amplification results from stimulated emission from the $^4I_{13/2}$ to the $^4I_{15/2}$ level. Each level includes a number of sublevels whose degeneracy is lifted as a result of Stark splitting due to the electric fields the Er ions experience in the glass matrix. This Stark splitting of the different sublevels, which is represented schematically in Fig. 1.3.2, is responsible for the broad cross section spectra of Fig. 1.3.3. The Stark-level energies of the $^4I_{15/2}$ and $^4I_{13/2}$ manifolds were evaluated by spectroscopic measurements of fluorescence and absorption in an erbium-doped fiber[1.3.23-24]. Since the homogeneous broadening at room temperature of the λ_0=1.531 μm laser line is approximately 49 cm^{-1} (or 11.5 nm)[1.3.25] and the splitting between the individual Stark levels is 17-82 cm^{-1}, the laser transitions starting from neighboring levels in the $^4I_{15/2}$ and $^4I_{13/2}$ manifolds have significant spectral overlap. The inhomogeneous broadening being also 49 cm^{-1}, a strong overlap between the light waves emitted from ions belonging to different atomic sites can be inferred. These facts explain the essentially homogeneous behavior of aluminosilicate Er-doped fibers and the broad fluorescence spectra observed at room temperature.

The spectral dependence of gain saturation is an important issue, especially for applications involving wavelength division multiplexing. The gain saturation exhibits a strong spectral dependence, showing more gain compression at short wavelengths near 1.53 μm than at longer wavelengths.

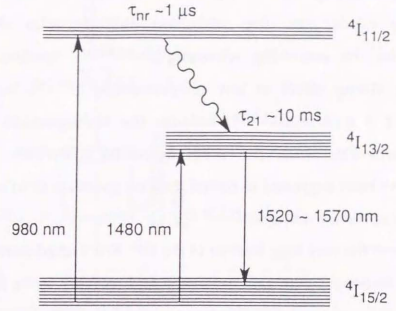

Fig. 1.3.2 Level scheme of Er^{3+} in silica glass. τ_{nr} is the life time of the $^4I_{11/2}$ level for nonradiative decay to the $^4I_{13/2}$ and τ_{21} is the life time of the $^4I_{13/2}$ for spontaneous emission (after Ref. 1.3.22).

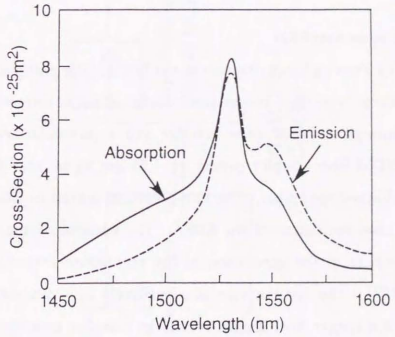

Fig. 1.3.3 Absorption and emission cross section spectra for erbium-doped fiber with alumino-germano-silicate core (after Ref. 1.3.22).

This strong spectral dependence of gain saturation can be described by the homogeneous model and the saturation charactersitics show little dependence on the saturating wavelength[1.3.25-26]. Spectral gain hole burning is a strong effect at low temperatures[1.3.27-28], but at room temperature it is quit weak[1.3.26] because the homogeneous linewidth becomes comparable with the inhomogeneous linewidth. Various techniques have been suggested to flatten the gain spectrum or to compensate for spectrally dependent saturation[1.3.29-31].

Because of the very long lifetime of the Er^{3+} first excited state (τ~10 ms) the transients associated with gain saturation and recovery in the EDFA have characteristic times on the order of 0.1 to 1 ms[1.3.32]. Thus, the intersymbol interference in high bit rate systems and interchannel crosstalk in wavelength division multiplexed systems will be damped out for frequencies above 1 kHz and will be negligible for high bit rates characteristic of optical communications systems.

Basic Properties as an Amplifier

Figure 1.3.4 shows a block diagram of the EDFA. The pump source is a 1.48 μm Fabry-Perot type high power laser diode, which is coupled into an erbium fiber through a WDM fiber coupler and a non-polarized optical isolator. The WDM fiber coupler passes the 1.55 μm signal and the pump beam into an erbium-doped fiber. The non-polarized optical isolator greatly suppresses the laser oscillation of the EDFA. The spectral components can effectively contribute to the generation of the population inversion of the erbium ions[1.3.33]. The combination of a relatively low concentration of erbium ions and a longer fiber length results in a higher gain than can be achieved with a high concentration and a shorter fiber length[1.3.34]. This low

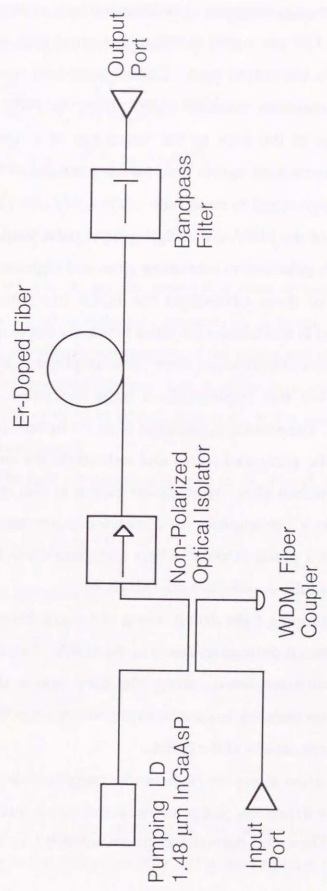

Fig. 1.3.4 Block diagram of an erbium-doped fiber amplifier (EDFA). It consists of five main components; an LD pump source, a WDM coupler, a non-polarized isolator, an erbium-doped fiber, and a narrowband filter.

doping can suppress the concentration quenching which reduces the pumping efficiency. The 1.55 μm signal is fed to the input port and the amplified signal exits from the output port. Optical amplifiers inevitably suffer from amplified spontaneous emission (ASE) from the EDFA. The suppression of ASE is one of the keys to the realization of a low noise amplifier. In this case a narrowband optical filter with a passband of 1~3 nm is installed, resulting in a high signal to noise ratio.

Typical advantages of the EDFA are a high gain of more than 30 dB, low noise, wide bandwidth, polarization insensitive gain, and high saturation output power. Because of these advantages the EDFA has three main applications[1.3.35]. The first is as a booster amplifier which is used to increase the signal power input into a transmission fiber. This amplifier is installed after the light source. For this application, a large saturation output characteristic is required. The second application is as an optical repeater which is used to amplify the attenuated signal and re-transmit the amplified signal into the next transmission fiber. High power output is also required. The third application is as a pre-amplifier to increase receiver sensitivity. This is installed in front of a photo detector, where low noise characteristics are required. EDFAs can be fully applied in these categories.

In the EDFA, the pumping light decays along the z axis because the pump beam is absorbed when it propagates down in the EDFA. As a result, a nonuniform population inversion occurs along the fiber, where the gain coefficient and the saturation intensity I_{sat} can be expressed as a function of z. Below, we describe some basic aspects of the EDFA.

The signal gain variation along the fiber can be roughly estimated by rate equation analysis. We define the pump intensity and signal intensity as I_p and I_s, respectively. Then, the normalized pump intensity $\bar{I}_p$ and the

normalized signal intensity $\bar{I}_s$ at amplifier length z in the forward pumping configuration are written as[1.3.9]

$$\frac{d\bar{I}_p}{dz} = -\frac{k_s\bar{I}_s + 1}{\bar{I}_p + (1+k_s)\bar{I}_s + 1}\rho\sigma_p^a\bar{I}_p\,, \tag{1.3.1}$$

$$\frac{d\bar{I}_s}{dz} = \frac{k_s\bar{I}_p - 1}{\bar{I}_p + (1+k_s)\bar{I}_s + 1}\rho\sigma_s^a\bar{I}_s\,, \tag{1.3.2}$$

$$\bar{I}_p = I_p/(h\nu_p/\sigma_p^a\tau), \tag{1.3.3}$$

$$\bar{I}_s = I_s/(h\nu_s/\sigma_s^a\tau)\,, \tag{1.3.4}$$

where σ_p^a and σ_s^a are the absorption cross section at the pump wavelength and the signal wavelength, respectively, ρ is the erbium concentration, $h\nu_P$ and $h\nu_S$ are the photon energies of the pump and signal waves, respectively, τ is the fluorescence lifetime, and α is the background loss of the fiber. We define the ratio k_s as σ_s^e/σ_s^a, where σ_s^e is the emission cross section at the signal wavelength.

The gain coefficient g defined as $d\bar{I}_s/dz = g\bar{I}_s$ is expressed from Eq. (1.3.2) as

$$g = \left[1 + \bar{I}_s/\left(\frac{\bar{I}_p + 1}{1 + k_s}\right)\right]^{-1}\frac{k_s\bar{I}_p - 1}{\bar{I}_p + 1}\rho\sigma_s^a, \tag{1.3.5}$$

which is rewritten as

$$g = \frac{g_0}{1 + \bar{I}_s/\bar{I}_{sat}}\,. \tag{1.3.6}$$

Here

$$\bar{I}_{sat} = \frac{\bar{I}_p + 1}{1 + k_s}\,, \tag{1.3.7}$$

and

$$g_0 = \frac{k_s\bar{I}_p - 1}{\bar{I}_p + 1}\rho\sigma_s^a\,. \tag{1.3.8}$$

Since $\bar{I}_{sat}$ and g_0 are functions of the pump intensity, they change with a decrease in the pump intensity along the amplifier length.

The pump power P_p and the signal power P_s are expressed as $P_p=I_pA_p$ and $P_s=I_sA_s$, respectively, where A_p and A_s are the effective core areas for the pump and signal waves. The saturation signal power P_{sat} is given by

$$P_{sat} = A_s(h\nu_s/\sigma_s^a\tau)\bar{I}_{sat} . \quad (1.3.9)$$

Figure 1.3.5(a) shows the gain $G = P_s^{out}/P_s^{in}$ by solving Eqs. (1.3.1) and (1.3.2) as a function of the input signal power P_s^{in}, where the input pump power is 59 mW. The length and the erbium concentration of the EDFA were 100 m and 92 ppm, respectively. The signal wavelength was 1.545 μm. The optical losses at the pump and signal wavelengths were 0.13 dB/m and 0.42 dB/m, respectively. The small-signal gain G_0 was 24.5 dB and the 3 dB saturation input power P_{3dB}^{in} was -15.2 dBm. Experimental data (open circles) are also shown in this figure. For small-signal input levels the gain is constant; but for moderate signal levels, the gain saturates with an increase in the input signal power. Gain as a function of the input pump power P_p is given in Fig. 1.3.5(b), where the open circles and the solid line represent experimental results and the theoretical curve, respectively.

In order to realize a high gain amplifier with a low pump power, it is important that the pump intensity is closely confined, so that an efficient excitation is achieved. To achieve this, special attention has been paid to structural optimization by doping erbium ions only into the center of the fiber core, so that the high intensity part of the pump field interacts with the erbium ions, resulting in efficient pumping. EDFA gain characteristics with a high gain coefficient thus obtained are shown in Figs. 1.3.6(a) and (b). An erbium-doped fiber with a high relative refractive-index ratio was used, in which the erbium is doped only into the high-index core region. The glass composition is Er:GeO_2-SiO_2-Al_2O_3. The mode field diameter, relative refractive-index difference, erbium concentration, and Al concentration were

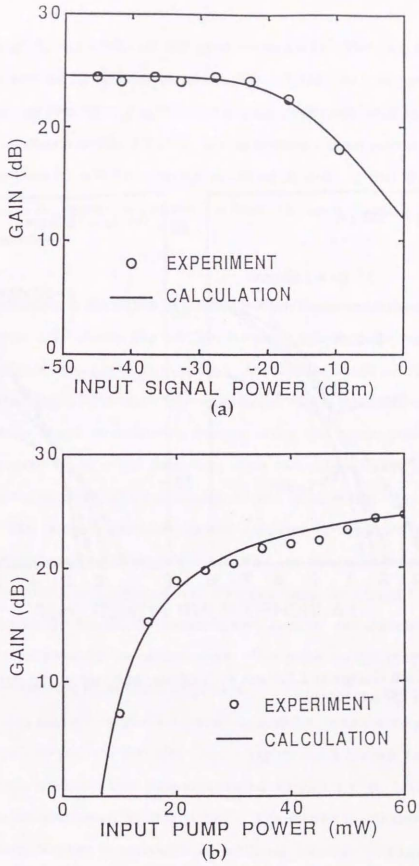

Fig. 1.3.5 Change in gain of EDFA as a function of the input signal power (a) and change in gain of EDFA as a function of the input pump power (b).

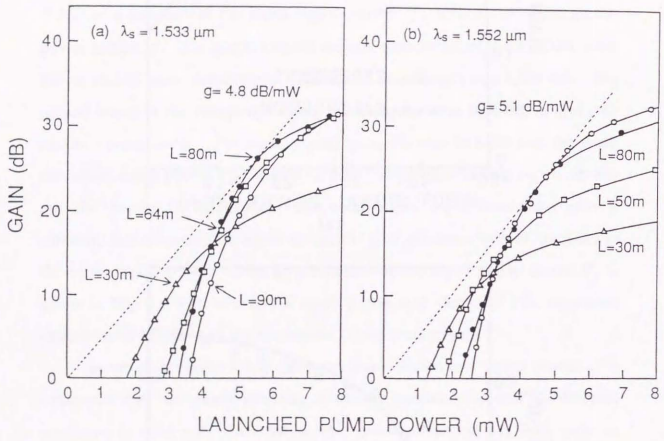

Fig. 1.3.6 Gain change at 1.533 μm vs. 1.48 μm launched pump power for (a) and that at 1.552 μm for (b).

4.8 μm, 1.67 %, 210 ppm, and 500 ppm, respectively. The gain coefficient at 1.553 μm was 4.8 dB/mW as shown in Fig. 1.3.6(a). At 1.552 μm the pump threshold was less than 2 mW and the gain coefficient was as high as 5.1 dB/mW as shown in Fig. 1.3.6(b). The saturation output power at 1.552 μm was more than 30 mW for a pump power of 50 mW, so that the EDFA can operate as a power amplifier, which is very useful for soliton communication.

1.3.3 Application of the EDFA to Optical Soliton Communications

Figure 1.3.7 shows the relation between soliton pulse width and its peak amplitude throughout propagation. The data for loss(Γ)=0.01 and 1.0 are illustrated in Fig. 1.3.7(a) and (b), respectively. The upper half of the figure shows pulse shape (amplitude) change along the propagation distance, assuming sech(t) as an input pulse (i.e., exact N=1 soliton). The lower half of the figure shows the product of amplitude and pulse width. For Fig. 1.3.7(a) (Γ=0.01), this product remains almost constant throughout propagation, which means that perturbation theory is valid and the pulse propagates as an N=1 soliton over a long distance. On the other hand, for a large Γ of 1.0 given in Fig. 1.3.7(b), the amplitude decreases very rapidly, and therefore the pulse width can not preserve the soliton state. This pulse cannot propagate as an N=1 soliton because of its small amplitude.

In long distance optical transmission systems, periodic amplification is required to compensate for fiber loss. Figure 1.3.8 shows two types of amplification scheme. One uses distributed amplifier (Fig. 1.3.8a) and the other uses lumped amplifier (Fig. 1.3.8b). The former is suitable for soliton transmission because it provides an artificial loss-free transmission line, while the latter is very simple and easy to construct.

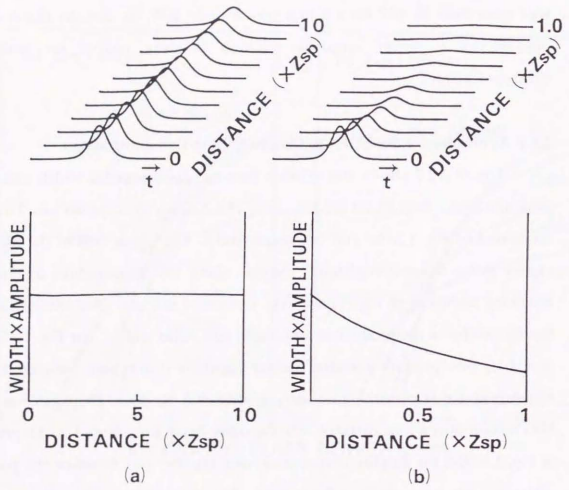

Fig. 1.3.7 Relation between the soliton pulse width and its peak amplitude during propagation. The upper half of the figure shows pulse shape (amplitude) change along the propagation distance and the lower half of the figure shows the product of amplitude and pulse width. (a) G=0.01, (b) G=1.0.

The Raman amplifier (1.3.8 a-1) is a typical distributed amplifier. That is, a conventional optical fiber itself becomes an amplifying medium through the Raman process. An Erbium-doped fiber with a low Er ion concentration can also be used as a distributed amplifier (1.3.8 a-2). In the Raman amplifier, the pump intensity decreases due to the intrinsic fiber loss and pump depletion. In an Er-doped fiber amplifier, the pump intensity decreases due to fiber loss and absorption by Er ions. These amplifiers act as a pure distributed gain medium only when the gain distributes uniformly. Hasegawa pointed out that the decreases in pump intensity produce a periodic perturbation to the solitons, and either gain or loss dominates at certain positions. The transmission loss of the soliton can only be compensated for by the overall periodic Raman gain[1.3.36]. When Γ is small, the soliton pulse behaves as described in Fig. 1.3.7(a), and the pulse propagates as an N=1 soliton over many multiples of Z_{sp}.

Based on this idea, long distance soliton transmission using periodic amplification by Raman amplifier is proposed[1.3.37]. Smith and Mollenauer have demonstrated pulse transmission over more than 6000 km in a recirculating 42-km fiber loop with a Raman amplifier[1.3.38]. The conditions of their system are L=41.7 km (loop length), Z_{sp}=66 km, γ=0.22 dB/km (fiber loss coefficient for signal), and α=0.29 dB/km (fiber loss coefficient for pump). The loop length L (amplifier spacing) is of the order of Z_{sp}. In that case, even though they use a Raman amplifier, it cannot be described as an ideal distributed amplifier system. Γ at the input of the fiber becomes +0.58, at which the perturbation theory cannot be applied.

On the other hand, laser diode (LD) amplifiers and erbium-doped fiber amplifiers (EDFAs) can be used as lumped amplifiers for soliton communication (Fig. 1.3.8b). An advantage of the lumped amplifier is its

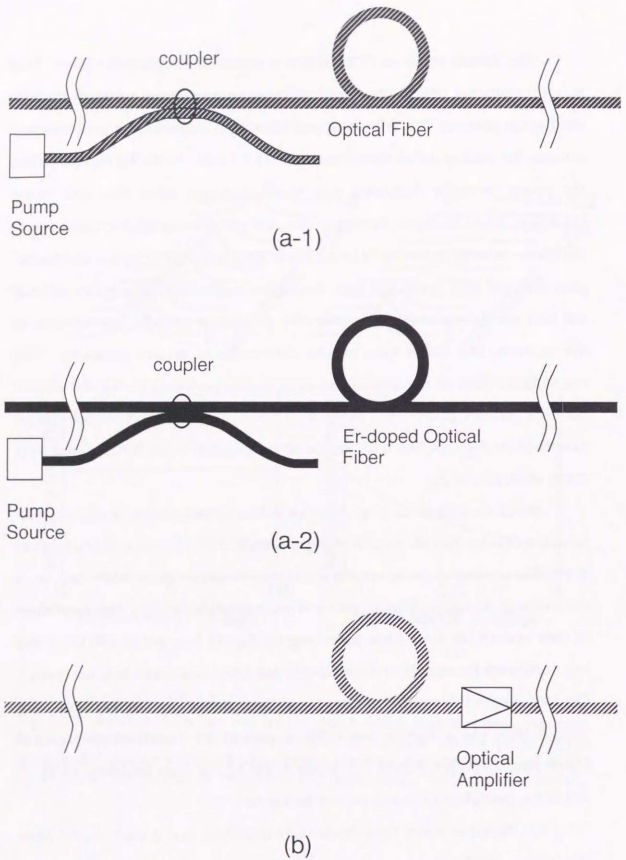

Fig. 1.3.8 Two types of amplification scheme used for long distance optical transmission systems. (a) distributed amplifier, (b) lumped amplifier.

simple configuration, i.e., the amplifier region is clearly separated from the transmission line. The LD amplifier is very compact and reliable, but it has polarization dependent gain and slight fluctuation in the transmitting signal pattern (patterning effect) due to the fast gain-recovery time which is comparable to transmitting speed. In contrast, the EDFA has the excellent characteristics of polarization insensitivity, high gain, low insertion loss, and no pattern effect because of its very slow gain-recovery time. Since the EDFA needs a pumping laser, it was very important to discover a compact and efficient pumping source. Nakazawa et al. showed 12.5 dB gain could be obtained by an EDFA pumped by an 1.48 μm distributed feedback laser diode (DFB LD)[1.3.17], and the current gain thus achieved exceeds 45 dB[1.3.39]. It was also demonstrated that picosecond and femtosecond solitons can be amplified by the EDFA[1.3.40-43]. Recently, the EDFA has been widely used for optical amplification in the 1.5 μm region in addition to its optical soliton application.

1.4 Outline of This Thesis

This thesis summarizes the results of the research on propagation characteristics of femtosecond optical soliton in an EDFA and also generation of femtoseocnd infrared pulse for the study of soliton propagation.

The thesis consists of 6 chapters. Chapter I provides an overview of soliton propagation in optical fibers and general features of an EDFA that are important for understanding the propagation characteristics in an EDFA discussed in chapters III~V. Chapter II describes our femtosecond infrared light source which we have newly developed and used in our experiments in later chapters. Chapter III describes amplification characteristics of femtosecond pulses under various pumping condtions for EDFAs. Adiabatic

and nonadiabatic amplification characteristics of a femtosecond soliton are presented in an EDFA which consists of a short length of erbium-doped fiber with a high doping concentration of erbium ions. Chapter IV describes femtosecond soliton transmission characteristics in an ultralong distributed EDFA (DEDFA) which consists of an 18 km erbium-doped fiber with a very low doping concentration. Chapter V describes mutual interactions between femtosecond solitons in a DEDFA. Propagation characteristics of a soliton pair in a DEDFA are presented which are strongly modified by a higher-order nonlinear effect, soliton self-frequency shift (SSFS), in a femtosecond region. Chapter VI summarizes the results obtained through the studies and describes the future of research on ultrashort optical nonlinear wave propagation in optical fibers.

References

section 1.1

[1.1.1] A. Hasegawa and F. D. Tappert, "Transmission of stationary nonlinear optical pulses in dispersive dielectric fibers. I," Appl. Phys. Lett. vol. 23, p. 142, 1973.

[1.1.2] R. J. Mears, L. Reekie, S. B. Poole, and D. N. Payne, "Neodymium-doped silica single-mode fibre lasers," Electron. Lett. vol. 21, p. 738, 1985.

[1.1.3] S. B. Poole, D. N. Payne, and M. E. Fermann, "Fabrication of low-loss optical fibres containing rare-earth ions," Electron. Lett. vol. 21, p. 737, 1985.

[1.1.4] E. Desurvire, J. R. Simpson, and P. C. Becker, "High gain erbium-doped traveling-wave fiber amplifier," Opt. Lett., vol. 12, p. 888, 1987.

[1.1.5] E. Snitzer, H. Po, F. Hakimi, R. Tuminelli, and B. C. McCollum, "Erbium fiber laser amplifiers at 1.55 μm with pump at 1.49 μm and Yb sensitized Er oscillator," in Proc. Opt. Fiber Commun. Conf., 1988, paper PD2.

[1.1.6] M. Nakazawa, Y. Kimura, and K. Suzuki, "Efficient Er^{3+}-doped optical fiber amplifier pumped by a 1.48 μm InGaAsP laser diode," Appl. Phys. Lett., vol. 54, p. 295, 1989.

[1.1.7] K. Suzuki, Y. Kimura, and M. Nakazawa, "Pumping wavelength dependence on gain factor of a 0.98 μm pumped Er^{3+} fiber amplifier," Appl. Phys. Lett., vol. 55, p. 2573, 1989.

[1.1.8] Y. Kimura, K. Suzuki and M. Nakazawa, "46.5 dB gain in Er^{3+}-doped fibre amplifier pumped by 1.48 μm GaInAsP laser diodes," Electron. Lett., vol. 25, p. 1656, 1989.

[1.1.9] M. Nakazawa, K. Suzuki, and Y. Kimura, "3.2-5 Gbit/s, 100 km Error-free soliton transmission with erbium amplifiers and repeaters," IEEE Photon. Technol. Lett., vol. 2, p. 216, 1990.

[1.1.10] H. Kubota and M. Nakazawa, "Long-distance optical soliton transmission with lumped amplifiers," IEEE J. Quantum Electron., vol. 26, p. 692, 1990.

[1.1.11] K. Suzuki, M. Nakazawa, E. Yamada, and Y. Kimura, "5 Gbit/s, 250 km error-free soliton transmission with Er^{3+}-doped fibre amplifiers and repeaters," Electron. Lett., vol. 26, p. 551, 1990.

[1.1.12] M. Nakazawa, K. Suzuki, E. Yamada, H. Kubota, Y. Kimura and M. Takaya, "Experimental demonstration of soliton data transmission over unlimited distances with soliton control in time and frequency domains," Electron. Lett., vol. 29, p. 729, 1993.

[1.1.13] M. Nakazawa, K. Suzuki, E. Yoshida, E. Yamada, T. Kitoh and M. Kawachi, "160 Gbit/s soliton data transmission over 200 km," Electron. Lett., vol. 31, p. 565, 1995.

[1.1.14] M. Suzuki, I. Morita, N. Edagawa, S. Yamamoto, H. Taga and S. Akiba, "Reduction of Gordon-Haus timing jitter by periodic dispersion compensation in soliton transmission," Electron. Lett., vol. 31, p. 2027, 1995.

[1.1.15] L. F. Mollenauer, P. V. Mamyshev and M. J. Neubelt, "Demonstration of soliton WDM transmission at up to 8 X 10 Gbit/s, error-free over transoceanic distances," in Technical Digest OFC '96, paper, PD22, 1996.

[1.1.16] I. Morita, M. Suzuki, N. Edagawa, S. Yamamoto, H. Taga, and S. Akiba, "20-Gb/s Single-Channel Soliton Transmission Over 9000 km Without Inline Filters," IEEE Photon. Technol. Lett., vol. 8, p. 1573, 1996.

section 1.2

[1.2.1] J. S. Russell, Reports of the Meeting of the British Association for the Advancement of Science, London: John Murray (London meeting, 1844), p. 311; (Liverpol meeting, 1838), p. 417.

[1.2.2] D. J. Korteweg and G. deVries, Philos. Mag. vol. 39, p. 422, 1895.

[1.2.3] H. Washimi and T. Taniuti, "Propagation of ion-acoustic solitary waves of small amplitude," Phys. Rev. Lett. vol. 17, p. 996, 1966.

[1.2.4] H. Ikezi, R. J. Taylor, and D. B. Baker, "Formation and interaction of ion-acoustic solitons," Phys. Rev. Lett. vol. 25, p. 11, 1970.

[1.2.5] H. Hasimoto, J. Fluid Mech. vol. 51, p. 477, 1972.

[1.2.6] W. P. Su, J. R. Schrieffer, and A. J. Heeger, "Solitons in polyacetylene," Phys. Rev. Lett. vol. 42, p. 1698, 1979.

[1.2.7] A. Hasegawa and F. D. Tappert, "Transmission of stationary nonlinear optical pulses in dispersive dielectric fibers. I," Appl. Phys. Lett. vol. 23, p. 142, 1973.

[1.2.8] L. F. Mollenauer, R. H. Stolen, and J. P. Gordon, "Experimental observation of picosecond pulse narrowing and solitons in optical fibers," Phys. Rev. Lett., vol. 45, p. 1095, 1980.

[1.2.9] N. J. Zabusky and M.D. Kruskal, "Interaction of "solitons" in a collisionless plasma and the recurrence of initial states," Phys. Rev. Lett., vol. 15, p.240, 1965.

[1.2.10] V. E. Zhakharov and A. B. Shabat, "Exact theory of two-dimensional self-focusing and one-dimensional self-modulation of waves in nonlinear media," Zh. Eksp. Teor. Fiz. vol. 61, p. 118, 1971. [Trans. Sov. Phys. JETP vol. 34, p. 62, 1972.]

[1.2.11] J. P. Gordon, "Interaction forces among solitons in optical fibers," Opt. Lett. vol. 8, p. 596, 1983.

[1.2.12] B. Hemmerson and D. Yevik, "Numerical investigation of soliton interaction," Electron. Lett. vol. 19, p. 570, 1983.

[1.2.13] P. L.Chu and C. Desem, "Mutual interaction between solitons of unequal amplitudes in optical fibre," Electron. Lett. vol. 21, p. 1133, 1985.

[1.2.14] A. Haegawa and Y. Kodama, "Signal transmission by optical solitons in monomode fiber," Proc. IEEE vol. 69, p. 570, 1983.

[1.2.15] K. J. Blow and N. J. Doran, "Soliton in optical communications," IEEE J. Quantum Electron. vol. QE-19, p. 1883, 1983.

[1.2.16] E. Shiojiri and Y. Fujii, "Transmission capacity of an optical fiber communication system using index nonlinearity," Appl. Opt. vol. 24, p. 358, 1985.

[1.2.17] A. Hasegawa, "Numerical study of optical soliton transmission amplified periodically by the stimulated Raman process," Appl. Opt. vol. 23, p. 3302, 1984.

[1.2.18] L. F. Mollenauer and K. Smith, "Demonstration of soliton transmission over more than 4000 km in fiber with loss periodically compensated by Raman gain," Opt. Lett. vol. 13, p. 675, 1988.

[1.2.19] M. Nakazawa, Y. Kimura, and K. Suzuki, "Soliton amplification and transmission with Er^{3+} - doped fibre repeater pumped by GaInAsP laser diode," Electron. Lett. vol. 25, p. 199, 1989.

[1.2.20] A. Hasegawa and Y. Kodama, "Guiding-center solitons in optical fibers," Opt. Lett. vol. 15, p. 1443, 1990.

[1.2.21] L. F. Mollenauer, S. G. Evangelides, and H. A. Haus, "Long distance soliton propagation using lumped amplifiers and dispersion-shifted fiber," IEEE Lightwave Technol. vol. 9, p. 194, 1991.

[1.2.22] K. J. Blow and N. J. Doran, "Average soliton dynamics and the operation of soliton systems with lumped amplifiers," IEEE Photo Tech. Lett. vol. 4, p.639, 1991.

[1.2.23] M. Nakazawa, K. Suzuki, E. Yamada, H. Kubota, Y. Kimura and M. Takaya, "Experimantal demonstration of soliton data transmission over unlimited distances with soliton control in time and frequency domains," Electron. Lett., vol. 29, p. 729, 1993.

[1.2.24] M. Nakazawa, K. Suzuki, E. Yoshida, E. Yamada, T. Kitoh and M. Kawachi," 160 Gbit/s soliton data transmission over 200 km," Electron. Lett., vol. 31, p. 565, 1995.

[1.2.25] M. Suzuki, I. Morita, N. Edagawa, S. Yamamoto, H. Taga and S. Akiba, "Reduction of Gordon-Haus timing jitter by periodic dispersion compensation in soliton transmission," Electron. Lett., vol. 31, p. 2027, 1995.

[1.2.26] L. F. Mollenauer, P. V. Mamyshev and M. J. Neubelt, "Demonstration of soliton WDM transmission at up to 8 X 10 Gbit/s, error-free over transoceanic distances," in Technical Digest OFC '96, paper, PD22, 1996.

[1.2.27] H. A. Haus and M. N. Islam, "Theory of the soliton laser," IEEE J. Quantum Electron. vol. QE-21, p. 1172, 1985.

[1.2.28] G. P. Agrawal, Nonlinear Fiber Optics (Academic Press, San Diego, 1989).

[1.2.29] L. F. Mollenauer, R. H. Stolen, and J. P. Gordon, "Extreme picosecond pulse narrowing by means of soliton effect in single-mode optical fibers," Opt. Lett. vol. 8, p. 289, 1983.

[1.2.30] J. Satsuma and N. Yajima, "Initial value problems of one-dimensional self-modulation of nonlinear waves in dispersive media," Suppl. Prog. Theor. Phys. vol. 55, p.284, 1974.

[1.2.31] D. Marcuse, "Pulse distortion in single-mode fibers," Appl. Opt. vol. 19, p. 1653, 1980.

[1.2.32] F. De Martine, C. H. Townes, T. K. Gustafson and P. L. Kelly, "Self-steeping of light pulses," Phys. Rev. vol. 164, p. 312, 1967.

[1.2.33] J. P. Gordon, "Theory of the soliton self-frequency shift," Opt. Lett. vol. 11, p. 662, 1986.

[1.2.34] F. M. Mitschke and L. F. Mollenauer, "Discovery of the soliton self frequency shift," Opt. Lett. vol. 11, p. 659, 1986.

[1.2.35] R. H. Stolen and E. P. Ippen, "Raman oscillation in glass optical waveguide," Appl. Phys. Lett. vol. 20, p. 62, 1972.

[1.2.36] M. N. Islam, Ultrafast Fiber Switching Devices and Systems (Cambridge University Press, NY, 1992).

[1.2.37] H. A. Haus and M. Nakazawa, "Theory of the fiber Raman soliton laser," J. Opt. Soc. Am. vol. B 4, p. 652, 1987.

[1.2.38] J. P. Gordon, "Interaction forces among solitons in optical fibers," Opt. Lett., vol. 8, p. 596, 1983.

[1.2.39] C. Desem and P. L. Chu, "Reducing soliton interaction in single-mode optical fibres," IEE Proc., vol. 134, Pt. J, p. 145, 1987.

[1.2.40] V. I. Karpman and V. V. Solovev, "A perturbational approach to the two-soliton systems," Physica, vol. 3D, p. 487, 1981.

[1.2.41] K. J. Blow and N. J. Doran, "Bandwidth limits of nonlinear (soliton) optical communication systems," Electron. Lett., vol. 19, p. 429, 1983.

[1.2.42] C. Desem and P. L. Chu, "Soliton interaction in the presence of loss and periodic amplification in optical fibers," Opt. Lett., vol. 12, p. 349, 1987; "Soliton propagation in the presence of source chirping and mutual interaction in single-mode optical fibres," Electron. Lett., vol. 23, p. 260, 1987.

[1.2.43] E. M. Dianov, Z. S. Nikonova and V. N. Serkin, "Influence of frequency modulation on the interaction of pulses in fiber waveguides," Sov. J. Quantum Electron. vol. 16, p. 1148, 1986.

[1.2.44] P. L. Chu and C. Desem, "Optical fibre communication using solitons," in Technical Digest IOOC '83, Tokyo, p. 52, 1983; "Effect of third-order dispersion of optical fibre on soliton interaction," Electron. Lett., vol. 21, p. 228, 1985.

[1.2.45] F. M. Mitschke and L. F. Mollenauer, "Experimental observation of interaction forces between solitons in optical fibers," Opt. Lett., vol. 12, p. 355, 1987.

[1.2.46] Y. Kodama and K. Nozaki, "Soliton interaction in optical fibers," Opt. Lett., vol. 12, p. 1038, 1987.

section 1.3

[1.3.1] E. Snitzer and R. Woodcock, "Yb^{3+} - Er^{3+} glass laser," Appl. Phys. Lett., vol. 6, p. 45, 1965.

[1.3.2] C. J. Koester and E. Snitzer, "Amplification in a fiber laser," Appl. Opt., vol. 3, p. 1182, 1964.

[1.3.3] J. Stone and C. A. Burrus, "Neodymium-doped fiber lasers: Room temperature CW operation with an injection laser pump," Appl. Opt., vol. 13, p. 1256, 1974.

[1.3.4] J. Hegarty, M. M. Broer, B. Golding, J. R. Simpson, and J. B. MacChesney, "Photon echoes below 1 K in Nd^{3+}-doped glass fiber," Phys. Rev. Lett., vol. 51, p. 2033, 1983.

[1.3.5] S. B. Poole, D. N. Payne, R. J. Rears, M. E. Fermann, and R. I. Laming, "Fabrication and characterization of low-loss optical fibers containing rare-earth ions," J. Lightwave Technol., vol. LT-4, p. 870, 1986.

[1.3.6] R. J. Mears, L. Reekie, S. B. Poole, and D. N. Payne, "Low-threshold tunable CW and Q-switched fiber laser operating at 1.55 μm," Electron. Lett., vol. 22, p. 159, 1986.

[1.3.7] R. J. Mears, L. Reekie, I. M. Jauncey, and D. N. Payne, "Low-noise erbium-doped fiber amplifier operating at 1.54 μm," Electron. Lett., vol. 23, p. 1026, 1987.

[1.3.8] R. Wyatt, "High-power broadly tunable erbium-doped silica fiber laser," Electron. Lett., vol. 25, p. 1498, 1989.

[1.3.9] E. Desurvire, J. R. Simpson, and P. C. Becker, "High gain erbium-doped traveling-wave fiber amplifier," Opt. Lett., vol. 12, p. 888, 1987.

[1.3.10] C. R. Giles, E. Desurvire, J. R. Talman, J. R. Simpson, and P. C. Becker, "2 Gbit/s signal amplification at λ=1.53 μm in an erbium-doped single-mode fiber amplifier," J. Lightwave Technol., vol. 7, p. 651, 1989.

[1.3.11] E. Desurvire, C. R. Giles, and J. R. Simpson, "Gain saturation effects in high-speed, multichannel erbium-doped fibre amplifiers at λ=1.53 μm," J. Lightwave Technol., vol. 17, p. 2095, 1989.

[1.3.12] T. J. Whitley, "Laser diode pumped operation of erbium-doped fibre amplifier," Electron. Lett., vol. 24, p. 1537, 1988.

[1.3.13] J. R. Armitage, C. G. Atkins, R. Wyatt, B. J. Ainslie, and S. P. Craig, "Spectroscopic studies of Er-doped single mode silica fiber," in Tech. Dig. Conf. Lasers and Electro-Optics (Opt. Soc. Amer., Washington, DC), 1988, paper TUM 27.

[1.3.14] R. I. Laming, M. C. Farries, P. R. Morkel, L. Reekie, D. N. Payne, P. L. Scrivener, F. Fontana and A. Righetti, "Efficient pump wavelengths of erbium-doped fibre optical amplifiers," Electron. Lett., vol. 25, p. 12, 1989.

[1.3.15] S. E. Fisher, D. Fekete, G. B. Feak, and M. J. Ballantyne, "Ridge waveguide injection laser with a GaInAs strained-layer quantum well (λ=1 μm)," Appl. Phys. Lett., vol. 50, p. 714, 1987.

[1.3.16] E. Snitzer, H. Po, F. Hakimi, R. Tuminelli, and B. C. McCollum, "Erbium fiber laser amplifiers at 1.55 μm with pump at 1.49 μm and Yb sensitized Er oscillator," in Proc. Opt. Fiber Commun. Conf., 1988, paper PD2.

[1.3.17] M. Nakazawa, Y. Kimura, and K. Suzuki, "Efficient Er^{3+}-doped optical fiber amplifier pumped by a 1.48 μm InGaAsP laser diode," Appl. Phys. Lett., vol. 54, p. 295, 1989.

[1.3.18] K. Hagimoto, "Dynamic evolution of advanced optical networks in Japan," in Tech. Dig. First Optoelectronics and Communications Conf. (OECC'96), paper 17A1-9, Makuhari, 1996.

[1.3.19] W. C. Barnett, H. Takahira, J. C. Baroni, and Y. Ogi, "The TPC-5 cable network," IEEE Comm. Magazine, vol. 34, p. 36, 1996.

[1.3.20] P. Trischitta, M. Colas, M. Green, G. Wuzniak, and J. Arena, "The TAT-12/13 cable network," IEEE Comm. Magazine, p. 24, 1996.

[1.3.21] D. R. Gunderson, A. Lecroart, and K. Tatekura, "The Asia pacific cable network," IEEE Comm. Magazine, p. 42, 1996.

[1.3.22] J. L. Zyskind, "Erbium-doped fiber amplifiers," in proceeding of SPIE Fiber Laser Sources and Amplifiers III, vol. 1581, p. 14, 1991.

[1.3.23] W. L. Barnes, P. R. Morkel, L. Reekie, and D. N. Payne, "High-quantum-efficiency Er^{3+} fiber lasers pumped at 980 nm," Opt. Lett., vol. 14, p. 1002, 1989.

[1.3.24] E. Desurvire and J. R. Simpson, "Evaluation of $^4I_{15/2}$ and $^4I_{13/2}$ Stark-level energies in erbium-doped aluminosilicate glass fibers," Opt. Lett., vol. 15, p. 547, 1990.

[1.3.25] E. Desurvire, J. W. Sulhoff, J. L. Zyskind, and J. R. Simpson, "Study of spectral dependence of gain saturation and effect of inhomogeneous broadening in erbium-doped aluminosilicate fiber amplifiers," IEEE Photo. Tech. Lett., vol. 2, p. 653, 1990.

[1.3.26] M. Tachibana, R. I. Laming, P. R. Morkel and D. N. Payne, "Spectral gain cross saturation and hole-burning in wideband erbium-doped fiber amplifiers," in Tech. Dig. on Optical Amplifiers and Their Applications (Opt. Soc. Amer., Washington, DC), vol. 13, paper, ThB1-1, p. 104, Snowmass, 1991.

[1.3.27] E. Desurvire, J. L. Zyskind, and J. R. Simpson, "Spectral gain hole-

burning at 1.53 μm in erbium-doped fiber amplifiers," IEEE Photo. Tech. Lett., vol. 2, p. 246, 1990.

[1.3.28] J. L. Zyskind, E. Desurvire, J. W. Sulhoff and D. J. DiGiovanni, "Determination of homogeneous linewidth by spectral gain hole-burning in an erbium-doped fiber amplifier with GeO_2:SiO_2 core," IEEE Photo. Tech. Lett., 2, p. 869, 1990.

[1.3.29] C. R. Giles and D. J. DiGiovanni, "Dynamic gain equalization in a two-stage amplifier," IEEE Photo. Tech. Lett., vol. 2, p. 866, 1990.

[1.3.30] M. Tachibana, R. I. Laming, P. R. Morkel and D. N. Payne, "Gain-shaped erbium-doped fiber amplifier (EDFA) with broad spectral bandwidth," in Tech. Dig. on Optical Amplifiers and Their Applications (Opt. Soc. Amer., Washington, DC), paper, MD1, Monterey, 1991.

[1.3.31] A. M. Holl, D. B. Payne, K. J. Blyth, D. S. Forrester, J. W. Arklight, R. Wyatt, J. F. Massicott, R. A. Lobbett, P. Smith and T. G. Hodgkinson, "7203-user WDM broadcast network employing one erbium-doped fibre power amplifier," Electron. Lett., vol. 26, p. 605, 1990.

[1.3.32] C. R. Giles, E. Desurvire and J. R. Simpson, "Transient gain and crosstalk in erbium-doped fiber amplifiers," Opt. Lett., vol. 14, p. 880, 1989.

[1.3.33] Y. Kimura, K. Suzuki and M. Nakazawa, "Pump wavelength dependence of the gain factor in 1.48 μm pumped Er^{3+}-doped fiber amplifiers," Appl. Phys. Lett., vol. 56, p. 1611, 1990.

[1.3.34] E. Desurvire, C. R. Giles, J. R. Simpson and J. L. Zyskind, in Tech. Dig. Conf. Lasers and Electro-Optics (Opt. Soc. Amer., Washington, DC), 1989, paper PD20.

[1.3.35] S. Shimada, "Impact of Erbium-doped amplifiers on optical communication systems," Optics & Photonics News, Opt. Soc. Amer., vol. 1, p. 6, 1990.

[1.3.36] A. Hasegawa, "Numerical study of soliton transmission amplified periodically by the stimulated Raman process," Appl. Opt. vol. 23, p. 3302, 1984.

[1.3.37] L. F. Mollenauer, J. P. Gordon and M. N. Islam, "Soliton propagation in long fibers with periodically compensated loss," IEEE J. Quantum Electron. vol. QE-22, p. 157, 1986.

[1.3.38] R. G. Smith and L. F. Mollenauer, "Experimental observation of adiabatic compression and expansion of soliton pulses over long fiber paths," Opt. Lett., vol. 14, p. 751, 1989.

[1.3.39] Y. Kimura, K. Suzuki and M. Nakazawa, "46.5 dB gain in Er^{3+}-doped fibre amplifier pumped by 1.48 μm GaInAsP laser diodes," Electron. Lett., vol. 25, p. 1656, 1989.

[1.3.40] M. Nakazawa, K. Suzuki and Y. Kimura, "Soliton amplification and transmission with Er^{3+}-doped fibre repeater pumped by GaInAsP laser diode," Electron. Lett., vol. 25, p. 199, 1989.

[1.3.41] B. J. Ainslie, K. J. Blow, A. S. Gouveia-Neto, P. G. J. Wigley, A. S. B. Sombra, and J. R. Taylor, "Femtosecond soliton amplification in erbium doped silica fibre," Electron. Lett., vol. 26, p. 186, 1990.

[1.3.42] I. Yu. Khrushchev, A. B. Grudinin, E. M. Dianov, D. V. Korobkin Jun, V. A. Semenov, and A. M. Prokhorov," Amplification of femtosecond pulses in Er^{3+}-doped single-mode optical fibres," Electron. Lett., vol. 26, p. 456, 1990.

[1.3.43] M. Nakazawa, K. Kurokawa, H. Kubota, K. Suzuki and Y. Kimura, "Femtosecond erbium-doped optical fiber amplifier," Appl. Phys. Lett., vol. 57, p. 653, 1990.

CHAPTER II. FEMTOSECOND INFRARED (IR) LIGHT SOURCE

2.1 Introduction

In this chapter, we describe our femtosecond infrared light source which we have newly developed and used in our experiments in this thesis.

Generation of ultrashort pulses in the wavelength region between 1.3 and 1.6 μm have aroused considerable interest in view of their applications in time resolved spectroscopy and in optical communications. Subpico- and femtosecond pulses in the near infrared region have been generated so far from a synchronously pumped infrared dye laser[2.1], and from a soliton laser[2.2]. These methods generate the pulses at high repetition rates but with low energies and narrow spectral tunability. Tunable infrared subpicosecond pulses have been obtained by difference frequency generation(DFG)[2.3] or parametric amplification[2.4] by using a white-light subpicosecond continuum. Although these techniques allow the generation of tunable ultrashort pulses with a high peak power, the repetition rate is low. Stimulated Raman scattering is also useful to generate subpicosecond continuum pulses around 2.4 μm[2.5]. 97 fs pulses at a rate of 50 MHz have been obtained at 1.5 μm by mixing a femtosecond dye laser and a picosecond YAG laser[2.6]. Although high repetition rate, infrared femtosecond pulses are generated with this method, the power of the generated pulse is low.

Then, we have succeeded in generating high peak-power, high repetition-rate, tunable subpico- and femtosecond pulses in the 1.4~1.6-μm region by mixing a 1.064 μm Nd:YAG laser pulse and a visible subpicosecond pulse from a cavity dumped, synchronously pumped dye laser[2.7]. Pulses as short as 94 fs with a peak power of 8.4 kW have been obtained with a KTP crystal at a rate of 3.8 MHz. Recently, high power, femtosecond infrared

pulses are easily obtained by using an optical parametric oscillator pumped by mode-locked Ti:Al_2O_3 laser[2.8].

2.2 Experimental Setup

The experimental arrangement is shown in Fig. 2.1. A cavity dumped, synchronously pumped dye laser supplies 600~640 nm subpicosecond pulses at a repetition rate of 3.8 MHz. The dye laser consists of six mirrors, two dye jets, four Brewster-angled prisms, an adjustable spatial filter, and a double-pass cavity dumper[2.9]. The laser was pumped by a frequency-doubled cw Nd:YAG laser with 1.35 W average power, 80 ps width and 76 MHz repetition rate. The gain medium was a mixture of Rh6G(0.7×10^{-3} mol/l) and Kiton Red S (KRS)(1.2×10^{-3} mol/l). The mixed saturable dyes DODCI(1.2×10^{-4} mol/l) and DQOCI(1.9×10^{-4} mol/l) in ethylene glycol were used to obtain stable mode-locked pulses.

The visible subpicosecond pulses from the cavity dumped dye laser were combined collinearly by dichroic mirror with a 1.064-μm pulse from a Nd:YAG laser. The cw modelocked power from the YAG laser was 20 W and it was reduced to 18 W after frequency-doubling in KTP. The visible subpicosecond pulse and 1.064-μm pulse were directed through a 4 cm focal-length lens into a nonlinear crystal. Temporal overlap of the two pulses was obtained by adjusting the variable delay. First, the delay was roughly adjusted by using a fast photodiode. Fine adjustment was maid to optimize the output power of the generated infrared pulses. A half-wave plate was installed in each optical path of the two pulses in order to change the polarization directions. The polarization of the 1.064-μm pulse was linearized with a Glan-Thompson prism. After passing an attenuator, a telescope, and the prism, 1.064-μm power coupled into the crystal was 5-6 W. The infrared

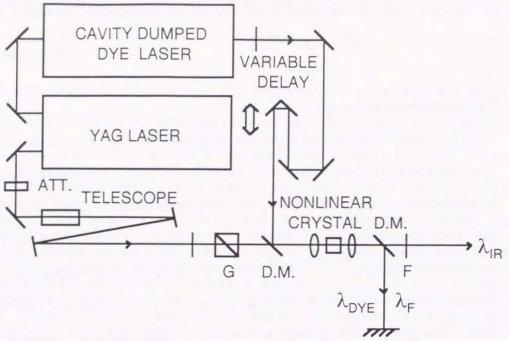

Fig. 2.1 Experimental setup for the generation of femtosecond infrared pulses by difference frequency generation(DFG). ATT. is the attenuator; $\lambda/2$, the half-wave plate; G, Glan-Thompson prism; D.M., dichroic mirrors; F, Filter; λ_{DYE}, λ_F and λ_{IR} are the wavelengths of the dye laser, of the Nd:YAG laser and of the generated infrared pulses, respectively.

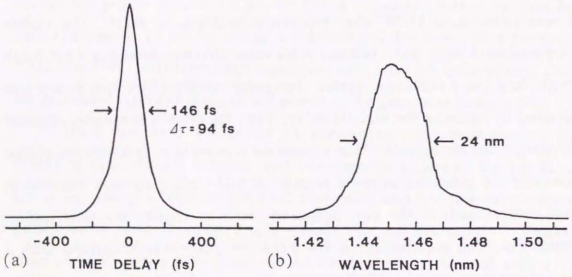

Fig. 2.2. (a) Autocorrelation trace and (b) frequency spectrum of the generated infrared pulse in KTP.

pulses generated by DFG were separated from the two input pulses by dichroic mirror.

2.3 Experimental Results and Discussion

Three kinds of nonlinear crystals, KTP, $LiNbO_3$, and β-BaB_2O_4 (BBO) were used for DFG. These nonlinear crystals are the most widely used crystals for second harmonic generators.

The KTP crystal was 3.4 mm long and was cut so that its z axis made an angle of 76° to the face normal. We adopted type II collinear phase-matching, that is, $E(\lambda_{IR})$ and $E(\lambda_F)$ were of orthogonal polarization, where $E(\lambda_{IR})$ and $E(\lambda_F)$ are the electric fields of the generated infrared pulse and the fundamental pulse (λ=1.064 μm) of the Nd:YAG laser, respectively. The polarization of the visible subpicosecond pulse from the dye laser was orthogonal to the polarization of the generated IR pulse.

The $LiNbO_3$ crystal was 3 mm long and was cut so that its optic axis made an angle of 61° to the face normal. In the case of $LiNbO_3$, the phase matching was type I, that is, $E(\lambda_{IR})$ and $E(\lambda_F)$ had the same polarization. The polarization of the visible subpicosecond pulse was orthogonal to those of the generated IR pulse and the 1.064-μm pulse. The BBO crystal used in the experiment was 5 mm long and was cut so that its optic axis made an angle of 23° to the face normal. We adopted type I collinear phase-matching.

The visible input pulse into the KTP crystal was 129 fs and the average power was 65 mW at a repetition rate of 3.8 MHz. The oscillation wavelength was 614 nm and the full width at half-maximum (FWHM) of the spectrum was 3.1 nm. The average power of the 1.064-μm pulse was 5.6 W at a repetition rate of 76 MHz, and the pulse width was 100 ps.

The output of the infrared (IR) pulse thus obtained is shown in Fig. 2.2. The autocorrelation trace of the generated IR pulse is shown in Fig. 2.2(a). The FWHM of the trace is 146 fs, which corresponds to a pulse width of 94 fs by assuming a $(sech)^2$ intensity profile. The average output power was 3 mW at a repetition rate of 3.8 MHz. The peak power was as high as 8.4 kW. The spectrum of the generated IR pulse is shown in Fig. 2.2(b). The wavelength of the IR pulse was 1.45 μm and the FWHM of the spectrum was 24 nm. Pulses with a duration of 94 fs and a spectral width of 24 nm give a time-bandwidth product of 0.32, which means that the pulses are transform limited.

In the generation of femtosecond IR pulses by DFG, pulse broadening due to group velocity dispersion (GVD) in the nonlinear crystal should be considered. For KTP, the calculated values of GVD at 614 nm and at 1.45 μm are 1.6 fs/nm mm and 6.4×10^{-2} fs/nm mm, respectively. These values are so small that the pulse broadening due to GVD is negligible at both wavelengths.

The angle-tuned phase-matching curve was investigated by tuning the wavelength of the visible subpicosecond pulses from the dye laser. The result is shown in Fig. 2.3. The phase-matching angle in Fig. 2.3 is the value of θ at $\phi=0$, where θ and ϕ are polar coordinates referring to z axis and x axis, respectively. By rotating a birefringent filter in the laser cavity, the wavelength of the visible pulses was tuned from 600 nm to 640 nm, corresponding to the generated IR wavelength from 1.4 μm to 1.6 μm. The circles in Fig. 2.3 show the measured phase-matching angles corresponding to the visible pump wavelengths. The Sellmeier equations of the H. Vanherzeele et al.[2.10] were used to calculate the phase-matching angle-variation with changes of the visible pump wavelength, which is given by a solid curve. It is clearly seen that both agree well and infrared pulses between

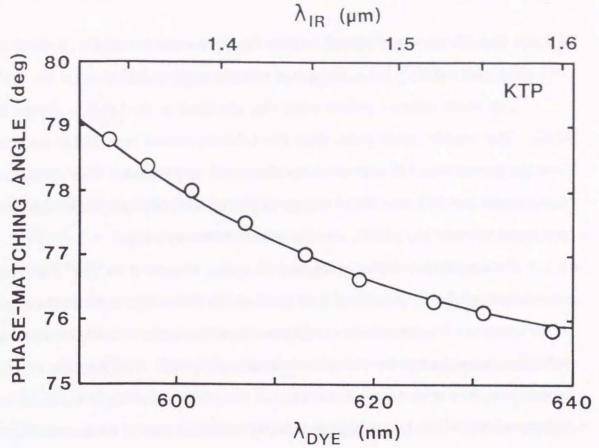

Fig. 2.3. Measured (o) and calculated (line) KTP phase-matching angle versus dye laser wavelength (λ_{DYE}). Idler wavelength is 1.064 μm.

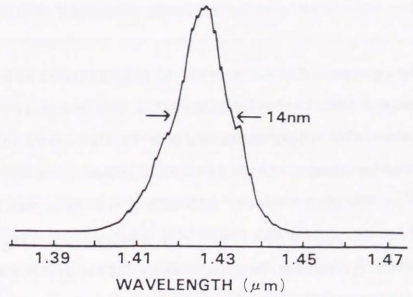

Fig. 2.4. Frequency spectrum of the generated infrared pulse by DFG with a $LiNbO_3$ crystal.

1.4 μm and 1.6 μm are obtained within an angle variation of 2° . Since the refractive index of KTP is 1.8, the actual rotation angle is 3.6° .

Ultrashort infrared pulses were also obtained in the $LiNbO_3$ crystal by DFG. The visible input pulse into the $LiNbO_3$ crystal was 190 fs and the average power was 100 mW at a repetition rate of 3.8 MHz. The oscillation wavelength was 610 nm. The average power of the 1.064-μm pulse was 5.6w at a repetition rate of 76 MHz, and the pulse width was 100 ps.

The spectrum of the generated IR pulse is shown in Fig. 2.4. The wavelength of the IR pulse was 1.43 μm and the full width at half maximum of the spectrum was 14 nm. In the present experiment the $LiNbO_3$ crystal was optically damaged by the visible subpicosecond pulse. The average output power was 30 μw at a repetition rate of 3.8 MHz. Although we used an autocorrelator which had a high sensitivity sufficient for the measurement of the pulses from laser diodes, the power of the generated IR pulse was still below the sensitivity of the autocorrelator. Therefore, an autocorrelation trace of the generated IR pulse could not be obtained. However, we have confirmed with an ultrafast photodetector that the IR signal is a very short pulse. The pulse width was limited by the picosecond response time of the detector.

The generated IR pulse width is roughly estimated as follows. In the subpicosecond DFG in the $LiNbO_3$ crystal, the group-velocity mismatch between the visible subpicosecond pulse and the generated IR pulse during the propagation causes a large temporal broadening of the generated IR pulse[2.11]. The group-velocity mismatch β was calculated by using the Sellmeier equations of Hobden et al.[2.12] β is defined as $\beta = |v_g^{-1}(\lambda_{DYE}) - v_g^{-1}(\lambda_{IR})|$, where $v_g(\lambda_{DYE})$ is the group velocity at the pump wavelength and $v_g(\lambda_{IR})$ is the group velocity at the wavelength of the generated IR pulse. For

$LiNbO_3$, β is calculated as 400 fs/mm at λ_{IR}=1.43 μm. The interaction length l of the input pulses is limited by the aperture length l_a which is defined as,

$$l_a = (\pi)^{1/2} w_0/\rho, \qquad (2.1)$$

where w_0 is the Gaussian beam spot radius and ρ is the walk-off angle[2.13]. The walk-off angle of the optically damaged $LiNbO_3$ is calculated to be 3.9×10^{-2} rad (2.2°) at 1.43 μm as we will refer below. Taking w_0 =50 μm, the aperture length is 2.3 mm and the interaction length l of the input pulses is 2.3 mm. By using the values of β=400 fs/mm and l=2.3 mm, the pulse width of the generated IR pulse is roughly estimated to around 0.9 ps.

For $LiNbO_3$, the calculated values of group velocity dispersion (GVD) at 610 nm and 1.43 μm are 3.0 fs/nm mm and 0.14 fs/nm mm, respectively. These values are so small that the pulse broadening due to GVD is negligible at both wavelengths. Therefore, the pulse duration of the generated IR pulse is longer than the input visible pulse due to the group-velocity mismatch and is roughly estimated to around 0.9 ps. The measurement of the pulse width of the generated IR pulse is our future investigation by using a more sensitive autocorrelator than that used in the present experiment.

In the subpicosecond down-conversion with $LiNbO_3$ there is a problem of optical damage. The crystal burn density of $LiNbO_3$ is reported to be 50-140 MW/cm^2[2.14]. The $LiNbO_3$ crystal was optically damaged by the visible subpicosecond pulse in the present DFG experiment. This optical damage causes the visible light to diverge and also the beam quality to be decreased. When the $LiNbO_3$ crystal is illuminated by intense light, the extraordinary index of refraction in the illuminated region decreases by as much as 10^{-3}, while the change of the ordinary index is much smaller[2.15]. According to the Ref. 2.15, the effect is attributed to the drifting of photoexcited electrons

out of the illuminated region followed by their retrapping near the beam periphery. The space-charge field between these retrapped electrons and the positive ionized centers in the illuminated region causes the change of refractive indices via the electro-optic effect of the crystal.

In the present experiment, the visible pulse propagates in $LiNbO_3$ as an extraordinary ray, and the 1.064-μm pulse and the generated IR pulse propagate as ordinary rays. Thus, only the visible pulse is an extraordinary ray and is affected by the optically induced change of refractive index in $LiNbO_3$ caused by the visible subpicosecond pulse. In the present experiment, we estimate that the damage threshold of the $LiNbO_3$ crystal for the visible subpicosecond pulse is 100-200 MW/cm^2. When the power of the visible pulse was just above the damage threshold of the $LiNbO_3$ crystal, the optical damage grew with time. On the other hand, the damage reached its steady state as soon as the crystal was illuminated by intense visible pulses which we used in the present DFG experiments. The optical damage in the $LiNbO_3$ crystal was irreversible. The damage threshold of $LiNbO_3$ is lower than the other nonlinear crystals such as KTP or β-BaB_2O_4 (BBO). It is disadvantageous for nonlinear use that the damage threshold of $LiNbO_3$ is low.

Infrared pulses between 1.4 μm and 1.6 μm are obtained with an angle variation of 5° . Since the refractive index of $LiNbO_3$ is 2.2, the actual rotation angle is as large as 11° which is much larger than that for KTP. Therefore, a large realignment is required to change the IR wavelength from 1.4 μm to 1.6 μm.

Ultrashort pulses were also obtained in the BBO crystal by DFG. The input pulses into the nonlinear crystal were 75 mW, 260 fs pulses at 608 nm, and 6 W, 100 ps pulses at 1.064 μm. The phase-matching angle was 21.0° or

the pump pulse at 608 nm. The average power of the generated IR pulses at 1.42 μm was 50 μW at a repetition rate of 3.8 MHz.

Since the power of the generated IR pulse was below the sensitivity of the autocorrelator, an autocorrelation trace of the generated IR pulse could not be obtained. However, the generated IR pulse width is roughly estimated as follows. The group-velocity mismatch β is calculated to be 54 fs/mm at λ_{IR}=1.42 μm by using the Sellmeier equations of K. Kato.[2.16] Since β (= 54 fs/mm) is very small, the pulse width of the generated IR pulse can be estimated to be almost the same as the input visible pulse width after passing through the 5 mm long BBO crystal. For BBO, the calculated values of GVD at 608 nm and at 1.42 μm are 0.54 fs/nm mm and 1.6×10^{-3} fs/nm mm, respectively. These values are so small that the pulse broadening due to GVD is negligible.

The peak power of the generated IR pulse, P_{IR}, at the difference frequency is given in the small gain limit at phase matching as follows,

$$P_{IR} = \frac{\omega_{IR}^2 d_{eff}^2 l_{eff}^2 P_F P_{DYE}}{n_{IR} n_F n_{DYE} \varepsilon_0 c^3} \tag{2.2}$$

where P_{IR}, P_F and P_{DYE} are the peak powers in the crystal at the wavelengths of λ_{IR}, λ_F and λ_{DYE}, respectively. n_{IR}, n_F and n_{DYE} are the refractive indices at λ_{IR}, λ_F and λ_{DYE}, respectively. d_{eff} is the effective nonlinear coefficient and l_{eff} is the useful crystal length.

KTP is a positive biaxial crystal of orthorhombic symmetry class mm2, $d_{eff} \sim d_{24} \sin(\theta_{PM})$. Here, $d_{24} = 7.6\times10^{-12}$ m/v,[2.17] and θ_{PM}, the phase-matching angle at ϕ=0, is 76.9° at 614 nm. Therefore, $d_{eff} \sim 7.4\times10^{-12}$ m/v. $LiNbO_3$ is a negative uniaxial crystal of the triclinic symmetry class 3m, $d_{eff} \sim d_{31} \sin(\theta_{PM})$. Here, $d_{31} = (5.82\pm0.70)\times10^{-12}$ m/v [2.18] and the phase-matching angle θ_{PM} of the optically damaged $LiNbO_3$ is 60.4° at 610 nm. Therefore, d_{eff}

~ 5.1×10^{-12} m/v. This value is smaller than the value of d_{eff} for KTP, which is 7.2×10^{-12}m/v. BBO is a negative uniaxial crystal of trigonal symmetry class 3, $d_{eff} \sim d_{11} \cos(\theta_{PM})$. Here, $d_{11}=1.6 \times 10^{-12}$ m/v [2.19] and $\theta_{PM}=21.0^{\circ}$. Therefore, $d_{eff} \sim 1.5 \times 10^{-12}$ m/v and the value of d_{eff} for BBO is the smallest of the three.

The useful crystal length is limited mainly by two effects in generating femtosecond IR pulses by DFG. One is the Poynting vector walk-off or the aperture effect. The aperture length l_a is defined by, $l_a = (\pi)^{1/2} w_0/\rho$, where w_0 is the Gaussian beam spot radius and ρ is the walk-off angle. Calculated walk-off angles for KTP, BBO, and $LiNbO_3$ are shown in Figs. 2.5 and 2.6. For KTP, the walk-off angle is 2.3×10^{-2} rad at 1.45 μm. Taking w_0 =50 μm, l_a becomes 3.9 mm. The aperture length l_a is longer than the KTP crystal length of 3.4 mm. Therefore, the limitation of the useful crystal length by the aperture effect is negligible in this case.

The walk-off angle for BBO was calculated with the use of the Sellmeier equations of K. Kato[2.16], and was 5.1×10^{-2} rad at 608 nm. Taking w_0 =50 μm, l_a becomes 1.7 mm. The aperture length l_a is shorter than the BBO crystal length of 5 mm. Therefore, the useful crystal length is limited to 1.7 mm by the aperture effect. For $LiNbO_3$, the walk-off angle of $LiNbO_3$ is 3.8×10^{-2} rad (2.2°) at 1.43 μm. When $LiNbO_3$ is optically damaged and the extraordinary refractive index decreases by 1.2×10^{-3} [2.15], the walk-off angle is 3.9×10^{-2} rad (2.2°) at 1.43 μm. Taking w_0 =50 μm, the aperture length for the optically damaged $LiNbO_3$ crystal is 2.3 mm and the useful crystal length is limited to 2.3 mm by the aperture effect.

Another limitation on the useful crystal length lies in the group-velocity mismatch between the pump pulse and the generated IR pulse in the crystal. In this case, group-velocity mismatch between the pump pulse and the 1.064-μm pulse is less important for determining the useful crystal length, because

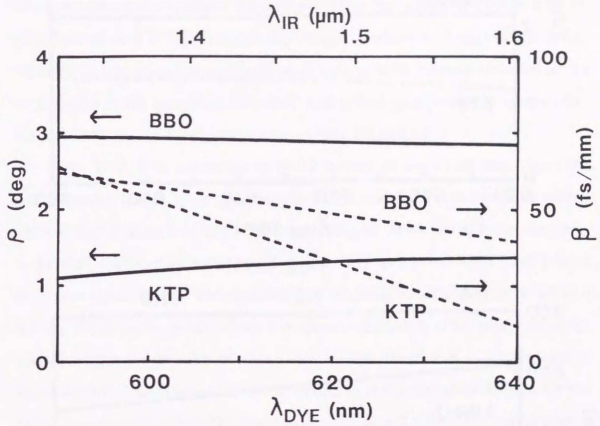

Fig. 2.5. Calculated walk-off angles ρ (solid lines) and group-velocity mismatches β (dashed lines) of KTP and β-BaB_2O_4 (BBO) crystals as a function of dye laser wavelength.

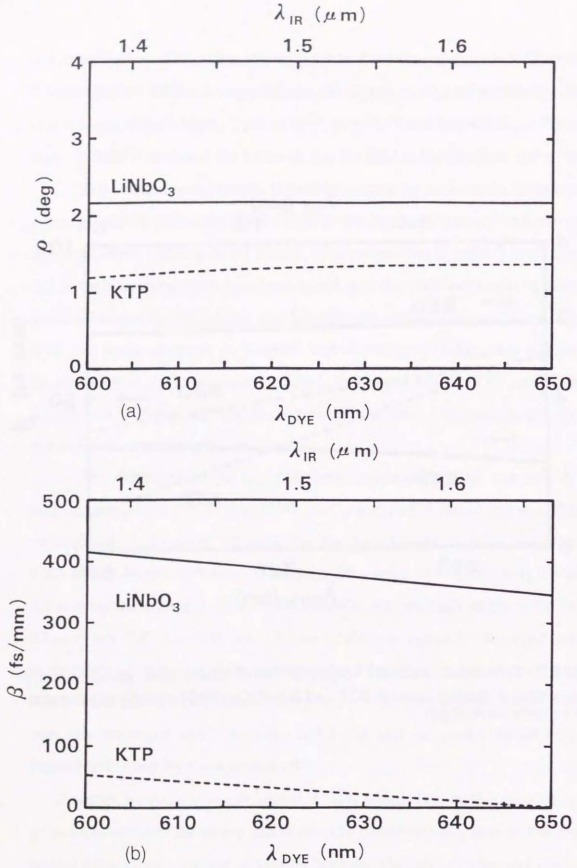

Fig. 2.6. (a)Calculated walk-off angles ρ of $LiNbO_3$ (solid line) and KTP (dashed line) crystals as a function of dye laser wavelength. (b)Calculated group-velocity mismatches β of $LiNbO_3$ (solid line) and KTP (dashed line) crystals as a function of dye laser wavelength.

the pulse width of the 1.064-μm pulse is 100 ps and is much longer than the pulse width of the visible pump pulse. The useful crystal length l_{eff} is limited by[2.4],

$$l_{eff} \leqq l_\beta \, (= \tau/\beta), \tag{2.3}$$

where τ is the pulse width of the pump and β is the group velocity mismatch. β is defined as $\beta = |v_g^{-1}(\lambda_{DYE}) - v_g^{-1}(\lambda_{IR})|$, where $v_g(\lambda_{DYE})$ is the group velocity at the pump wavelength and $v_g(\lambda_{IR})$ is the group velocity at the wavelength of the generated IR pulse. Calculated group-velocity mismatches for KTP, BBO, and $LiNbO_3$ are shown in Figs. 2.5 and 2.6.

For KTP, β is calculated to be 39 fs/mm at λ_{IR} =1.45 μm. Then the useful crystal length l_β is calculated to be 3.3 mm for the pump pulse with τ =129 fs, and is almost equal to our crystal length. Since the aperture length l_a is 3.9 mm, the useful crystal length l_{eff} for KTP is 3.3 mm. For BBO, β is 54 fs/mm at λ_{IR}=1.42 μm. The useful crystal length l_β is calculated to be 4.8 mm for the 260-fs pump pulse. Since the aperture length l_a is 1.7 mm, the useful crystal length l_{eff} is 1.7 mm. For $LiNbO_3$, β is calculated as 400 fs/mm at λ_{IR}=1.43 μm. Then the useful crystal length l_β is calculated as 0.5 mm for the 190-fs pump pulse. Since the aperture length l_a is 2.3 mm, the useful crystal length l_{eff} is 0.5 mm.

By using Eq. (2.2) with the value of the useful crystal length l_{eff} discussed above, the generated IR power can now be calculated. Calculated ratio of the IR power for KTP and for $LiNbO_3$ gives $P_{IR}(LiNbO_3)/P_{IR}(KTP) = 7.1 \times 10^{-3}$. The experimental value was estimated to be 1.1×10^{-3}. The large difference between the calculated ratio and the experimental one may be mainly due to the optical damage of the $LiNbO_3$ crystal. $LiNbO_3$ is less suitable than KTP for DFG with femtosecond pulses, because of the large

value of the group velocity mismatch β and the low threshold power of the optical damage.

Calculated ratio of the IR power for KTP and for BBO gives P_{IR} (BBO)/P_{IR} (KTP) =7.7×10^{-3}. The experimental value was estimated to be 6.0×10^{-3} and was almost the same as the calculated value. In the case of BBO, d_{eff} for BBO is about 1/5 of that for KTP and l_{eff} for BBO is about 1/2 of that for KTP. Hence, the power of the generated IR pulse with BBO is much smaller than that with KTP because the output peak power is proportional to $(d_{eff} \times l_{eff})^2$, as shown in Eq. (2.2).

2.4 Conclusion

Tunable subpicosecond infrared pulses have been generated in the 1.4-1.6 μm region by mixing a 1.06 μm Nd:YAG laser pulse and a visible subpicosecond pulse from a cavity dumped, synchronously pumped dye laser.

Three kinds of nonlinear crystal, KTP, $LiNbO_3$, and β-BaB_2O_4(BBO) were used for DFG. It is found that KTP is the most suitable crystal of the three for femtosecond DFG. Pulses as short as 94 fs with a peak power of 8.4 kW have been obtained with a KTP crystal at a rate of 3.8 MHz.

Because of the large value of the group velocity mismatch β and the low threshold of the optical damage, $LiNbO_3$ is less suitable than KTP for DFG with femtosecond pulses. However, $LiNbO_3$ is a suitable crystal for DFG with ps pulses, because the value of d_{eff} for $LiNbO_3$ is almost as large as that for KTP and the cost of the $LiNbO_3$ crystal is lower than that of the KTP crystal.

BBO is a less suitable nonlinear crystal than KTP for femtosecond difference frequency generation because of the smaller effective nonlinear coefficient d_{eff} and the larger walk-off angle ρ than those for KTP.

References

[2.1] P. Beaud, B. Zysset, A. P. Schwarzenbach, and H. P. Weber, "1.3-μm subpicosecond pulses from a dye laser pumped by compressed Nd:YAG-laser pulses," Opt. Lett., vol. 11, p. 24, 1986.

[2.2] F. M. Mitschke and L. F. Mollenauer, "Ultrashort pulses from the soliton laser," Opt. Lett. vol. 12, p. 407, 1987.

[2.3] D. S. Moore and S. C. Schmidt, "Tunable subpicosecond infrared pulse generation to 4 μm," Opt. Lett. vol. 12, p. 480, 1987.

[2.4] I. Ledoux, J. Badan, J. Zyss, A. Migus, D. Hulin, J. Etchepare, G. Grillon and A. Antonetti, "Generation of high-peak-power tunable infrared femtosecond pulses in an organic crystal: application to time resolution of weak infrared signals," J. Opt. Soc. Am. vol. B4, p. 987, 1987.

[2.5] J. H. Glownia, J. Misewich and P. P. Sorokin, "Subpicosecond time-resolved infrared spectral photography," Opt. Lett. vol. 12, p. 19, 1987.

[2.6] A. Mokhtari, L. Fini, and J. Chesnoy, "Efficient frequency mixing of a cw femtosecond laser synchronously pumped by a frequency doubled Nd:YAG laser," Opt. Commun. vol. 61, p. 421, 1987.

[2.7] K. Kurokawa and M. Nakazawa, "Femtosecond 1.4-1.6 mm infrared pulse generation at a high repetition rate by difference frequency generation," Appl. Phys. Lett. vol. 55 p. 7, 1989.

[2.8] Q. Fu, G. Mak, and H. M. van Driel, "High-power, 62-fs infrared optical parametric oscillator synchronously pumped by a 76-MHz Ti:sapphire laser," Opt. Lett. vol. 17, p. 1006, 1992; see also, W. S. Pelouch, P. E. Powers, and C. L. Tang, "Ti:sapphire-pumped, high-repetition-rate femtosecond optical parametric oscillator," Opt. Lett. vol. 17, p. 1070, 1992.

[2.9] M. Nakazawa, T. Nakashima, H. Kubota, and S. Seikai, "55 kW, 240 fs pulse generation from a cavity dumped, synchronously pumped dye laser and

its application to pulse compression," Appl. Phys. Lett. vol. 51, p. 728, 1987; see also K.Kurokawa, H.Kubota, and M.Nakazawa, "48 fs, 190 kW pulse generation from a cavity dumped, synchronously pumped dye laser," Opt. Commun. vol. 68, p. 287, 1988.

[2.10] H. Vanherzeele, J. D. Bierlein, and F. C. Zumsteg, "Index of refraction measurements and parametric generation in hydrothermally grown $KTiOPO_4$," Appl. Opt., vol. 27, p. 3314, 1988.

[2.11] A. M. Weiner, "Effect of group velocity mismatch on the measurement of ultrashort optical pulse via second harmonic generation," IEEE J. Quantum Electron. vol. QE-19, p. 1276, 1983.

[2.12] M. V. Hobden and J. Warner, "The temperature dependence of the refractive indices of pure lithium niobate," Phys. Lett. vol. 22, p. 243, 1966.

[2.13] G. D. Boyd, A. Ashkin, J. M. Dziedzic, and D. A. Kleinman, "Second-harmonic generation of light with double refraction," Phys. Rev. A vol. 137, p. 1305, 1965.

[2.14] R. L. Byer, in: Quantum Electronics: a Treatise, eds. H. Robin and C.L. Tang, (Academic Press, New York, 1975).

[2.15] F. S. Chen, "Optically induced change of refractive indices in $LiNbO_3$ and $LiTaO_3$,"J. Appl. Phys. vol. 40, p. 3389, 1969.

[2.16] K. Kato, "Second-harmonic generation to 2048 $\mathring{A}$ in β-BaB_2O_4," IEEE J. Quantum Electron. vol. QE-22, p. 1013, 1986.

[2.17] F. C. Zumsteg, J. D. Bierlein, and T. E. Gier, "$K_xRb_{1-x}TiOPO_4$: a new nonlinear optical material," J. Appl. Phys. vol. 47, p. 4980, 1976.

[2.18] M. M. Choy and R. L. Byer, "Accurate second-order susceptibility measurements of visible and infrared nonlinear crystals," Phys. Rev. B vol. 14, p. 1693, 1976.

[2.19] D. Eimerl, L. Davis, S. Velsko, E. K. Graham, and A. Zalkin, "Optical, mechanical, and thermal properties of barium borate," J. Appl. Phys. vol. 62, p. 1968, 1987.

CHAPTER III. AMPLIFICATION CHARACTERISTICS OF A FEMTOSECOND SOLITON IN AN ERBIUM-DOPED OPTICAL FIBER AMPLIFIER (EDFA)

3.1 Introduction

Recent progress on erbium-doped fiber amplifiers (EDFA) has been very rapid since they show a great potential for opening a new field in high-speed optical communication[3.1-3]. Their typical advantages are a high gain of more than 30 dB at a 1.5 μm region, low noise, wide bandwidth, polarization insensitive gain, and high saturation output power. Among these excellent characteristics, the wideband property, greater than 30 nm, is very useful not only for high speed communication, but also for amplifying ultrashort pulses including optical solitons.

Nakazawa et al. have reported picosecond (9~20 ps) ~ subpicosecond (0.7~0.9 ps) soliton amplification using EDFAs[3.4-5], in which the soliton period was much longer than the length of the EDFA (3~5 m) and the peak power of the amplified pulse reached as high as 96 W. It should be noted that the EDFA gain is determined by the average input power, not by the peak power, since the gain recovery time is of the order of milliseconds. Zhu et al. reported the application of an erbium-doped fiber to the coupled-cavity mode locking of a KCl:Ti femtosecond laser[3.6], and Ainslie et al.[3.7] and Khrushchev et al.[3.8] reported the amplification of femtosecond soliton pulses. Dianov et al. reported the change in the frequency spectrum of the amplified femtosecond soliton as the pulse propagates down the EDFA, in which the center wavelength of the soliton pulse was set at the 1.54 μm region[3.9]. If the full bandwidth of approximately 30 nm can be utilized, a 100 fs pulse could be amplified.

In this chapter, we describe amplification characteristics of femtosecond pulses under various pumping conditions for EDFAs[3.10-12]. Section 3.2 shows that a femtosecond pulse can be amplified in an EDFA. Section 3.3 describes adiabatic and nonadiabatic amplification characteristics of a femtosecond soliton in an EDFA. Adiabatic soliton narrowing occurs due to the optical gain. By increasing the pump power to the EDFA a considerable soliton narrowing takes place with the soliton self-frequency shift (SSFS)[3.13] which is enhanced by the gain narrowing effect. In section 3.4, wavelength-dependent amplification characteristics of a femtosecond soliton are described. And we show our conclusion of chapter III in section 3.5.

3.2 Amplification Characteristics of Femtosecond Pulses in an EDFA

Figure 3.1 shows the experimental setup. Femtosecond infrared pulses in the 1.5 μm region are generated by using difference frequency mixing in a KTP crystal as shown in chapter II. The pulse repetition rate is 3.8 MHz and the output pulse has a width of 250 fs with peak powers of 2 ~ 4 kW.

These femtosecond pulses are coupled into an EDFA through a 1.48 μm/1.55 μm WDM fiber coupler. The EDFA is pumped by InGaAsP laser diodes[3.14]. The length of the erbium fiber is 3~5 m and the doping concentration of erbium ions is 1900 ppm. Al_2O_3 with a concentration of 500 ppm was co-doped to increase optical gain bandwidth. Figure 3.2 shows the absorption spectrum of the erbium fiber. As shown in Fig. 3.2, there are two peaks at 1.534 μm and 1.550 μm which correspond to the transitions between the Stark components of the $^4I_{15/2}$ and $^4I_{13/2}$ manifolds as described in Sec. 1.3.2. The optical loss was 8.9 dB/m at 1.552 μm. The zero group velocity dispersion, spot size, and cut-off wavelength are 1.45 μm, 3.5 μm, and 1.28 μm, respectively. Since the group velocity dispersion at 1.552 μm is 6.4 ps/km nm,

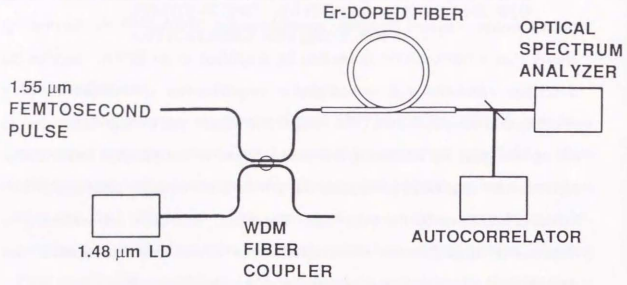

Fig. 3.1 Experimental setup for femtosecond pulse amplification in an erbium-doped fiber amplifier (EDFA).

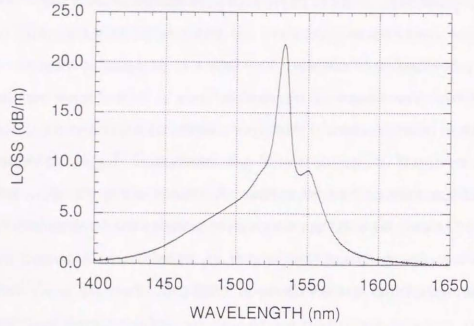

Fig. 3.2 Absorption spectrum of an erbium-doped optical fiber.

the N=1 soliton peak power for 250 fs input is approximately 120 W, which can be easily generated by the present difference frequency mixing technique. The pulse width and the spectrum of the amplified output solitons are monitored using an autocorrelator with a resolution of less than 100 fs and a spectrum analyzer.

When erbium fibers about 100 m long with a doping concentration of 100 ppm or 20 m long with a concentration of 470 ppm are used for the EDFA, the self-frequency shift becomes quite large and the continuum spectrum broadens to 1.75 μm from 1.55 μm. In this case, the spectral component of the soliton has already moved outside the EDFA gain profile, so high gain is not obtained. The key to achieving efficient femtosecond pulse amplification is to use a shorter erbium fiber with a relatively high doping concentration of between 1000 ppm and 2000 ppm.

Gain characteristics for 266 fs input pulses are shown in Fig. 3.3. The peak power of the pulse and the repetition rate are 31 W and 3.8 MHz. The average input power was 30 μm (-15.2 dBm). Figure 3.3(a) is the input spectrum and (b) is the output spectrum at a pump power of 20 mW for the EDFA. (c) and (d) are input and output pulse waveforms corresponding to (a) and (b), respectively. It should be noted that one division is 206 fs in (c) and 323 fs in (d). In trace (a), the center wavelength of the pulse is 1.551 μm which is one of the EDFA gain peaks. The spectral width $\Delta\lambda$ is 10.3 nm and the FWHM of the pulse waveform from (c) is 266 fs. Hence, the pulse width-bandwidth product, $\Delta\tau\Delta\nu$, is 0.32~0.34, which means that the pulse is a transform-limited sech waveform.

From trace (b), the input pulse was successfully amplified and a gain of 9 dB was obtained for a pump power of 20 mW. The amplified spectrum is accompanied by a small pedestal in the shorter wavelength region around

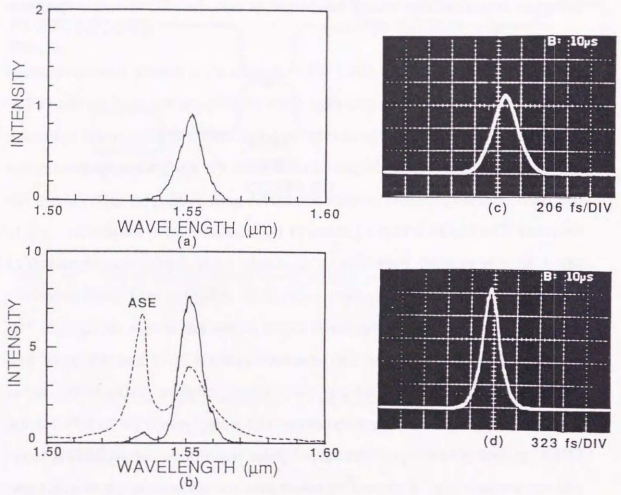

Fig. 3.3 Gain characteristics of EDFA for 266 fs input pulses at 1.551 μm. (a) is the input spectrum of the 266 fs pulse and (b) is the spectrum of the amplified pulse. (c) and (d) are the corresponding input and output waveforms, respectively.

1.535 μm, which is due to the existence of a gain peak at that wavelength in the EDFA. It is also noted that the spectral width of the output pulse is 9.3 nm which is a little narrower than that of the input pulse. This is attributed to the fact that the EDFA has a parabolic gain profile at around 1.552 μm, so that the input spectral profile is modified when it is amplified. For convenience, an amplified spontaneous emission (ASE) profile is shown in (b) by a dashed line. According to trace (b) and output photo (d), $\Delta\tau\Delta\nu$ is equal to 0.31 ~ 0.32, which means that the output pulse is a transform-limited sech pulse. When a non-transform-limited pulse with a broader spectral width and the same pulse width is coupled into the EDFA, the output pulse also remains at 250 fs and the spectral width is limited around 9~10 nm. These results indicate that a strong spectral shaping exists at around 1.552 μm, so that non-transform-limited pulses can be converted into transform-limited pulses by active spectral windowing.

Here, we discuss the soliton property of the input pulse. The group velocity dispersion (GVD) at 1.552 μm is 6.4 ps/kmnm and the pulse width of 266 fs gives an N=1 soliton peak power, $P_{N=1}$, of 120 W and a soliton period, Z_{sp}, of 4.4 m. Since the gain is 9 dB for an input peak power of 31 W, this produces output pulses with a peak power of about 260 W. Based on a gain coefficient of 3 dB/m (9 dB gain for an erbium fiber length of 3 m), N=1 soliton is excited at around 2 m from the fiber end. This means that the EDFA can amplify femtosecond soliton pulses. When the pump power is further increased, the SSFS appears and the carrier wavelength of the input soliton starts to move toward a longer wavelength region, so that the gain can not be measured exactly.

Figure 3.4 shows the gain spectrum of the erbium doped fiber at the pump power of 25 mW, where the input signal is a cw beam emitted from a

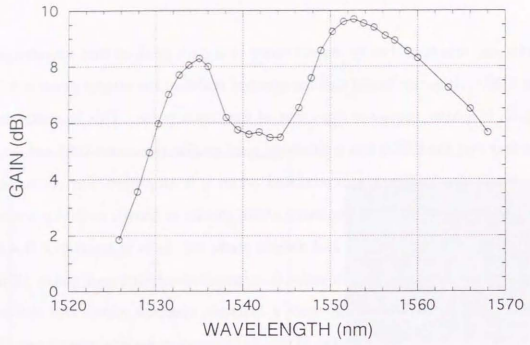

Fig. 3.4 Gain spectrum of a 3 m-long EDFA. The input signal is a cw beam emitted from a single-wavelength laser diode. The pump power is 25 mW and the input signal power is -15.2 dBm.

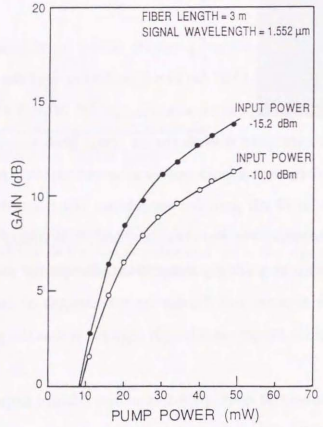

Fig. 3.5 Changes in EDFA gain at 1.552 μm as a function of pump power. The input signal is a cw beam emitted from a single-wavelength laser diode.

single-wavelength laser diode and the input signal power was -15.2 dBm. The gain bandwidth around 1.55 μm is about 18 nm which is large enough to amplify the 266 fs pulse. Figure 3.5 shows gain changes at 1.552 μm of the EDFA as a function of pump power, where the input signal is a cw beam emitted from a single-wavelength laser diode. As seen, the gain for an average input power of -15.2 dBm is about 8.5 dB for a pump power of 20 mW, which corresponds to the condition of the present femtosecond pulse amplification. If the pulse repetition rate is of the order of 100 Hz, the gain will be greatly increased since the gain recovery time of the erbium ions is of the order of milliseconds. When the repetition rate is larger than a few hundred kHz, the characteristics can be completely described by the average input power. For an average input power of - 10 dBm (0.1 mW ave.), the gain for a pump power of 20 mW decreases to 6.5 dB, which is due to gain saturation.

In summary, we have shown that the femtosecond pulses can be amplified in an erbium-doped optical fiber amplifier. A gain of 9 dB has been obtained for input pulses with a peak power of 30 W, an average power of 30 μW (-15.2 dBm), and a pulse width of 260 fs.

3.3 Adiabatic and Nonadiabatic Amplification of a Femtosecond Optical Soliton

Changes in the pulse width of the output soliton and nonsoliton pulses as a function of the pump power are given in Fig. 3.6, where the symbols ● , □, and ○ correspond to the peak powers (the average powers) of 30 W (27 μW), 55 W (50 μW), and 219 W (200 μW), respectively. The input pulse width was 240 fs, the erbium fiber length was 3 m and the center wavelength of the input pulse was 1.557 μm. A pulse width of 240 fs and a

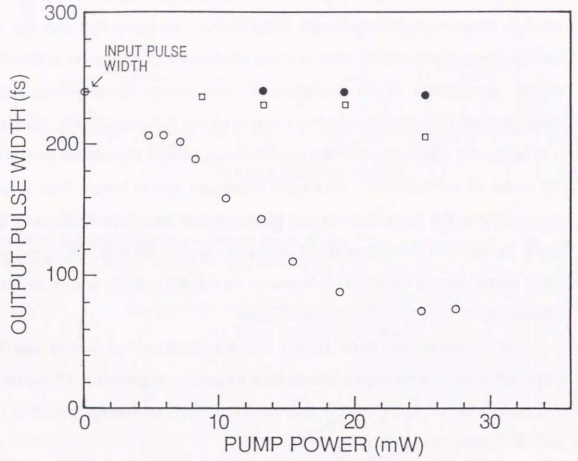

Fig. 3.6 Changes in output soliton width as a function of the EDFA pump power. The input pulse width was 240 fs. For pump powers smaller than 5 mW, the EDFA acts as a loss medium, so that the output power is too small to measure the pulse width with an autocorrelator. Symbols ●, □, and ○ correspond to the peak powers (the average powers) of 30 W (27 μW), 55 W (50 μW), 219 W(200 μW), respectively.

GVD of 6.8 ps/kmnm at 1.557 μm give an N=1 soliton peak power of 140 W and a soliton period, Z_{sp}, of 3.3 m. When the input peak power was as low as 30 W (●) which corresponded to an N=0.46 soliton, no pulse shortening or pulse spectrum changes occur, although the EDFA gain for an average input power of 27 μW was 9 dB for a pump power of 25 mW. This is because the propagation distance as a N=1 soliton was too short in the erbium fiber. When the input peak power was 55 W (□) which corresponded to an N=0.63 soliton, a small amount of soliton narrowing from 240 fs to 206 fs was observed, since the peak power of the propagating pulse was already in the N=1 soliton power regime.

Drastic changes in the output pulse width were observed for an input peak power of 219 W (○), corresponding to an N=1.2~1.3 soliton. The soliton width decreases linearly with an increase in the pump power (the optical gain). When the average input power for the soliton input was 200 μW (- 7 dBm), the gain was approximately 5 dB (a gain coefficient of 1.67 dB/m) for a pump power of 19~20 mW because of gain saturation. When the pump power was 20~24 mW, the pulse narrowing stopped and the pulse width was 74 fs. With a slow scan autocorrelator, the value of 74 fs measured in the fast scan mode was estimated to be 60 fs. It is clearly seen in Fig. 3.6 that adiabatic soliton narrowing occurs with an increase in the gain as long as the gain is moderate.

Figure 3.7 and 3.8 show how the spectrum and the waveform of the output soliton pulse change for the symbol ○ shown in Fig. 3.6. The dashed profile in Fig. 3.7(a) is the spectral profile of the 240 fs input soliton pulse with a center wavelength of 1.557 μm. The FWHM of the spectrum was 12.7 nm and the $\Delta\nu\Delta\tau$ product of the input pulse was 0.37. Waveform of the input soliton is shown in Fig. 3.8(a-1). The pulse width became 203 fs for an EDFA

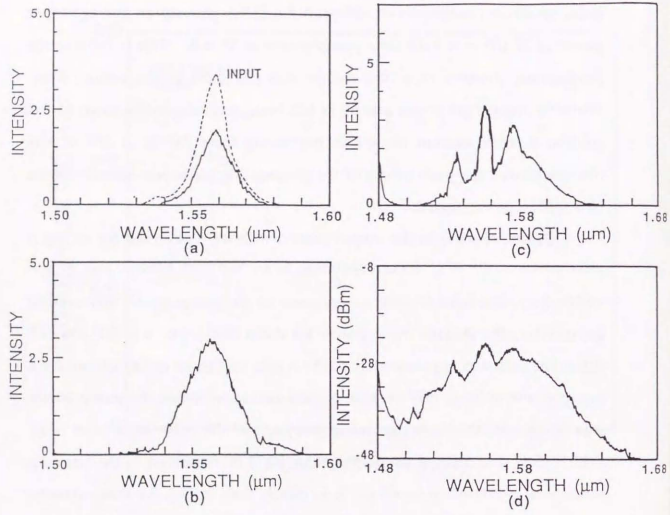

Fig. 3.7 Adiabatic soliton narrowing and enhanced soliton self-frequency shift controlled by the pump power to the EDFA. (a)~(c) are output spectra for pump powers of 7.2 mW, 13.2 mW, and 25 mW, respectively. The dashed curve in (a) is the spectral profile of an input soliton. The spectrum shown in (c) is log-transformed into (d).

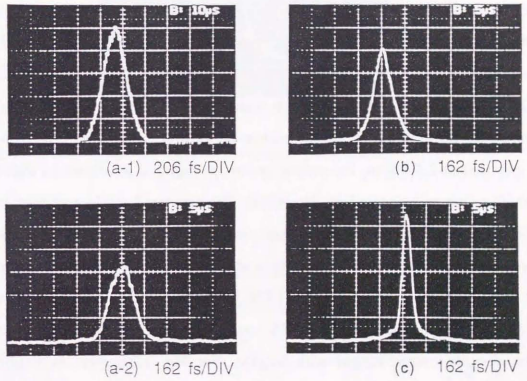

Fig. 3.8 Adiabatic soliton narrowing and enhanced soliton self-frequency shift controlled by the pump power to the EDFA. Photo (a-1) is an input soliton pulse. Photos (a-2)~(c) correspond to output spectra Fig. 3.4(a)~(c), respectively.

pump power of 7~7.5 mW where the gain was zero, indicating the pump threshold. In this case, the spectrum broadened to 13.5 nm as shown by the solid line in Fig. 3.7(a), where $\Delta\nu\Delta\tau$ was 0.34. The waveform of the output soliton is shown in Fig. 3.8(a-2). This pulse shortening is due to an excitation of the N=1.2~1.3 soliton. By increasing the pump power to 13 mW, corresponding to a gain coefficient of 0.83 dB/m, the output soliton width shortened to 142 fs as shown in Fig. 3.6 and the spectrum broadened to 21.3 nm as shown in Fig. 3.7(b). The waveform of the output soliton is shown in Fig. 3.8(b). Here, $\Delta\nu\Delta\tau$ was 0.37, which means that the output pulse was almost transform-limited. For a pump power of 25 mW, corresponding to a gain coefficient of 2.3 dB/m, the output spectrum changed as shown in Fig. 3.7(c), which is log-transformed in Fig. 3.7(d). The spectral broadening observed in Fig. 3.7(b) disappeared. The spectrum component at 1.557 μm is rather less and two new peaks have appeared; One is at 1.535 μm which is another gain peak of the EDFA and the other is at 1.576 μm which is due to the soliton self-frequency shift (SSFS). The SSFS causes a shift of the soliton carrier wavelength toward longer wavelengths. For Fig. 3.7(c), the corresponding pulse width was 60 fs in a slow scan mode. Fig. 3.8(c) shows the waveform of the output. Such a pulse compression is of considerable practical importance as it can be used to amplify and compress femtosecond pulses simultaneously. When the pump power was further increased, pedestal components appeared on the wing of the amplified soliton pulse as shown in Fig. 3.9 and a further shift of the spectrum due to the SSFS was observed. However, no further pulse shortening was observed.

An interesting feature exists in the transition process between Fig. 3.7(b) and Fig. 3.7(c). The physics behind Fig. 3.7(b) can be explained by the adiabatic soliton narrowing. When the gain is less than a few dB, the system

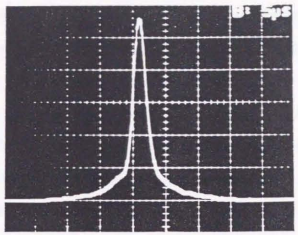

Fig. 3.9 Autocorrelation trace of the output pulse for a pump power of 28 mW.

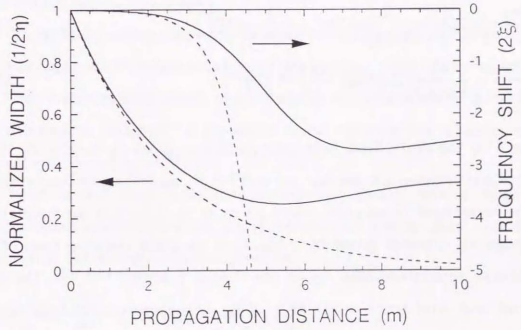

Fig. 3.10 Transient behavior of the trapped soliton with adiabatic narrowing. Changes in soliton width and frequency as a function of distance (Perturbation theory).

is adiabatic, where the soliton pulse narrows adiabatically without the red shift of the spectrum due to the SSFS. In Fig. 3.7(c), the EDFA gain of 7 dB no longer acts adiabatically, so that the input soliton amplitude is simply increased and the pulse compression due to the nonlinear effect exceeds the pulse broadening due to the GVD, resulting in a further shortening of the pulse width. The situation is in another words the excitation of higher-order solitons which cause large pulse compression[3.15] as shown in section 1.2. In this case, the SSFS occurs strongly because of the considerable shortening of the pulse width even if the EDFA gain is bandwidth limited.

Using the perturbation theory for the N=1 soliton[3.17] as a rough analysis at the first step, the soliton intensity (or inverse of the width) 2η and the frequency shift 2ξ for a perturbed soliton with gain and SSFS can be described as[3.17,18]

$$\frac{d(2\eta)}{dq} = 2\eta 2G\left[1 - \frac{1}{3(\omega_g\tau_0)^2}(2\eta)^2 - \frac{1}{(\omega_g\tau_0)^2}(2\xi)^2\right] \tag{3.1}$$

$$\frac{d(2\xi)}{dq} = -\left[\frac{4G}{3(\omega_g\tau_0)^2}(2\eta)^2(2\xi) + \frac{8}{15}\left(\frac{\tau_n}{\tau_0}\right)(2\eta)^4\right]. \tag{3.2}$$

Here, G is the normalized field gain coefficient given by $G=gZ_0$, Z_0 is the normalized distance, g is the gain per unit length, ω_g is the gain bandwidth, τ_0 is the normalized input pulse width given by $\tau_{in}/1.76$, q is the normalized propagation distance given by z/Z_0, τ_n is the finite response time of the nonlinear refractive-index n_2 or the Raman process[3.17,3.13]. The first, second, and third terms in the r.h.s. of Eq. (3.1) represent adiabatic soliton narrowing, gain decrease due to the gain dispersion, and gain decrease due to the soliton frequency shift, respectively. The first and second terms in Eq. (3.2) are the frequency pulling effect toward the center of the gain bandwidth and

the SSFS. It has been shown that the soliton pulse has a steady-state carrier wavelength which satisfies $d\xi/dz=0$[3.17,18]. In addition, from Eq. (3.1), there exists a steady-state soliton amplitude caused by balancing the adiabatic gain narrowing and the gain dispersion with the SSFS. The pulse width change ($1/2\eta$) and the frequency change 2ξ as a function of the distance are given in Fig. 3.10 by solving Eqs. (3.1) and (3.2), where τ_{in}=250 fs, D=5 ps/kmnm, Z_0=3.16 m, $\omega_g\tau_0$=3, $\tau_n/\tau_0=4\times10^{-2}$, g=0.19 m^{-1} (~5 dB for 3 m), and $G=gZ_0$=0.6. As can be clearly seen a steady state $1/2\eta$ and 2ξ exist when the soliton propagates down the erbium fiber. The dashed lines in Fig. 3.10 show the changes in the pulse width and the frequency when the gain is independent of the frequency, that is, a flat gain. As can be seen, the pulse width decreases monotonously and the frequency strongly shifts toward longer wavelengths by the SSFS. These numerical results indicate that bandwidth-limited amplification can suppress the soliton self-frequency shift.

At 3.0 m, soliton narrowing to about $0.37\tau_{in}$ and a frequency shift of 2ξ= – 0.26 occur, which means a frequency change $\delta\omega=0.09\omega_g$. Since τ_{in} is 250 fs, $0.37\tau_{in}$ becomes 93 fs which roughly agrees with the 80~90 fs output pulse width that we observed. It should be noted that complete adiabatic soliton narrowing occurs when G << 1.

It is not clear from the perturbation theory how a large gain nonadiabatically modifies the input solitons. To analyze this, a perturbed nonlinear Schrödinger equation given by

$$(-i)\frac{\partial u}{\partial q} = \frac{1}{2}\frac{\partial^2 u}{\partial s^2} + |u|^2 u - iG\left[u + \frac{1}{(\omega_g\tau_0)^2}\frac{\partial^2 u}{\partial s^2}\right] - \frac{\tau_n}{\tau_0}u\frac{\partial}{\partial s}|u|^2 \tag{3.3}$$

was computer-run. The output soliton width as a function of the optical gain is given in Fig. 3.11. Here A=1.0 and 1.2, the fiber length is 3.0 m and other parameters are the same as those in Fig. 3.10. As shown in Fig. 3.11, for the A=1.2 soliton input, the pulse shortening is offset, as is well known from the initial value problem of the nonlinear Schrödinger equation[3.16]. For a gain of 5 dB (1.67 dB/m, 3 m) at A=1.2, the pulse narrowing is approximately 1/2.6 of the input soliton, which agrees with our experimental result shown in Fig. 3.6.

The corresponding spectrum changes for the A=1.2 soliton are shown in Fig. 3.12(a)~(d), where (a)~(d) refer to g=1.0 dB/m, 1.5 dB/m, 2.0 dB/m, and 2.5 dB/m, respectively. The dashed profile is the input spectrum of the soliton and the FWHM of the input spectrum is 1/3 of the gain bandwidth. In Fig. 3.11 and 3.12(a), the adiabatic narrowing of the soliton is clearly seen, in which the center frequency of the soliton does not change. It should be noted that a propagation distance of 3 m is comparable to the soliton period. The gain of 2 dB/m for 3 m shown in Fig. 3.12(c) produces G=0.73, which means that the condition is no longer adiabatic. Here the nonadiabatic gain contribution becomes larger, resulting in the further shortening of the soliton and the large frequency shift due to the SSFS. That is why small humps appear on the wing of the spectrum in Fig. 3.12(c). Figure 3.13 shows the linear plot of Fig. 3.12(c). As can be seen in Fig. 3.13 which corresponds to total gains of 6 dB, a numerical result qualitatively agrees with the corresponding experimental result shown in Fig. 3.7(c), although the center-peak wavelength in Fig. 3.13 is 1.55 μm because the input signal is 1.55 μm in numerical calculation.

Figures 3.14 shows the evolution of a soliton in the range z=0~4 m for an amplifier gain of 2.5 dB/m. In the range z=0~3 m the most noteworthy feature of Fig. 3.14 is the pulse compression. The pulse width is reduced by

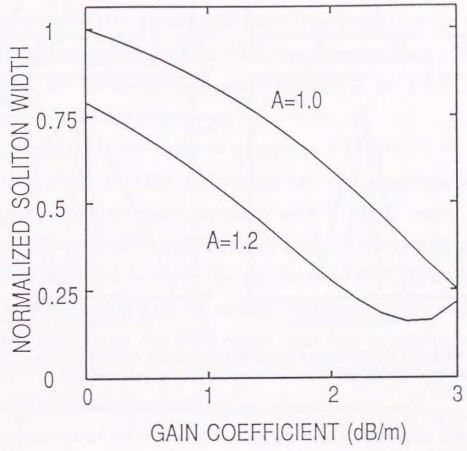

Fig. 3.11 Transient behavior of the trapped soliton with adiabatic narrowing. Changes in output soliton width at 3 m as a function of the gain coefficient (Direct calculation of the nonlinear Schrödinger equation).

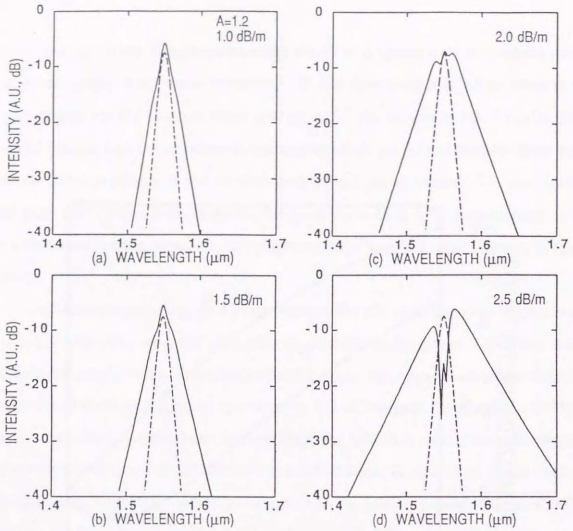

Fig. 3.12 Changes in the spectrum of the calculated output solitons. (a)~(d) refer to gain coefficients of 1.0, 1.5, 2.0, and 2.5 dB/m, respectively.

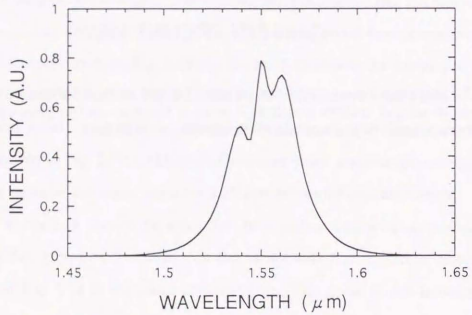

Fig. 3.13 Linear plot of the spectrum corresponding to Fig. 12 (c) refer to gain coefficients of 2.0 dB/m.

approximately a factor of 4.1 at z=3 m. Beyond z=3 m the pulse shifts to the right side, and a new pulse begins to form. The shift is due to the SSFS and results from a transfer of pulse energy toward longer-wavelength components that travel slower than the original pulse in the anomalous dispersion regime. Figure 3.15 shows the pulse spectra corresponding to the waveforms in Fig. 3.14. Considerable spectral broadening occurs beyond z=2.5 m. In the range z≥3m the large frequency-downshift due to the SSFS is observed, and the spectral component around 1.55 μm builds up which corresponds to the new pulse beyond z=3 m in Fig. 3.14.

According to the numerical analysis by G. Agrawal[3.19], when the amplifier gain is very large, for example, 20 dB per dispersion length, the input pulse splits into many subpulses, each of which evolves toward a chirped solitary wave[3.20] with a width of $T_2/\sqrt{3}$. In this case the generation of many subpulses is caused by the gain dispersion[3.19]. In an experiment with a net gain of 21.5 dB the autocorrelation trace of the output pulse indicated splitting of the 180-fs input pulse into at least five separate pulses[3.8] as shown in Fig. 3.16, which qualitatively agrees with the numerical analysis by G. Agrawal.

In summary, we have shown adiabatic and nonadiabatic amplification characteristics of a femtosecond optical soliton in an EDFA. When the gain is moderate, we have experimentally observed adiabatic narrowing of a femtosecond fundamental soliton. By increasing the amplifier gain to nonadiabatic region, pulse compression by as much as a factor 4 has been observed by using 240-fs pulses. In this case the frequency of the soliton strongly shifts toward longer wavelength region outside the EDFA gain bandwidth. Therefore, when the gain is very high, the process of the femtosecond soliton amplification is stopped by the SSFS. It should be noted

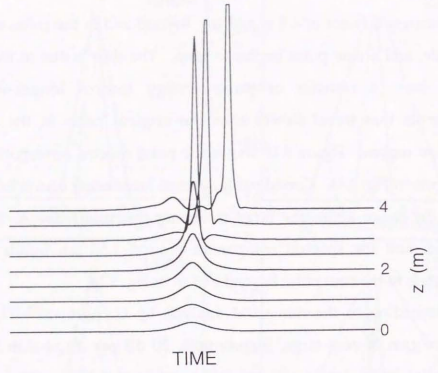

Fig. 3.14 Evolution of a calculated soliton waveform in the range z=0~4 m for an amplifier gain of 2.5 dB/m. The input pulse is an A=1.2 soliton with a pulse width of 250 fs.

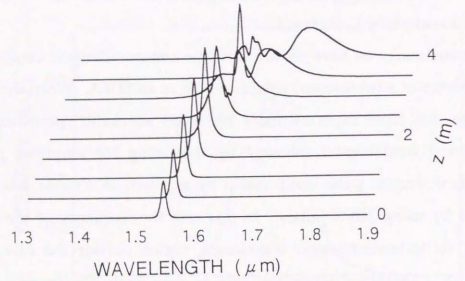

Fig. 3.15 Evolution of a calculated soliton spectrum corresponding to the waveforms in Fig. 3.14.

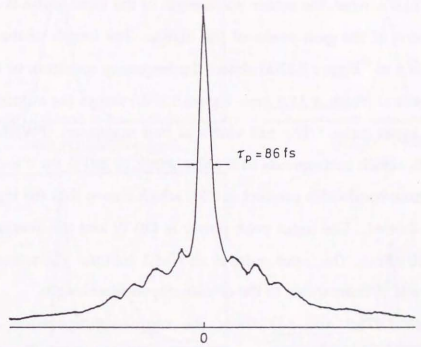

Fig. 3.16 Autocorrelation trace of the output pulse after 4 m of erbium-doped fiber amplifier where the optical gain is 21.5 dB. (after Ref. 3.8).

that we have to develop a method for suppressing the SSFS in order to realize strong amplification of femtosecond optical soliton.

3.4 Wavelength-Dependent Amplification Characteristics of a Femtosecond Optical Soliton in an EDFA

Figure 3.17 shows input and amplified output soliton characteristics through the EDFA when the center wavelength of the input pulse is 1.535 μm which is at one of the gain peaks of the EDFA. The length of the erbium-doped fiber is 5 m. Figure 3.17(a) shows the frequency spectrum of the input pulse. Its spectral width is 11.8 nm. Figure 3.17(b) shows the autocorrelation trace of the input pulse. The full width at half maximum (FWHM) of the trace is 320 fs, which corresponds to a pulse width of 210 fs for a sech^2 pulse shape. The time-bandwidth product is 0.31, which means that the input pulse is transform-limited. The input peak power is 120 W and the average power is 99 μW (- 10 dBm). The input pulse is an N=1.1 soliton. The soliton period Z_{sp} is 4.6 m and is comparable to the erbium-doped fiber length.

Figures 3.17(c) and (d) show the frequency spectrum and the autocorrelation trace of the output pulse when the pump power is 29 mW which corresponds to 7.3 dB gain at 1.535 μm. So the amplification process is nonadiabatic. Here the soliton self-frequency shift (SSFS) occurs and the soliton carrier wavelength is shifted to 1.56 μm. When this happens, the autocorrelation trace of the output pulse changes as shown in Fig. 3.17(d). The base line is shown by an arrow. The pulse width narrows to 80 fs and large pedestal components appear on the wings of the soliton pulse due to the fact that the spectral component has been split into two at 1.535 μm and 1.56 μm. The wing component in Fig. 3.17(d) could result from the amplification of the non-soliton component at 1.535 μm after the frequency downshift of

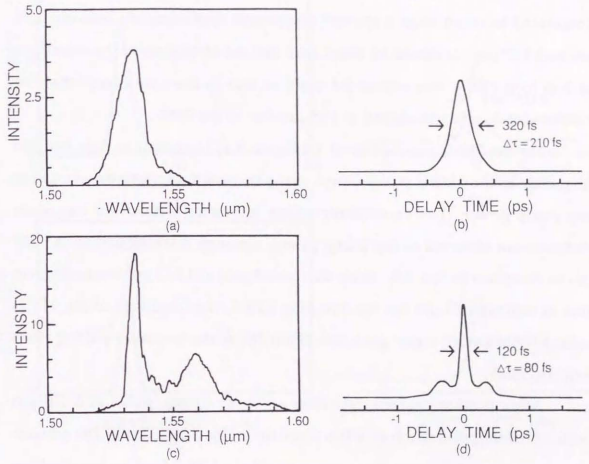

Fig. 3.17 Amplification characteristics of EDFA using 210 fs pulses at 1.535 μm.(a) is the input spectrum of the 210 fs pulse and (b) is the autocorrelation trace of the input pulse. (c) and (d) are the frequency spectrum and the autocorrelation trace of the output pulse. The base line is shown by an arrow. The fiber length is 5 m.

the input soliton due to the SSFS. This situation is considered to be similar to the soliton pulse evolution at 1.55 μm numerically shown in Figs. 3.14 and 3.15. When an 80 fs pulse at 1.56 μm with a $sech^2$ pulse shape is transform-limited, its spectral width is 32 nm. Hence the output pulse width of 80 fs is considered to result from a spectral component approximately between 1.54 μm and 1.57 μm. It should be noted here that the amplification characteristics in 3-m long EDFA was almost the same as that in this case except that the soliton wavelength was shifted to 1.55 μm due to the SSFS.

For the 210 fs input pulse at 1.535 μm, it is important to note that the frequency of the output pulse always changed toward a longer wavelength at any pump power. That is, adiabatic soliton narrowing without the frequency shift was not observed at any pump power, although it was observed at 1.557 μm as described in Sec. 3.3. Since the optical gain at 1.535 μm is smaller than that at around 1.55 μm for the 5-m long EDFA, the frequency of the 210 fs soliton shifts toward a gain peak at 1.55 μm due to the frequency-pulling effect and the SSFS.

Amplification characteristics for an input soliton pulse at 1.530 μm with a broader pulse width of 470 fs is shown in Fig. 3.18(a) - (d). The erbium-doped fiber length is 3 m. The spectral profile in 3.18(a) is of an input soliton with a center wavelength of 1.530 μm, whose waveform is given in 3.18(b). The pulse width is 470 fs. The gain bandwidth at 1.535 μm is broader than the bandwidth of a 470 fs pulse, so that the 470 fs pulse can be amplified within the bandwidth. The input peak power is 50 W (average power of 90 μW; -10.5 dBm). The input pulse becomes an N=1.7 soliton. Z_{sp} is 24 m.

Figure 3.18(c) and (d) show the frequency spectrum and the autocorrelation trace of the output pulse for a pump power of 25 mW which corresponds to 4~5 dB gain at 1.53 μm. Since the fiber length of 3 m is about

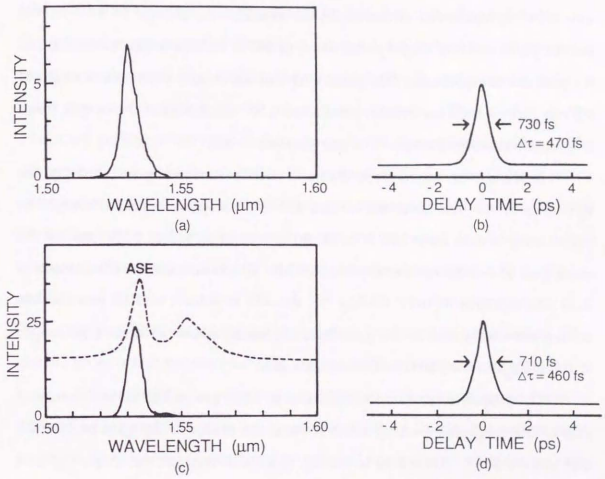

Fig. 3.18 Changes in frequency spectrum and pulse waveform for 470 fs input pulses at 1.530 μm. (a) and (b) are the frequency spectrum and the waveform of the input pulse. (c) and (d) are the frequency spectrum and the waveform of the output pulse. The fiber length is 3 m. The dashed line in (c) shows an amplified spontaneous emission (ASE) profile.

$0.1Z_{sp}$, the amplification process is nonadiabatic. As shown in 3.18(c), the center wavelength is 1.533 μm, shifting toward a gain peak at 1.535 μm. The FWHM of the spectrum is 6.2 nm. The dashed line in 3.18(c) shows an amplified spontaneous emission (ASE) profile. As shown in 3.18(d), the output pulse width is slightly shortened to 460 fs and the pulse waveform has no pedestal components. The pulse width of 460 fs and the spectral width of 6.2 nm gives a time-bandwidth product of 0.36, which means the output pulse is almost transform-limited. The gain is about 5 dB.

It should be noted here that the soliton narrowing induced by the optical gain was not observed for the 470 fs pulses at 1.53 μm, although the pulse compression from 240 fs to 80~90 fs was observed at 1.557 μm for the same gain of 4~5 dB as described in Sec. 3.3. This is because the fiber length of 3 m corresponds to only $0.1Z_{sp}$ for the 470 fs soliton at 1.53 μm and the soliton narrowing due to the gain does not occur, while the same fiber length is about Z_{sp} for the 240 fs soliton at 1.557 μm.

The frequency shift from 1.530 μm to 1.533 μm in Fig. 3.18(c) is mainly due to the frequency-pulling effect toward the center of the gain bandwidth and not the SSFS. According to the Eq. (1.2.35) in Sec. 1.2, the frequency shift due to the SSFS is proportional to τ^{-4}, where τ is the pulse width. Therefore, the frequency shift for the 470 fs pulse in this case should be much less than 1/15 smaller than the shift of 19 nm for the 240 fs pulse as shown in Fig. 3.7(c), because the output pulse width in Fig. 3.7(c) narrowed from 240 fs to 60 fs. Since the SSFS is small, efficient amplification is attained at 1.530 μm.

Amplification characteristics of the EDFA at other wavelengths are investigated using a femtosecond soliton pulse. Figure 3.19 shows the amplification characteristics of an input pulse with a wavelength of 1.564 μm, which is the long wavelength tail of the gain profile at 1.552 μm. The spectral

profile in 3.19(a) is of an input soliton with a center wavelength of 1.564 μm. The length of the erbium-doped fiber is 3 m. The pulse width of the input pulse is 250 fs. The input peak power is 150 W and the input average power is 0.14 mW (- 8.5 dBm). The input pulse is an N=1.2 soliton. Z_{sp} is 4.8 m.

For a pump power of 19 mW(~4 dB gain), the output soliton spectrum changes as shown in Fig. 3.19(b). The peak wavelength of the output pulse is 1.561 μm and is shifted to the shorter wavelength. This is due to the frequency pulling effect toward the gain peak. A new spectral peak at 1.584 μm appears, which is due to the SSFS. Since the 250 fs input pulse is much shorter than the 470 fs pulse at 1.530 μm, the frequency shift due to the SSFS for the former pulse is much larger than that for the latter. In addition, a new spectral peak appears at 1.54 μm, which is considered to be due to a gain peak at 1.535 μm.

Figure 3.19(c) shows the autocorrelation trace of the output pulse. The output pulse width narrows to 90 fs and pedestal components appear on the wings of the soliton pulse. Since a sech^2 shaped, transform-limited pulse at 1.56 μm with a width of 90 fs has a spectral width of 28 nm, the output pulse width of 90 fs is mainly attributed to spectral components roughly between 1.56 μm and 1.59 μm. By further increasing the pump power, further spectral shift is observed because of the gain enhanced SSFS. In contrast, by decreasing the pump power, the frequency shift due to the SSFS is reduced and the spectral component at 1.54 μm becomes small.

In summary, the amplification characteristics of erbium-doped optical fiber amplifiers have been investigated using femtosecond soliton pulses with various wavelengths. No adiabatic soliton narrowing was observed for the 210 fs pulse at 1.535 μm at any pump power but the SSFS occurs, while the adiabatic soliton narrowing without the frequency shift was observed at 1.557

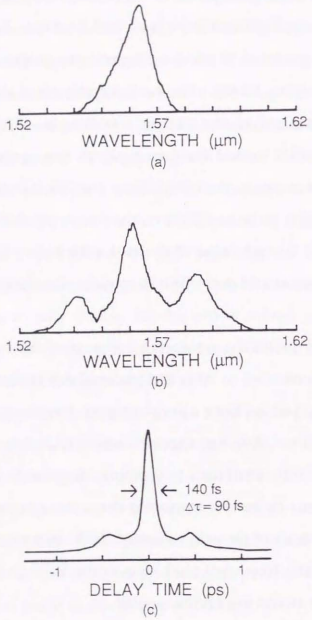

Fig. 3.19 Amplification characteristics of 250 fs input pulses at 1.564 μm. (a) is the frequency spectrum of the input pulse and (b) is the output spectrum. (c) is an autocorrelation trace of the output pulse. The fiber length is 3 m.

μm. This should be due to the frequency-pulling effect toward the optical gain at 1.55 μm. The output pulse width narrowed from 210 fs to 80 fs by the optical gain, which is similar to the observed pulse compression at 1.557 μm by the EDFA gain. On the other hand, the 470 fs soliton pulse was efficiently amplified without the SSFS by the optical gain at 1.535 μm, where the gain bandwidth is broader than the bandwidth of the input pulse. Here the pulse compression due to the optical gain was not observed because the Er-fiber length corresonded to only $0.1Z_{sp}$. The gain is about 5 dB for a pump power of 25 mW.

3.5 Conclusion

In this chapter we have shown the amplification characteristics of a femtosecond pulse in an erbium-doped optical fiber amplifier. A gain of 9 dB has been obtained in an EDFA for input pulses with a peak power of 30 W, an average power of 30 μW (- 15.2 dBm), and a pulse width of 260 fs.

When the input peak power is increased in the soliton power regime, interesting features peculiar to the optical soliton have been observed in the amplification process of the femtosecond pulses. When the gain is moderate, we have experimentally observed adiabatic narrowing of a femtosecond fundamental soliton at 1.55 μm. By increasing the amplifier gain to nonadiabatic region, pulse compression by as much as a factor 4 has been observed by using 240-fs pulses. This feature is very interesting since the pulse width of the output soliton can be fully controlled by changing the pump power. However, at the same time the frequency of the soliton strongly shifts toward longer wavelength region outside the EDFA gain bandwidth due to the SSFS. Therefore, when the gain is very high, the amplification process of the femtosecond soliton is stopped by the SSFS.

We have also investigated amplification characteristics of femtosecond soliton pulses with various wavelengths. No adiabatic soliton narrowing was observed for the 210 fs pulse at another gain peak of 1.535 μm at any pump power but the SSFS occurs. This should be due to the frequency-pulling effect toward the another optical gain peak at 1.55 μm. The output pulse width narrowed from 210 fs to 80 fs by the optical gain, which is similar to the observed pulse compression at 1.557 μm by the EDFA gain. On the other hand, the 470 fs soliton pulse was efficiently amplified without the SSFS by the optical gain at 1.535 μm, where the gain bandwidth is broader than the bandwidth of the input pulse.

It is important to note that the SSFS prevents from the efficient amplification of femtosecond soliton pulses by using an EDFA. Since the frequency shift Δf due to the SSFS is proportional to Dl/τ^4 as described in Eq. (1.2.26) in Sec. 1.2, the following should be necessary for the efficient amplification of the very short optical soliton;

1. dispersion parameter D is small,
2. fiber length l is short,
3. soliton pulse width τ is relatively broad.

In order to realize the condition 1, we need to prepare an erbium doped fiber which zero dispersion wavelength is close to the input soliton wavelength. For satisfying the condition 2 we have to prepare the erbium doped fiber with a relatively high doping concentration which can supply high optical gain in a short fiber. Because of the condition 3, it is difficult to efficiently amplify ultrashort femtosecond soliton pulses by using an EDFA. Of course, the pulse width range is also limited by the EDFA gain-bandwidth.

On the other hand, strong pulse compression in the amplification process accelerated the SSFS as described in Sec. 3.3. In order to suppress the

strong pulse compression, the erbium fiber length should be much shorter than the soliton period Z_{sp}. Since $Z_{sp} \propto \tau^2/D$, conditions 1 and 3 in the above is useful for increasing Z_{sp}. Therefore, the above three conditions are also useful for suppressing the pulse compression and the following acceleration of the SSFS in amplifying a femtosecond soliton pulses.

References

[3.1] R. J. Mears, L. Reekie, I. M. Jauncey, and D. N. Payne, "Low-threshold tunable CW and Q-switched fiber laser operating at 1.55 μm," Electron. Lett., vol. 23, p. 1026, 1987.

[3.2] E. Desurvire, J. R. Simpson, and P. C. Becker, "High gain erbium-doped traveling-wave fiber amplifier," Opt. Lett., vol. 12, p. 888, 1987.

[3.3] Y. Kimura, K. Suzuki, and M. Nakazawa, "46.5 dB gain in Er^{3+}-doped fibre amplifier pumped by 1.48 μm GaInAsP laser diodes," Electron. Lett., vol. 25, p. 1656, 1989.

[3.4] M. Nakazawa, Y. Kimura, K. Suzuki, "Soliton amplification and transmission with Er^{3+}-doped fibre repeater pumped by GaInAsP laser diode," Electron. Lett., vol. 25, p. 199, 1989.

[3.5] K. Suzuki, Y. Kimura, and M. Nakazawa, "Subpicosecond soliton amplification and transmission using Er^{3+}-doped fibers pumped by InGaAsP laser diodes," Opt. Lett., vol. 14, p. 865, 1989.

[3.6] X. Zhu, P. N. Kean, and W. Sibbett, "Coupled-cavity mode locking of a KCL:Tl laser using an erbium-doped optical fiber," Opt. Lett., vol. 14, p. 1192 (1989).

[3.7] B. J. Ainslie, K. J. Blow, A. S. Gouveia-Neto, P. G. J. Wigley, A. S. B. Sombra, and J. R. Taylor, "Femtosecond soliton amplification in erbium doped silica fibre," Electron. Lett., vol. 26, p. 186, 1990.

[3.8] I. Yu. Khrushchev, A. B. Grudinin, E. M. Dianov, D. V. Korobkin Jun, V. A. Semenov, and A. M. Prokhorov, "Amplification of femtosecond pulses in Er^{3+}-doped single-mode optical fibres," Electron. Lett., vol. 26, p. 457, 1990.

[3.9] E. M. Dianov, A.B. Grudinin, I. Y. Khrushchev, D. V. Korobkin, Jr, A. Y. Makarenko, A. M. Prokhorov, "Nonlinear dynamics of femtosecond soliton amplification in erbium doped fibers," in Proceedings of the Conference on Lasers and Electro-optics, Anaheim, paper, JTUA7, 1990.

[3.10] M. Nakazawa, K. Kurokawa, H. Kubota, K. Suzuki and Y. Kimura, "Femtosecond erbium-doped optical fiber amplifier," Appl. Phys. Lett., 57, p. 653, 1990.

[3.11] M. Nakazawa, K. Kurokawa, H. Kubota, and E. Yamada, "Observation of the trapping of an optical soliton by adiabatic gain narrowing and its escape," Phys. Rev. Lett. vol. 65, p. 1881, 1990.

[3.12] K. Kurokawa and M. Nakazawa, "Wavelength-dependent amplification characteristics of a femtosecond erbium-doped optical fiber amplifiers," Appl. Phys. Lett., vol. 58, p. 2871, 1991.

[3.13] J. P. Gordon, "Theory of the soliton self-frequency shift," Opt. Lett., vol. 11, p. 662, 1986; see also F. M. Mitschke and L. F. Mollenauer, "Discovery of the soliton self frequency shift," Opt. Lett., vol. 11, p. 659, 1986.

[3.14] M. Nakazawa, Y. Kimura, and K. Suzuki, "Efficient Er^{3+}-doped optical fiber amplifier pumped by a 1.48 μm InGaAsP laser diode," Appl. Phys. Lett., vol. 54, p. 295, 1989.

[3.15] L. F. Mollenauer, R. H. Stolen, and J. P. Gordon, "Extreme picosecond pulse narrowing by means of soliton effect in single-mode optical fibers," Opt. Lett. vol. 8, p. 289, 1983.

[3.16] J. Satsuma and N. Yajima, "Initial value problems of one-dimensional self-modulation of nonlinear waves in dispersive media," Suppl. Prog. Theoret. Phys., vol. 55, p. 284, 1974.

[3.17] H. A. Haus and M. Nakazawa, "Theory of the fiber Raman soliton laser," J. Opt. soc. Ame. vol. B-4, p. 652, 1987.

[3.18] K. J. Blow, N. J. Doran, and D. Wood, "Generation and stabilization of short soliton pulses in the amplified nonlinear Schrödinger equation," J. Opt. Soc. Ame. vol. B-4, p. 381, 1988.

[3.19] G. P. Agrawal, "Effect of gain dispersion and stimulated Raman scattering on soliton amplification in fiber amplifiers," Opt. Lett. vol. 16, p. 226, 1991.

[3.20] P. A. Belanger, L. Gagnon and C. Pare, "Solitary pulses in an amplified nonlinear dispersive medium," Opt. Lett. vol. 14, p. 943, 1989.

CHAPTER IV. TRANSMISSION CHARACTERISTICS OF A FEMTOSECOND SOLITON IN A DISTRIBUTED EDFA (DEDFA)

4.1 Introduction

With a view to the realization of ultrahigh speed optical communication, it has become more important to investigate ultrashort pulse propagation in long optical fibers[4.1-2]. In order to maintain soliton energy over long distances, it is important to compensate for fiber loss with optical amplifiers. Concerning about loss compensation, there are two types of long distance soliton transmission method. One is suitable for a lumped amplifier system. This method was realized by using EDFAs and its stability has been experimentally and theoretically proved, confirming it as a major method suitable for a lumped amplifier system[4.3-7]. Recently, field experiment of soliton transmission by this method has been succeeded with the use of dispersion-allocation technique[4.8] which enables us to use an already installed fiber cable for commercial systems to transmit optical solitons[4.9-10].

However, this method using a lumped amplifier system has a restriction that the repeater spacing should be less than or comparable to the soliton period. This is because nonsoliton components are generated when the repeater spacing is longer than the soliton period and the nonsoliton components prevent a long distance soliton transmission[4.6].

On the other hand, high bit-rate communication above 100 Gbit/s with a single carrier wavelength requires ultrashort optical pulses which pulse widths are in the subpico~femtosecond region. Since the soliton period is proportional to the square of the pulse width, the soliton periods for subpico~femtosecond pulses become very short. Therefore, the lumped

amplifier technique is not suitable for high bit-rate communication above 100 Gbit/s.

The other method is the distributed amplifier technique which can compensate for the fiber loss, resulting in an artificial loss-less transmission line except for the accumulation of amplified spontaneous emission (ASE) in the amplifier[4.11-13]. In this case, the concept of repeater spacing is irrelevant and very short soliton pulses can be transmitted at a high bit-rate with the aid of adiabatic soliton trapping in an active transmission line[4.14-18]. Nakazawa et al. have reported the picosecond (20 ps) soliton transmission characteristics of an 18.2 km long, distributed EDFA (DEDFA), at a repetition rate of 5 GHz[4.13].

In order to realize high speed optical communication systems with a bit-rate above 100 Gbit/s and a single carrier wavelength, the soliton pulse width should be in the subpico~ femtosecond region. However, such short solitons are unstable and eventually disperse because of the increase in additional perturbative terms such as soliton self-frequency shift[4.19-20] and third-order dispersion[4.21-22]. Several results on femtosecond soliton amplification in EDFAs[4.23-25] have been reported. To realize terabit/s systems with a single carrier wavelength, it is important to investigate femtosecond soliton transmission characteristics in an ultralong DEDFA.

In this chapter, we describe femtosecond soliton transmission over 18 km in a dispersion-shifted, DEDFA. In section 4.2, we describe our experimental setup for a soliton transmission over a long distance. In section 4.3, we show gain distribution along the 18.2 km-long distributed erbium doped fiber both experimentally and analytically. Experimental results on femtosecond soliton transmission in an 18.2 km-long DEDFA are described in section 4.4. Changes in transmission characteristics with different pumping

configurations are also shown in section 4.5. And we show our conclusion of chapter IV in section 4.6.

4.2 Experimental Setup

The experimental setup is shown in Fig. 4.1. Femtosecond pulses in the 1.5 μm region are generated by difference frequency mixing in a KTP crystal, as shown in chapter II. In the 1.5 μm region, the output pulse has a width of 250 fs with peak powers of 2~4 kW.

The experimental setup for measuring the amplification characteristics of an ultralong DEDFA is shown on the right hand side of Fig. 4.1. The femtosecond pulses are coupled with the pump light through a 1.48 μm/1.55 μm wavelength-division-multiplexing (WDM) fiber coupler. The femtosecond pulses and the pump light are coupled into an erbium-doped fiber after passing through a polarization-insensitive optical isolator. The isolator was installed to suppress laser oscillation. The pumping source is 1.48 μm InGaAsP laser diodes[4.26]. Here, we adopt three types of pumping scheme, that is, forward, backward, and bi-directional pumping (forward and backward pumping) configurations. The power ratio of forward to backward pumping in the bi-directional pumping configuration is 0.7:1. The amplified output pulse is detected with an autocorrelator and an optical spectrum analyzer.

An 18.2 km-long EDF was fabricated by the VAD method with the solution doping technique, in which a dehydration process using Cl_2 plays an important role in making low-loss distributed fiber by removing excess loss due to OH absorption[4.12]. The glass composition was Er:GeO_2-SiO_2 with a doping concentration of about 0.5 ppm. The fiber had a dual-shape core structure. The mode field diameter, cut-off wavelength, and zero dispersion

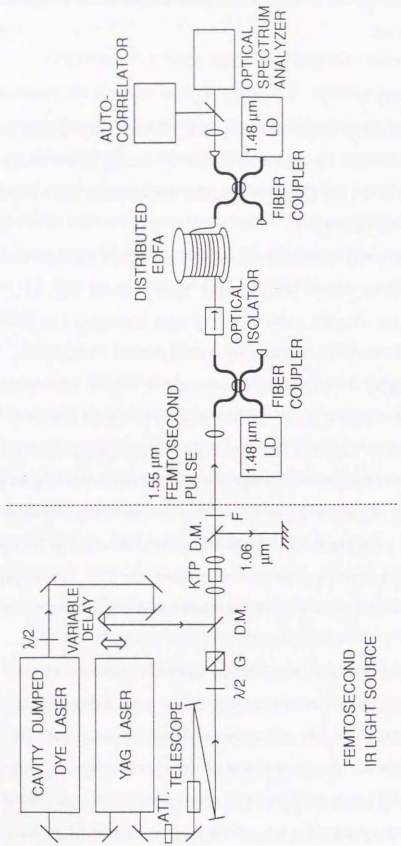

Fig. 4.1 Experimental setup for femtosecond soliton transmission in a distributed erbium-doped fiber amplifier (DEDFA). ATT. is the attenuator; $\lambda/2$, the half-wave plate; G, Glan-Thompson prism; D.M., dichroic mirror; LD, laser diodes.

wavelength were 7.7 μm, 1.2 μm, and 1.49 μm, respectively. The group velocity dispersion at 1.551 μm was 3.8 ps/km/nm.

The gain changes as a function of signal wavelength and pump power are shown in Fig. 4.2(a) and (b), respectively. The input average power in Fig. 4.2(a) was 22 μW(-16.6 dBm) and the total pump power was 33 mW. The maximum gain at 1.535 μm was 18 dB and that at 1.551 μm was 15 dB for a total pump power of 33 mW. The - 3 dB gain bandwidth at 1.535 μm was about 4.8 nm and that at 1.551 μm was 7.2 nm. As shown in Fig. 4.2(b), the gain threshold for input signal powers between 22 μW (-16.1 dBm) and 60 μW (-12.2 dBm) was given at a total pump power of as low as 14 mW. The signal wavelength was 1.551 μm. Although a larger gain saturation occurs for a signal power of - 12.2 dBm (open circle) than for one of - 16.6 dBm (closed circle), a gain of more than 10 dB can be obtained for a pump power of 30 mW. These high gain and wide-band characteristics enable us to amplify femtosecond solitons.

Figure 4.3 shows gain changes at 1.551 μm in the EDFA as a function of pump power, where triangles, circles, and squares correspond to forward, backward, and bi-directional pumping, respectively. The input signal was a cw beam emitted from a single-wavelength laser diode. The average input power of the signal was 60 μW (-12.2 dBm). This average power corresponds to the input average power in the experiment. The threshold pump powers, which give zero net gain, in the three pumping configurations are 14~16 mW. As seen, the gain for backward pumping is almost the same as that for bi-directional pumping. However, the gain for forward pumping is 2.5~3 dB lower than that of the other two pumping configurations for the measured pump power. This is due to signal gain saturation.

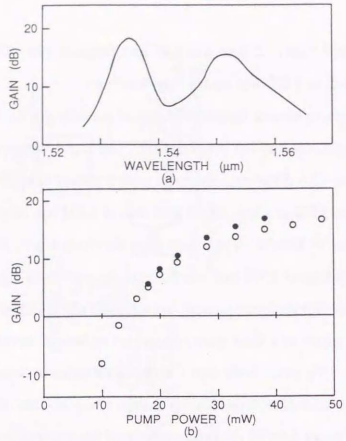

Fig. 4.2 Gain characteristics of 18.2 km-long dispersion-shifted, distributed erbium-doped fibre amplifier.
(a) Wavelength dependence of the gain (Input power ~ 22 μW, pump power =33 mW (Forward=13 mW, Backward=20 mW)).
(b) Gain at 1.551 μm vs. pump power (○ : -12.2 dBm input, ● :-16.6 dBm input). The power ratio of forward to backward pumping was 0.7:1

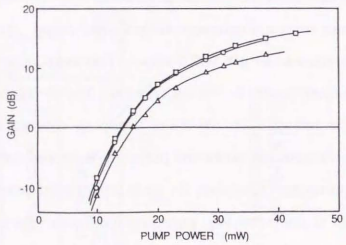

Fig. 4.3 Gain changes at 1.551 μm in an 18.2 km EDFA as a function of pump power. The input signal with an average power of -12.2 dBm is a cw beam emitted from a single-wavelength laser diode. Δ, ○, and □ correspond to forward, backward, and bi-directional pumping, respectively.

4.3 Gain Variation along the Erbium-Doped Fiber

A. Gain-Distribution Measurements Using Optical-Time-Domain Reflectometry

An investigation of the gain variation along the fiber is important for the analysis of femtosecond soliton transmission characteristics in a DEDFA. The changes in optical gain as a function of distance along a DEDFA can be measured using optical-time-domain reflectometry (OTDR)[4.27-28]. We used a commercially available optical-time-domain reflectometer with a correlation function. The average launched power for the OTDR was -38 dBm which was lower than the input power of -12.2 dBm, so the unsaturated gain distribution could be measured over long distances. Figure 4.4 shows the OTDR signals at 1.55 μm for pump powers of 0, 16, and 34 mW, where the dot-dashed, solid, and dashed lines correspond to forward, backward, and bi-directional pumping, respectively. At a pump power of 0 mW, shown by the solid line in Fig. 4.4, the fiber loss was 2.3 dB/km. This agrees with that obtained by the conventional transmission method. When the pump power was as low as 16 mW, the gains at 18.2 km with forward pumping and backward pumping were 0~1 dB and the gain with bi-directional pumping was 4 dB. It should be noted that the changes in gain along the fiber are quite different for forward pumping and backward pumping. With forward pumping, the gain increased up to 10 km and reached 5.5 dB. A decrease in gain was observed from 10 km to 18 km owing to intrinsic loss. On the other hand, a loss medium was created up to 8 km with backward pumping, and a gain medium was formed from 8 km to 18 km.

When the pump power was as high as 34 mW, the gains at 18.2 km with forward pumping and backward pumping increased to 13 dB and the gain with bi-directional pumping was about 15 dB. The signal was amplified

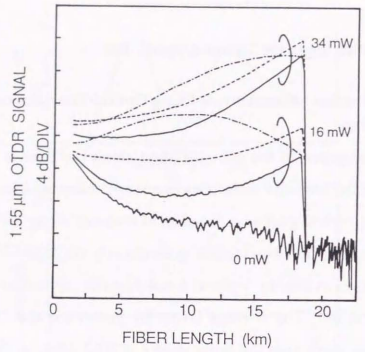

Fig. 4.4 OTDR signals for an 18.2 km distributed erbium amplifier. Dot-dashed, solid, and dashed lines indicate forward, backward, and bi-directional pumping, respectively. The average launched power for the OTDR is -38 dBm.

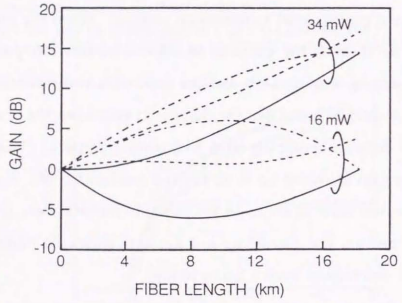

Fig. 4.5 Calculated signal gain variation along 18.2 km EDFA without the SSFS effect. Dot-dashed, dashed, and solid lines indicate forward, backward, and bi-directional pumping, respectively. The input signal power is -38 dBm.

from the early stage of the EDFA in all pumping configurations. The discrepancies between the zero levels of the OTDR signal at the input end may be caused by the high pump power. The signal gain per unit length with backward pumping is smaller than that with forward pumping in the first half of the EDFA.

B. Rate Equation Analysis of Gain Distribution

The signal gain variation along the fiber can be roughly estimated by rate equation analysis. We define the pump intensity and signal intensity as I_p and I_s, respectively. Then, the normalized pump intensity $\bar{I}_p$ and the normalized signal intensity $\bar{I}_s$ at amplifier length z in the forward pumping configuration are written as[4.29]

$$\frac{d\bar{I}_p}{dz} = -\left\{\frac{k_s\bar{I}_s + 1}{\bar{I}_p + (1+k_s)\bar{I}_s + 1}\rho\sigma_p^a + \alpha\right\}\bar{I}_p \tag{4.1}$$

$$\frac{d\bar{I}_s}{dz} = \left\{\frac{k_s\bar{I}_p - 1}{\bar{I}_p + (1+k_s)\bar{I}_s + 1}\rho\sigma_s^a - \alpha\right\}\bar{I}_s \tag{4.2}$$

$$\bar{I}_p = I_p/(h\nu_p/\sigma_p^a\tau) \tag{4.3}$$

$$\bar{I}_s = I_s/(h\nu_s/\sigma_s^a\tau) \tag{4.4}$$

where σ_p^a and σ_s^a are the absorption cross section at the pump wavelength and the signal wavelength, respectively, ρ is the erbium concentration, $h\nu_p$ and $h\nu_s$ are the photon energies of the pump and signal waves, respectively, τ is the fluorescence lifetime, and α is the background loss of the fiber. We define the ratio k_s as σ_s^e/σ_s^a , where σ_s^e is the emission cross section at the signal wavelength. The pump power P_p and the signal power P_s are expressed as $P_p = I_pA_p$ and $P_s = I_sA_s$, respectively, where A_p and A_s are the effective interaction areas for the pump and signal waves. It should be noted that $\rho\sigma_{p,s}^a$ represents the optical loss per unit length. The optical losses at the

pump and signal wavelengths and the background loss were taken from the experimental results.

The signal gain along the fiber given by $G(z)=P_s(z)/P_s^{in}$ is calculated numerically by using Eq. (4.2) in the forward pumping configuration, where P_s^{in} is the input signal power. The results for pump powers of 16 mW and 34 mW are shown with dot-dashed lines in Fig. 4.5, where the input signal power is -38 dBm. The value of k_s is approximately unity. The signal gain in the other pumping configurations are calculated in the same way, and the results are also shown in Fig. 4.5. The dot-dashed, solid, and dashed lines correspond to the forward, backward, and bi-directional pumping configurations, respectively. As shown in Fig. 4.5, the calculated gains at 18.2 km for a pump power of 16 mW are 0 dB with forward pumping and backward pumping and 4 dB with bi-directional pumping. These values agree with the experimental results shown in Fig. 4.4. The signal gain with forward pumping increases up to 10 km and a decrease in gain is observed from 10 km to 18 km. With backward pumping, on the other hand, a loss medium is formed up to 8 km and a gain medium is created from 8 km to 18 km. These values agree with the experimental results shown in Fig. 4.4. When the pump power is as high as 34 mW, the signal is amplified from the early stage of the EDFA in all pumping configurations, as shown in Fig. 4.5. The gains at 18.2 km for all three pumping configurations agree within experimental error with the experimental results shown in Fig. 4.4.

Figure 4.6 shows the calculated gain distribution for an input signal power of -12.2 dBm which is the input power of the femtosecond soliton pulse in the present experiment. The dot-dashed, solid, and dashed lines correspond to forward, backward, and bi-directional pumping, respectively. The pump powers are 16 mW and 38 mW. As shown in Fig. 4.6, the gains at

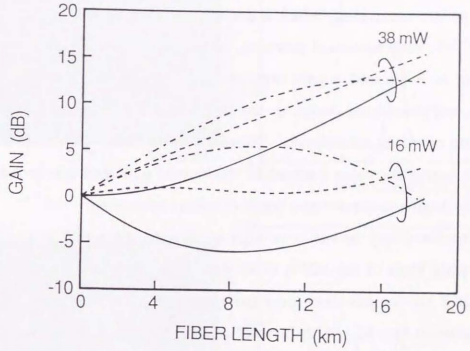

Fig. 4.6 Calculated signal gain variation along 18.2 km EDFA without the SSFS effect. Dot-dashed, dashed, and solid lines indicate forward, backward, and bi-directional pumping, respectively. The input signal power is -12.2 dBm.

18.2 km for a pump power of 16 mW are 0~3 dB for the three pumping configurations, which agrees with the experimental results shown in Fig. 4.3 where the threshold pump powers are 14~16 mW. With forward pumping, the gain increases up to 10 km and reaches about 5.5 dB. Thus, in the first half of the EDFA the signal power increases and the signal pulse narrows as a result of soliton narrowing, which enhances the soliton self-frequency shift (SSFS)[4.17-18]. With backward pumping, on the other hand, a loss medium is created up to 8 km and a gain medium is formed from 8 km to 18 km. Therefore, with backward pumping, the signal power first decreases and the signal pulse broadens adiabatically. However, in the latter half of the EDFA, the signal power increases because of the optical gain and the broadened signal pulse begins to narrow as a result of soliton narrowing.

When the pump power is as high as 38 mW, the signal is amplified from the early stage of the EDFA in all three pumping configurations. The gains at 18.2 km for the three configurations agree with the experimental results shown in Fig. 4.3. With forward pumping, a loss medium is created near the far end of the EDFA even for a pump power as high as 38 mW, as shown in Fig. 4.6. It should be noted that the gain with backward pumping is 0 dB or a little lower near the input end of the EDFA for a pump power of 38 mW.

4.4 Transmission Characteristics in an 18 km-Long DEDFA

In this section, we describe femtosecond soliton transmission over 18 km in a dispersion-shifted, DEDFA. The DEDFA was pumped by a bi-directional pumping configuration to generate uniform gain distribution.

Femtosecond soliton transmission characteristics are shown in Fig. 4.7, where the soliton wavelength was 1.551 μm and the soliton pulse width was

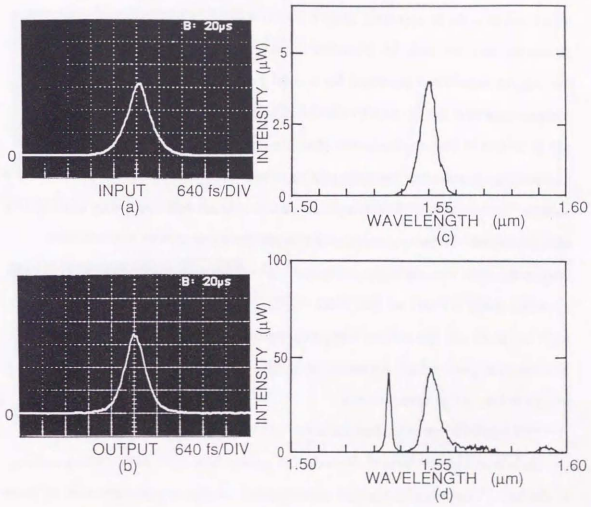

Fig. 4.7 Soliton transmission characteristics for 454 fs soliton.
(a) 454 fs input soliton waveform (autocorrelator output)
(b) Output soliton waveform (433 fs)
(c) Input soliton spectrum
(d) Output soliton spectrum

454 fs with an autocorrelator. One division of Fig. 4.7(a) and (b) is 640 fs, corresponding to 416 fs for a sech pulse. The normalised soliton amplitude, A, was approximately 1.2, corresponding to an average power of 60 μW. Fig. 4.7 (a) is an input soliton waveform and Fig. 4.7(c) is the spectral profile of the input soliton. $\Delta\lambda$ is approximately 6.2 nm, so that $\Delta\tau\Delta\lambda$ ~0.35. The soliton pulses transmitted over 18. 2 km are shown in Fig. 4.7(b) and (d). Fig. 4.7(b) is the output waveform obtained for a total pump power of 38 mW which corresponds to a cw gain of 15 dB (0.8 dB/km). The output soliton width is 433 fs which is slightly narrower that the input. This is due to soliton narrowing. Interesting features can be observed in the spectrum of the output soliton. In the longer wavelength region, a soliton self-frequency shift (SSFS) was observed. When we increased the soliton peak power further, this frequency shift was strongly enhanced. $\Delta\lambda$ of the output spectrum is approximately 6.1 nm, so that $\Delta\tau\Delta\lambda$ ~0.33. The gain for this soliton was as high as 10~11 dB. No soliton trapping appeared at this EDFA gain bandwidth. The spectral peak which appeared at 1.535 μm was due to ASE, which did not produce any pulse components.

Transmission characteristics for shorter pulses at a lower power level are shown in Fig. 4.8, where the average power was ~ 35 μW, corresponding to A=0.67. The most important investigation in this experiment was to know how short a pulse can be transmitted over 18 km. Thus, the input pulse, which was almost at a soliton power level, was set as short as 260 fs as shown in Fig. 4.8(a), corresponding to a peak power of 35.4 W. The spectrum is shown in Fig. 4.8(c), where $\Delta\lambda$ of the input spectrum is approximately 9.5 nm, so that $\Delta\tau\Delta\lambda$ ~0.31. The output pulse waveform and the spectrum are shown in Fig. 4.8(b) and (d), respectively, in which the total pump power was 38 mW. The output pulse width was broadened up to 471 fs. From the output

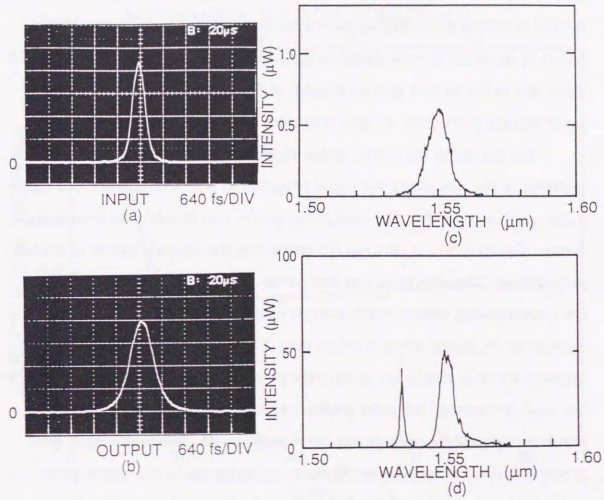

Fig. 4.8 Amplification characteristics for 260 fs near soliton pulse.
(a) 260 input soliton waveform (autocorrelator output)
(b) Output soliton waveform (471 fs)
(c) Input soliton spectrum
(d) Output soliton spectrum

spectrum, we also observed a small SSFS and ASE at 1.535 μm. The Δλ of the output spectrum is approximately 5.5 nm, so that ΔτΔλ ~0.32. Although the gain could not be evaluated exactly since the input width is different from the output width, it was more than 10 dB. When we increased the peak power of the 260 fs soliton pulse, further SSFS appeared. In our experiment, shorter pulses of about 200 fs were always broadened up to around 400 fs. This may be attributed to the limited gain bandwidth of 7~8 nm which depends on the input average power due to gain saturation.

The change in the output pulse width for different input power levels is shown in Fig. 4.9, where the signal wavelength was 1.551 μm and the input pulse width was 405 fs. The total pump power was 33 mW. An interesting feature observed here is that Fig. 4.9 represents the inherent nature of soliton propagation. The transverse axis represents average input power, and also the corresponding soliton number A. A soliton can be formed when A>0.5. As seen in the figure, when A is less than 0.5, enormous pulse broadening appears, which is due to the group velocity dispersion. The nonlinearity is too weak to maintain the pulse width. Around A~0.63 the output pulse width was almost the same as the input pulse width. When the input peak power is further increased (A=0.63~A=1.5), the change in the output pulse width is almost flat around 500 fs, but is gradually broadened with an increase in the input A number. This is due to the excitation of the SSFS in the early stage of the DEDFA.

4.5 Changes in Transmission Characteristics with Different Pumping Configurations

In this section, the transmission and amplification characteristics of femtosecond soliton pulses are described for various pumping conditions.

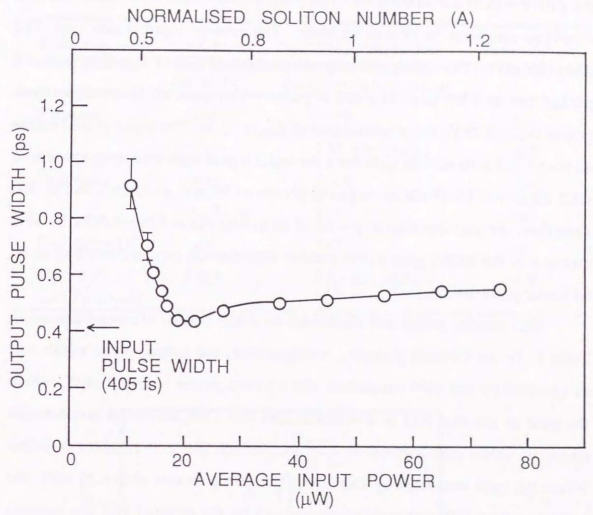

Fig. 4.9 Change in the output pulse width as a function of the different soliton intensity. The soliton pulse width is 405 fs, the wavelength is 1.551 μm, and the total pump power is 33 mW (Forward=13 mW, Backward=20 mW)

The input pulse was a transform-limited 440 fs pulse for all three pumping configurations. The full width at half maximum (FWHM) of the input pulse spectrum was 5.6 nm. The center wavelength was 1.551 μm which was one of the gain peaks of the EDFA[4.14]. The peak power of the input pulse and the repetition rate were 36 W and 3.8 MHz. The average input power was -12.2 dBm (60 μW). The group velocity dispersion (GVD) of the fiber was 3.8 ps/km/nm at 1.551 μm. The 440 fs pulse width gave an N=1 soliton peak power $P_{N=1}$ of 27 W and a soliton period Z_{sp} of 20 m. The input pulse became an N=1.1~1.2 soliton. The gain for a cw input signal with an average power of -12.2 dBm was 12~15 dB for a pump power of 38 mW as shown in Fig. 4.7. Therefore, the gain per soliton period of 20 m was about 0.013~0.017 dB. This means that the EDFA gain in the present experiments can be described as an adiabatic perturbation.

Our results, which are described in detail below, are summarized in Table I. In the forward pumping configuration, the output pulse width was determined by the SSFS component for a pump power below 20 mW, where the gain in the first half of the EDFA was low. An amplified spontaneous emission (ASE) was formed at 1.55 μm, which did not produce a pulse. When the gain was high by increasing the pump power above 30 mW, the output pulse width was mainly determined by the original 1.55 μm spectral component, where an output pulse corresponding to the SSFS component also existed.

In the backward pumping configuration, the output pulse width was also determined by the SSFS component when the gain in the first half of the EDFA was low by setting the pump power as low as 20 mW. Although an ASE was also generated at 1.55 μm, no pulse was formed. For a pump power of as high as 40 mW, the output pulse width was still determined by the SSFS

TABLE I

SUMMARY OF EXPERIMENTAL RESULTS

Pumping Configuration	Gain in the First Half of the EDFA	Spectral Components Corresponding to Autocorrelation Signal	Pump Power (mW)
Forward	low	SSFS	≤20
	high	1.55 μm, SSFS	≥30
Backward	low	SSFS	~20
	medium	SSFS	~40
Bi-directional	low	SSFS	~20
(Forward and Backward)	high	1.55 μm, SSFS	≥30

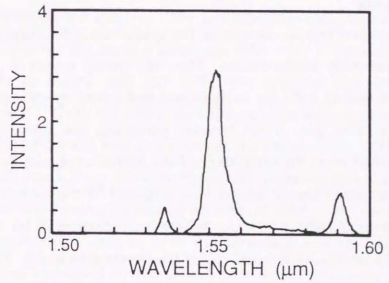

Fig. 4.10 Typical output spectrum with forward pumping. The pump power is 30 mW.

component for backward pumping but by the 1.55 μm spectral component for forward pumping. This is because the gain near the input end of the EDFA with backward pumping is still 0 dB or a little negative even for a pump power as high as 40 mW, as shown in Fig. 4.6. At 1.55 μm, the ratio of an ASE to the signal in the backward configuration was larger than that in the forward configuration. When the pump power further increases in the backward pumping configuration, the output pulse width will be determined by the original 1.55 μm spectral component.

In the bi-directional pumping configuration, the output pulse width was determined by the SSFS component when the gain in the first half of the EDFA was low. When the gain was high by setting the pump power above 30 mW, the output pulse width was mainly determined by the original 1.55 μm component, as with forward pumping. The output pulse corresponding to the SSFS component also existed. The details are described in the following subsections A~C.

A. Forward Pumping

Figure 4.10 shows typical changes in the spectrum of the output soliton in the forward pumping configuration. Here the pump power is 30 mW. The spectral component at 1.551 μm is dominant and a new spectral peak due to SSFS appears at 1.59 μm. With forward pumping, the signal pulse is adiabatically amplified from the early stage of the EDFA, as shown in Fig. 4.6. Based on the perturbation theory for the N=1 soliton,[4.25] the soliton pulse is shortened to approximately $1/(1+2\Delta)$, where perturbation Δ for the gain medium is given by $2\Delta=G_p/(10\log_{10}e)$. G_p is the power gain in dB. The pulse which is shortened by soliton narrowing causes a large SSFS, since the frequency shift due to SSFS is proportional to τ^{-4}, where τ is the pulse

width[4.18]. It is necessary to correct the spectrum, especially for wavelengths longer than 1.57 μm, because of the wavelength dependence of the coupling ratio of the fiber coupler which is connected to the output end of the 18.2 km erbium-doped fiber. The coupling ratio at 1.59 μm is 46 %. Therefore, the spectral component at 1.59 μm at the output end of the erbium-doped fiber is about 2.2 times larger than that shown in Fig. 4.10. This correction is required throughout the paper when the wavelength is longer than 1.57 μm.

The new spectral component at around 1.535 μm is an ASE, which does not produce pulse components. The output pulse width broadened from 440 fs to 700 fs. Changes in the output pulse width as a function of pump power are summarized in Fig. 4.11. Here, the triangles on the solid line correspond to forward pumping in an 18.2 km EDFA and the triangles on the dashed line correspond to that in a 9.4 km EDFA. In the 9.4 km EDFA the input pulse was an N=1.6 soliton and had a width of 370 fs. When the pump power was increased, the output pulse width decreased in both EDFAs.

It is important to note here that the output pulse width is mainly determined by the original 1.551 μm spectrum component for pump powers above 30 mW. By using a bandpass filter with a bandwidth of 29 nm, it is possible to select only the 1.551 μm spectral component or the SSFS component. Then, we found that the autocorrelation signal of the 1.551 μm spectral component was much larger than that of the SSFS component. On the other hand, only the autocorrelation signal of the SSFS component was obtained for a pump power of around 20 mW. By further increasing the pump power, the gain at 1.551 μm increased and the output soliton pulse width was shortened by the soliton narrowing, as shown by the triangles in Fig. 4.11. Since the pump power was insufficient over 18.2 km, there was little soliton narrowing.

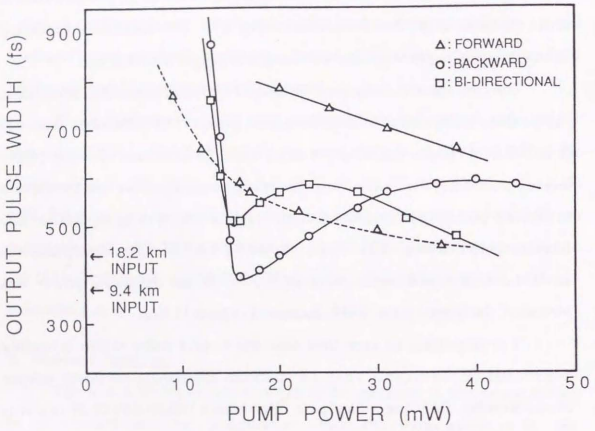

Fig. 4.11 Output pulse width changes in an 18.2 km EDFA as a function of pump power. Δ, ○, and □ indicate forward, backward, and bi-directional pumping, respectively. Triangles on a dashed line correspond to forward pumping in a 9.4 km EDFA.

It is important to note in Fig. 4.11 that the pulse broadening in the 9.4 km EDFA is smaller than that in the 18.2 km EDFA at the same pump power. Although the input pulse widths are different, a clearer difference can be found between the output pulse widths. This is because an absorptive region is formed in the far end of the 18.2 km EDFA as shown in Fig. 4.6 and the pulse intensity decreases, resulting in pulse broadening due to group velocity dispersion.

B. Backward Pumping

Figure 4.12 shows changes in the spectrum of the output solitons in the backward pumping configuration. When the pump power is 14 mW, the FWHM of the spectrum narrows from 5.6 nm to 3.9 nm as shown in Fig. 4.12(a). The dashed line in this figure shows the spectrum of the input pulse. The output pulse width broadens to 690 fs. Since the threshold pump power with backward pumping is 14~15 mW as shown in Fig. 4.3, the soliton pulse in the EDFA for a pump power of 14 mW is dispersive, and eventually it broadens due to the GVD of the erbium fiber. The pulse is broadened as a result of adiabatic broadening so that the spectrum is also modified. The another possible explanation of the spectral narrowing is that the spectral profile is modified since absorption saturation may occur only at the spectral peak of the pulse. The new spectral component at around 1.535 μm is an ASE, which does not produce pulse components.

By increasing the pump power to 16 mW, the center wavelength shifts to 1.555 μm due to SSFS as shown in Fig. 4.12(b) and the pulse width narrows to 400 fs. Figure 4.13 shows its autocorrelation trace. The output power was almost the same as the input power. Thus, a lossless transmission of 440 fs soliton pulses over 18.2 km has been achieved for a pump power of as low as

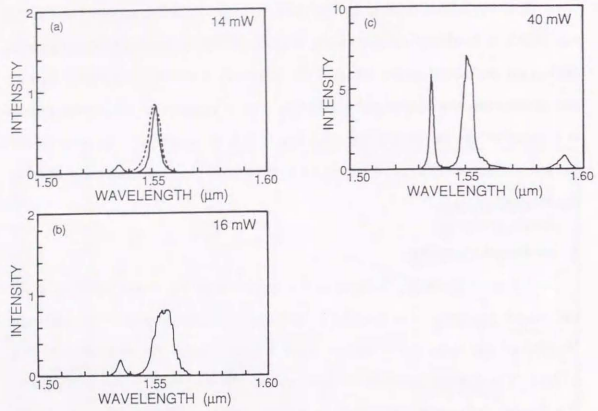

Fig. 4.12 Changes in the spectrum of the output pulse with backward pumping. Spectra (a)-(c) correspond to pump powers of 14, 16, and 40 mW, respectively. The dashed line in (a) shows the spectrum of the input pulse.

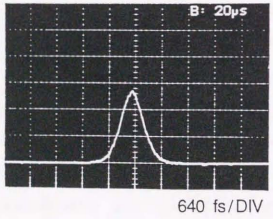

Fig. 4.13 Typical autocorrelation trace of the output pulse. This trace is of an output pulse when the pump power is 16 mW with backward pumping.

16 mW with backward pumping. When the pump power is increased to as high as 40 mW, the spectral peak shifts further to 1.592 μm as shown in Fig. 4.12(c) and the output pulse width broadens to 590 fs.

Changes in the output pulse width and in the frequency shift due to SSFS with backward pumping are summarized with open circles in Figs. 4.11 and 4.14, respectively. By using a bandpass filter as with forward pumping, it was found that for a pump power of above 16 mW, the autocorrelation signal of the SSFS component was much larger than that of the spectral component at 1.551 μm. Most of the spectral component at 1.551 μm is composed of an ASE. When the pump power is increased, the frequency shift increases as shown in Fig. 4.14 and the center wavelength is beyond the EDFA gain bandwidth. Here the lower-frequency edge of the gain bandwidth corresponds to a frequency shift of 1.6 THz for a pump power of 16 mW. The increase in the GVD value at the center wavelength of the frequency shifted soliton pulse requires broader pulses to maintain the same soliton power. Therefore, the output soliton pulse width broadens with increases in the pump power, as shown in Fig. 4.11.

Pulse broadening stops when the pump power is further increased to 40 mW. Here, the output pulse width is determined by the SSFS component at 1.59 μm. Due to the increase in the pump power, the spectral component within the gain bandwidth is efficiently amplified in the early stage of the EDFA as we can see from Fig. 4.16, resulting in an increase in the amplitude of the SSFS component. Thus soliton narrowing at 1.59 μm is greater than at lower pump powers and pulse narrowing occurs at a pump power of around 40 mW.

C. Bi-Directional (Forward and Backward) Pumping

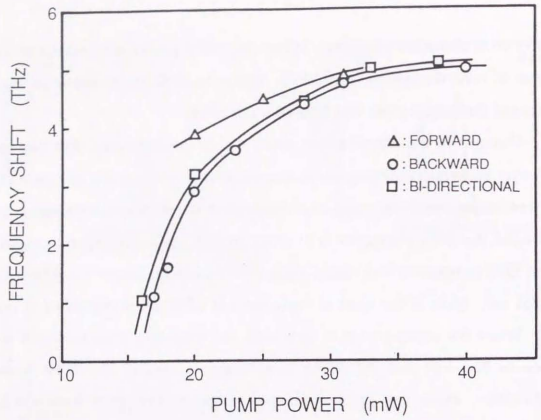

Fig. 4.14 Changes in the frequency shift due to SSFS as a function of pump power. △, ○, and □ indicate forward, backward, and bi-directional pumping, respectively.

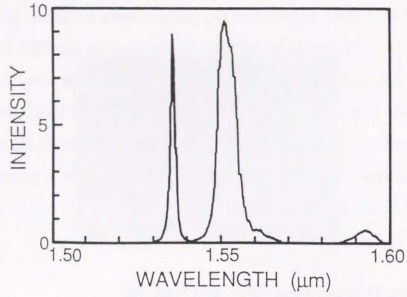

Fig. 4.15 Output spectrum at 38 mW pump power with bi-directional pumping.

As shown by the squares in Fig. 4.11, when the pump power is around 20 mW, the output pulse width in the bi-directional pumping configuration broadens as the pump power is increased. In the present case, it was found that the output pulse width was determined by the SSFS component. This is due to the fact that for a low pump power, the gain in the early stage of the EDFA is low as shown in Fig. 4.6. The output pulse width broadens with increases in the pump power, since the increase in the GVD value at the center wavelength of the frequency shifted soliton pulse requires a broader pulse to maintain the same soliton power.

On the other hand, when the pump power was higher than 30 mW, the autocorrelation signal of the 1.551 μm spectral component was larger than that of the SSFS component, since the gain in the early stage of the EDFA is high for a pump power of above 30 mW as shown in Fig. 4.6. The output pulse width narrows with an increase in the pump power, since the optical gain reduces the pulse width as a result of soliton narrowing.

Figure 4.15 shows a typical output pulse spectrum for a high pump power. The total pump power is as high as 38 mW (Forward 15 mW, Backward 23 mW). The 1.551 μm spectral component is efficiently amplified and the peak wavelength of the SSFS component shifts to 1.592 μm. The output pulse width changes to 480 fs. Here the gain for the spectral component at 1.551 μm is about 11 dB, which is smaller than the gain of 15 dB for the cw beam because of SSFS.

D. Soliton Self-Frequency Shift in the 18.2 km DEDFA

Figure 4.14 shows changes in the frequency shift due to SSFS as a function of pump power. Triangles, circles, and squares show the frequency shift in the forward, backward, and bi-directional pumping configurations,

respectively. As shown in Fig. 4.14, the frequency shift increases as the pump power increases for all pumping configurations. However, the frequency shift saturates when the pump power exceeds 20 mW. SSFS is linearly accelerated when the soliton spectrum is in the EDFA gain bandwidth, where the lower-frequency edge of the bandwidth corresponds to a 1.6 THz frequency shift for a pump power of 16 mW. When we increase the pump power, the frequency shift occurs in the early stage of the fiber and the soliton frequency is beyond the gain bandwidth of the EDFA. After that, the gain does not enlarge SSFS. Therefore, the frequency shift is not a linear function of the pump power.

When the pump power is below 30 mW, the frequency shift in the forward pumping configuration is much larger than that in the backward pumping configuration. The frequency shift Δf due to SSFS for the N=1 soliton is expressed as[4.18]

$$\Delta f \propto l\tau^{-4} \qquad (4.5)$$

where l is the propagation distance and τ is given by $1/2\eta$ where 2η is the amplitude of the soliton. As shown in Fig. 4.6, when the pump power is as low as 16 mW, the signal pulse with forward pumping is first amplified and the amplified signal pulse which is shortened by soliton narrowing causes a large SSFS in the first half of the 18.2 km EDFA. On the other hand, with backward pumping, the signal power first decreases and the signal pulse broadens, because the gain in the first half of the EDFA is negative as shown in Fig. 4.6. In the latter half of the EDFA, the signal power increases along the fiber and SSFS occurs. Therefore, when SSFS occurs, the soliton pulse with forward pumping is shorter than that with backward pumping. Furthermore, since the propagation distance in the forward pumping configuration, where effective SSFS occurs, is longer than that in the backward pumping

configuration, the total frequency shift with forward pumping is larger than that with backward pumping.

At higher pump powers, effective amplification can be realized in the first half of the erbium-doped fiber, even when the backward pumping configuration is adopted. This reduces the difference in frequency shift between forward pumping and backward pumping.

As shown by the present experimental results, SSFS occurs strongly when a femtosecond soliton pulse propagates in the DEDFA. These results indicate that the femtosecond soliton pulses are very weakly trapped in the EDFA gain bandwidth of 1.55 μm, and therefore it may not be possible to use the bandwidth limitation of the gain profile for soliton stabilization[4.14,16]. In soliton communication systems, SSFS causes large frequency fluctuations of the solitons and they are translated into pulse position jitter after propagation along a fiber. Therefore, SSFS imposes stringent limitations on the maximum data rates[4.30]. When the pump power is above 30 mW with bi-directional pumping, the output pulse width is determined by the 1.55 μm spectral component not by the SSFS component. Femtosecond soliton transmission may be possible with DEDFAs by eliminating the SSFS component with an optical bandpass filter which only transmits the 1.55 μm signal component.

4.6 Conclusion

We have experimentally investigated femtosecond optical soliton transmission characteristics in a dispersion-shifted, distributed erbium-doped fibre amplifier as long as 18.2 km. Solitons (A=0.7~1.2) with a pulse width of about 450 fs have been transmitted. However, a femtosecond soliton is very weakly trapped in the EDFA gain bandwidth of 1.55 μm and the soliton self-

frequency shift inevitably occurs. When the soliton width was reduced to 260 fs, the output pulse width always broadened up to around 470 fs because of the gain bandwidth of the DEDFA.

By changing the pumping configuration, the transmission characteristics of femtosecond optical solitons have been investigated in details. With backward pumping, a lossless transmission of 440 fs solitons at 1.55 μm has been realized with a pump power of 16 mW. Here the output pulse width is determined by the spectrum modified by the soliton self-frequency shift. On the other hand, in a bi-directional pumping configuration, 440 fs soliton pulses have been transmitted for a total pump power of 38 mW, where the output pulse width is determined by the original 1.55 μm spectrum. It should be noted here that in the forward pumping and the bi-directional pumping configurations, there are two output pulses when the pump power is above 30 mW. One is a frequency-downshifted pulse due to the SSFS and the other corresponds to the original 1.55 μm spectrum. And the autocorrelation signal of the former is much smaller than that of the latter because of the optical loss outside the gain bandwidth of the DEDFA. A new pulse at 1.55 μm may be generated by the amplification of the non-soliton component at 1.55 μm.

Finally, when the pulse width shortens to a femtosecond region a strong SSFS becomes a big problem in the realization of a long-distance transmission of an optical soliton with a DEDFA, as similar to the amplification process of a femtosecond optical soliton in an EDFA as described in chapter III. In order to reduce the SSFS in a long-distance transmission of a femtosecond optical soliton, we should use a DEDFA with a small dispersion and also have to develop other methods to suppress the SSFS.

References

[4.1] D. Marcuse, "Pulse distortion in single-mode fibers," Appl. Opt. vol. 19, p. 1653, 1980.

[4.2] K. Suzuki, Y. Kimura, and M. Nakazawa, "Subpicosecond soliton amplification and transmission using Er^{3+}-doped fibers pumped by InGaAsP laser diodes," Opt. Lett. vol. 14, p. 865, 1989.

[4.3] M. Nakazawa, Y. Kimura and K. Suzuki, "Soliton amplification and transmission with Er^{3+}-doped fibre repeater pumped by GaInAsP laser diode" Electron. Lett., vol. 25, p. 199, 1989.

[4.4] M. Nakazawa, K. Suzuki, and Y. Kimura, "3.2-5 Gbit/s, 100 km Error-free soliton transmission with erbium amplifiers and repeaters", IEEE Photon. Technol. Lett., vol. 2, p. 216, 1990.

[4.5] H. Kubota and M. Nakazawa, "Long-distance optical soliton transmission with lumped amplifiers", IEEE J. Quantum Electron., vol. 26, p. 692, 1990.

[4.6] A. Hasegawa and Y. Kodama, "Guiding-center soliton in optical fibers", Opt. Lett., vol. 15, p. 1443, 1990.

[4.7] L. F. Mollenauer, S. G. Evangelides and H. A. Haus, "Long distance soliton propagation using lumped amplifiers and dispersion-shifted fiber", IEEE J. Lightwave Technol. vol. 9, p. 194, 1991.

[4.8] M. Nakazawa and H. Kubota, "Optical soliton communication in a positively and negatively dispersion allocated optical fiber transmission line", Electron. Lett. vol. 31, p. 216, 1995.

[4.9] M. Nakazawa, Y. Kimura, K. Suzuki, H. Kubota, T. Komukai, E. Yamada, T. Sugawa, E. Yoshida, T. Yamamoto, T. Imai, A. Sahara, H. Nakazawa, O. Yamauchi and M. Umezawa, "Field demonstration of soliton transmission at 10 Gb/s over 2000 km in Tokyo metropolitan optical loop network", Electron. Lett. vol. 31, p. 992, 1995.

[4.10] M. Nakazawa, Y. Kimura, K. Suzuki, H. Kubota, T. Komukai, E. Yamada, T. Sugawa, E. Yoshida, T. Yamamoto, T. Imai, A. Sahara, O. Yamauchi and M. Umezawa, "Soliton transmission at 20 Gbit/s over 2000 km in Tokyo metropolitan optical network", Electron. Lett. vol. 31, p. 1478, 1995.

[4.11] S. P. Craig-Ryan, B. J. Ainslie, C. A. Millar, "Fabrication of long length of low excess loss erbium-doped optical fibre" Electron. Lett., vol. 26, p. 185, 1990.

[4.12] J, R. Simpson, L. F. Mollenauer, K. S. Kranz, P. J. Lemaire, N. A. Olsson, H. T. Shang, P. C. Becker, "A distributed erbium doped fiber amplifier" in Proc. OFC'90, (OSA/IEEE), paper, PD19-1, 1990.

[4.13] M. Nakazawa, Y. Kimura, and K. Suzuki, "Ultralong dispersion-shifted erbium-doped fiber amplifier and its application to soliton transmission" IEEE J. Quantum Electron., vol. 26, p. 2103, 1990.

[4.14] M. Nakazawa, H. Kubota, K. Kurokawa, and E. Yamada, "Femtosecond optical soliton transmission over long distances using adiabatic trapping and soliton standardization," J. Opt. Soc. Amer. B, vol. 8, p. 1811, 1991.

[4.15] H. A. Haus and M. Nakazawa, "Theory of the fiber Raman soliton laser," J. Opt. Soc. Am. vol. B 4, p. 652, 1987.

[4.16] K. J. Blow, N. J. Doran, and D. Wood, "Suppression of the soliton self-frequency shift by bandwidth-limited amplification," J. Opt. Soc. Am. vol. B 5, p. 1301, 1988.

[4.17] K. J. Blow, N. J. Doran, and D. Wood, "Generation and stabilization of short soliton pulses in the amplified nonlinear Schrödinger equation," J. Opt. Soc. Am. vol. B 5, p. 381, 1988.

[4.18] K. J. Blow, N. J. Doran, and D. Wood, "Trapping of energy into solitary waves in amplified nonlinear dispersive systems," Opt. Lett. vol. 12, p. 1011, 1987.

[4.19] F. M. Mitschke and L. F. Mollenauer, "Discovery of the soliton self-frequency shift," Opt. Lett. vol. 11, p. 659, 1986.

[4.20] J. P. Gordon, "Theory of the soliton self-frequency shift," Opt. Lett. vol. 11, p. 662, 1986.

[4.21] P. K. A. Wai, C. R. Menyuk, Y. C. Lee, and H. H. Chen, "Nonlinear pulse propagation in the neighborhood of the zero-dispersion wavelength of monomode optical fibers," Opt. Lett., vol. 11, p. 464, 1986.

[4.22] P. K. A. Wai, C. R. Menyuk, H. H. Chen, and Y. C. Lee, "Soliton at the zero-group-dispersion wavelength of a single-mode fiber," Opt. Lett., vol. 12, p. 628, 1987.

[4.23] M. Nakazawa, K. Kurokawa, H. Kubota, K. Suzuki, and Y. Kimura, "Femtosecond erbium-doped optical fiber amplifier" Appl. Phys. Lett., vol. 57, p. 635, 1990; see also M. Nakazawa, K. Kurokawa, H. Kubota, and E. Yamada, "Observation of the trapping of an optical soliton by adiabatic gain narrowing and its escape" Phys. Rev. Lett., vol. 65, p. 1881, 1990;see also K. Kurokawa and M. Nakazawa," Wavelength-dependent amplification characteristics of femtosecond erbium-doped optical fiber amplifier" Appl. Phys. Lett., vol. 58, p. 2871, 1991.

[4.24] B. J. Ainslie, K. J. Blow, A. S. Gouveia-Neto, P. G. J. Wigley, A. S. B. Sombra, and J. R. Taylor, "Femtosecond soliton amplification in erbium doped silica fibre," Electron. Lett., vol. 26, p. 186, 1990.

[4.25] I. Yu. Khrushchev, A. B. Grudinin, E. M. Dianov, D. V. Korobkin Jun, V. A. Semenov, and A. M. Prokhorov, "Amplification of femtosecond pulses in Er^{3+}-doped single-mode optical fibres," Electron. Lett., vol. 26, p. 457, 1990; see also E. M. Dianov, A.B. Grudinin, I. Y. Khrushchev, D. V. Korobkin, Jr, A. Y. Makarenko, A. M. Prokhorov, "Nonlinear dynamics of femtosecond soliton

amplification in erbium doped fibers," in Proceedings of the Conference on Lasers and Electro-optics, Anaheim, paper, JTUA7, 1990.

[4.26] M. Nakazawa, Y. Kimura, and K. Suzuki, "Efficient Er^{3+}-doped optical fiber amplifier pumped by a 1.48 μm InGaAsP laser diode," Appl. Phys. Lett., vol. 54, p. 295, 1989.

[4.27] M. Nakazawa, Y. Kimura, and K. Suzuki, "Gain-distribution measurements along an ultralong erbium-doped fiber amplifier using optical-time-domain reflectometry," Opt. Lett., vol. 15, p. 1200, 1990.

[4.28] D. L. Williams, S. T. Davey, D. M. Spirit, and B. J. Ainslie, "Transmission over 10 km of erbium doped fibre with ultralow signal power excursion," Electron. Lett., vol. 26, p. 1517, 1990.

[4.29] E. Desurvire, J. R. Simpson, and P. C. Becker, "High gain erbium-doped traveling wave fiber amplifier," Opt. Lett., vol. 12, p. 888, 1987.

[4.30] D. Wood, "Constraints on the bit rates in direct detection optical communication systems using linear or soliton pulses," J. Lightwave Technol., vol. 8, p. 1097, 1990.

CHAPTER V. FEMTOSECOND SOLITON INTERACTIONS IN A DISTRIBUTED EDFA (DEDFA)

5.1 Introduction

With a view to the realization of ultrahigh speed optical communication, it has become more important to investigate ultrashort pulse propagation in long optical fibers[5.1-2]. Distributed erbium-doped fiber amplifiers (DEDFAs) offer the very attractive prospect of achieving ultralong lossless transmission lines[5.3-4]. We have reported the femtosecond soliton transmission characteristics of an 18.2 km-long DEDFA[5.5-6]. Optical solitons have attracted a lot of attention as information carriers in ultrahigh speed optical communication. However, nonlinear interaction between solitons may result in a significant reduction in the bandwidth of a soliton-based optical communication system[5.7-14]. Therefore, it is important to investigate mutual interactions between ultrashort solitons in a DEDFA as a step forward the realization of ultrahigh speed optical soliton communication. The soliton self-frequency shift (SSFS) is a dominant factor in femtosecond soliton transmission because it is inversely proportional to τ^4 (τ: pulse width)[5.15-16]. Since τ is directly related to the soliton amplitude, fluctuation in the latter may cause significant changes in the femtosecond soliton-soliton interaction as a result of the SSFS.

In this chapter, we describe nonlinear interaction between femtosecond solitons in a DEDFA. Section 5.3.1 describes femtosecond soliton interaction with adiabatic gain narrowing. Section 5.3.2 shows that a small sub-pulse which is coherently added to or subtracted from a soliton pulse greatly modifies the soliton-soliton interaction, as a result of the SSFS. This study is very important because sub-pulses or small amplitude fluctuations are easily

generated by optical pulse reflection at the surfaces of optical components or by detuning the laser cavity. In section 5.3.3, it is shown that when the input femtosecond soliton pair is in phase, the SSFS is greatly accelerated through soliton interaction. And we show our conclusion of chapter V in section 5.4.

5.2 Experimental Setup

The experimental setup for soliton interaction is shown in Fig. 5.1. Femtosecond pulses were generated in the 1.5 μm region by difference frequency mixing in a KTP crystal, where a visible femtosecond pulse from a cavity dumped, synchronously pumped dye laser was mixed with a 1.064 μm pulse from a Nd:YAG laser. Two 1.55 μm femtosecond pulses were generated with a Michelson interferometer. The length of one of the interferometer arms was varied by using a stepping motor with a resolution of 0.05 μm. This resolution was quite sufficient to allow precision control of the relative phase between the two solitons. The pulse pairs and the pump light were coupled into a DEDFA through a 1.48 μm/1.55 μm wavelength-division-multiplexing fiber coupler. The pumping source was 1.48 μm InGaAsP laser diodes. After passing through the DEDFA the soliton pulse pairs were detected with an autocorrelator and an optical spectrum analyzer. The DEDFA was 1~10 km long and the erbium ion doping concentration was 0.5~2.8 ppm. The mode field diameter at 1.55 μm was 7.3~7.7 μm and the zero dispersion wavelength was 1.49~1.50 μm.

5.3 Femtosecond Soliton Interaction in a DEDFA

5.3.1 Femtosecond Soliton Interaction with Adiabatic Gain Narrowing

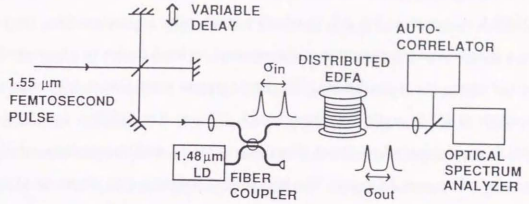

Fig. 5.1 Experimental setup for femtosecond soliton interaction in a DEDFA.

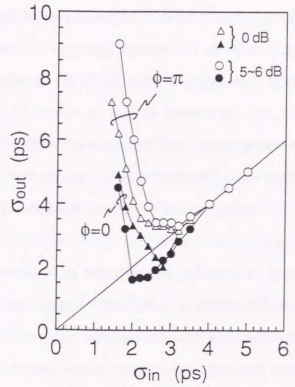

Fig. 5.2 Femtosecond soliton interaction in a 1 km DEDFA. The triangles and circles represent DEDFA optical gains of 0 and 5~6 dB, respectively. The closed (open) triangles and circles correspond to in phase (out of phase) condition.

An experimental result of femtosecond soliton-soliton interaction in a DEDFA is shown in Fig. 5.2, in which output pulse separation (σ_{out}) is plotted as a function of input soliton pulse separation (σ_{in}) under in phase (ϕ=0) and out of phase (ϕ=π) conditions. The input pulses were N=1.0~1.1 solitons with a width of 450 fs and a wavelength of 1.550 μm. The DEDFA was 1 km long, which corresponded to about 40 soliton periods, and the erbium ion doping concentration was 2.8 ppm. The first soliton collision was observed at σ_{in}=2.8 ps under a ϕ=0 condition when the optical gain of the DEDFA was 0 dB, as shown by the closed triangles. Here we define σ_c as σ_{in} at which the first collision occurs. Under the ϕ=π condition, soliton pulse repulsion was observed as shown by the open triangles.

When the optical gain was increased to 5~6 dB under the ϕ=0 condition, the two solitons coalesced at around σ_{in}=2.1 ps, as shown by the closed circles. Since the soliton period is 26 m, the optical gain per soliton period is 0.1~0.2 dB. This means that the gain of the DEDFA is adiabatic for soliton amplification. Thus, σ_c decreased to 2.1 ps when the optical gain was increased, where the output pulse width narrowed to 290 fs as a result of the adiabatic soliton narrowing. This narrowing may be useful for reducing the soliton interaction. The output wavelength changed to 1.555 μm due to the SSFS.

On the other hand, when the input pulse pair was out of phase, the output pulse separation for a gain of 5~6 dB was larger than that for a gain of 0 dB at σ_{in} values of less than 3~4 ps, although the pulse width narrowed to 290 fs. In order to analyze femtosecond soliton interactions with the SSFS effect, we computer-ran a perturbed nonlinear Schrödinger equation given by

$$(-i)\frac{\partial u}{\partial q}=\frac{1}{2}\frac{\partial^2 u}{\partial \tau^2}+|u|^2 u-\frac{\tau_n}{\tau_0}u\frac{\partial}{\partial \tau}|u|^2 \qquad (5.1)$$

Numerical results of a femtosecond soliton-soliton interaction are shown in Fig. 5.3, in which σ_{out} is plotted as a function of σ_{in} under a ϕ=π condition. Here we use a τ_n value of 5.9 fs and the fiber length is 800 m. The input pulses are N=1 solitons with a width of 450 fs, which corresponds to our experimental condition. The closed triangles in Fig. 5.3 show that two solitons repel each other under a ϕ=π condition when the optical gain is 0 dB. As shown with the closed circles in the figure, the σ_{out} values for a gain of 6 dB are larger than those for a gain of 0 dB at σ_{in} values of less than 3 ps. These numerical results agree well with the present experiment. The open triangles and open circles correspond to values of σ_{out} for a gain of 0 dB and 6 dB, respectively, when the SSFS is not included in the calculation. A numerical calculation without including the SSFS shows that under a ϕ=π condition, σ_{out} is reduced by the adiabatic soliton narrowing when the optical gain increases. Therefore, it is concluded that when the optical gain increases, the SSFS causes an increase in output pulse separation at σ_{in} values of less than 3~4 ps.

It should be noted that the noninstantaneous response of the nonlinear medium, that is SSFS, causes amplitude asymmetry between the two solitons when their tails overlap. When ϕ=π, the amplitude of the front soliton may decrease slightly because of the noninstantaneous response of the nonlinear medium, which makes the frequency downshift of the front soliton smaller than that of the rear soliton. Therefore, the output pulse separation between the front and rear solitons increases. When the optical gain is increased and the pulse widths of the two solitons are narrowed by the adiabatic soliton narrowing, this difference between the frequency downshift of the front and rear solitons increases, resulting in a larger output pulse separation.

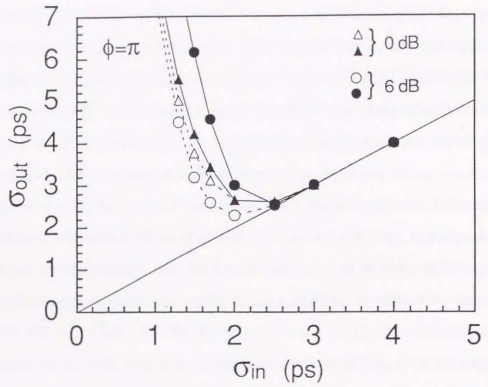

Fig. 5.3 Numerical results of femtosecond soliton interaction under out of phase condition. The triangles and circles represent DEDFA optical gains of 0 and 6 dB, respectively. The closed triangles and circles correspond to numerical results including the SSFS and the open ones correspond to those including no SSFS.

Here we show that a small difference between the amplitudes of two solitons in the femtosecond region causes a large change in σ_{out} due to the SSFS. Figure 5.4 shows the change in σ_{out} as a function of σ_{in} when the amplitudes of two solitons are different. The input pulses were N=1.2 solitons with a pulse width of 550 fs and a wavelength of 1.551 μm. The fiber length was 1 km and the optical gain was 2~3 dB. The output pulse width was reduced to about 400 fs by the adiabatic gain narrowing, where the output wavelength was 1.552~1.553 μm. The power of the front soliton pulse was the same in all cases. In this experiment σ_{in} was so large that there was negligible nonlinear interaction between two solitons with equal amplitudes, as shown with the circles in Fig. 5.4. When the power of the rear soliton pulse was increased by 13 % compared with that of the front soliton pulse, σ_{out} became about 1.3 ps larger than σ_{in} in spite of the σ_{in} values in the measurement, as shown by the triangles in Fig. 5.4. On the other hand, when the power of the rear soliton pulse was decreased to a level 13 % below that of the front soliton pulse, σ_{out} became about 1.3 ps smaller than σ_{in}, as shown by the squares in Fig. 5.4. The results in Fig. 5.4 were independent of the relative phase between the two solitons because of the larger separation.

The experimental results can be explained by the SSFS. From the perturbation theory, when an amplitude perturbation Δ is applied by coherent addition or subtraction, the soliton amplitude changes to $1\pm2\Delta$ (+ ; coherent addition, - ; coherent subtraction). Therefore, the soliton pulse width changes to $(1\pm2\Delta)^{-1}$. Since the frequency shift due to the SSFS is proportional to τ^{-4}, the amplitude perturbation Δ causes a frequency shift $\Delta f \propto (1\pm2\Delta)^4 \cong (1\pm8\Delta)$. Therefore, when the pulse width is in the femtosecond region, a small amplitude perturbation causes a large frequency shift due to the SSFS. When the amplitude of the rear soliton pulse is larger than that of the front soliton,

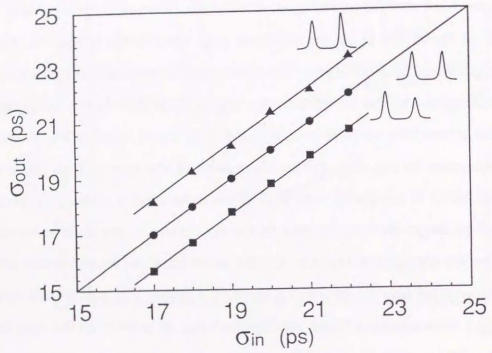

Fig. 5.4 Changes in σ_{out} for a soliton pulse pair with different amplitudes. The DEDFA is 1 km long.

●: equal amplitudes

▲: the power of the rear soliton pulse is 13 % greater than that of the front pulse.

■: the power of the rear soliton pulse is 13 % less than that of the front pulse.

the frequency downshift of the rear soliton pulse is larger than that of the front soliton, resulting in an increase in output pulse separation between the front and rear solitons, as shown by the triangles in Fig. 5.4. On the other hand, when the amplitude of the rear soliton pulse is smaller than that of the front soliton, the frequency downshift of the rear soliton pulse is smaller than that of the front soliton, resulting in a decrease in output pulse separation between the front and rear solitons, as shown by the squares in Fig. 5.4. Thus, a small difference between the amplitudes of two solitons causes an increase or decrease in the output pulse separation because the frequency shifts of the soliton carrier are different due to the SSFS.

5.3.2 Significant Modification of Femtosecond Soliton Interaction in a Gain Medium by Small Sub-Pulses

Experimental results of femtosecond soliton-soliton interactions are shown in Fig. 5.5, in which σ_{out} is plotted as a function of σ_{in} under $\phi=0$ and $\phi=\pi$ conditions. The input pulses were N=1.0~1.1 solitons with a width of 440 fs and a wavelength of 1.550 μm. The DEDFA was 1 km long and the doping concentration was 2.8 ppm. Large differences were observed between the in phase σ_{out} (closed triangles) and out of phase σ_{out} (open triangles) at around σ_{in}=2, 4, 10 ps, when the gain was 0 dB. Here the output wavelength was 1.551 μm, and the output pulse width was 440 fs which was the same as that of the input. When the pump power was increased to provide a gain of 5~6 dB, it was clearly seen that soliton-soliton interactions at around σ_{in}=4 ps and 10 ps are strongly enhanced, as shown by the circles. In addition, the output wavelength was shifted to 1.558 μm due to the SSFS, and the output pulse was shortened to 280 fs due to the optical gain. The experimental results can be also understood by an interaction between two solitons with different

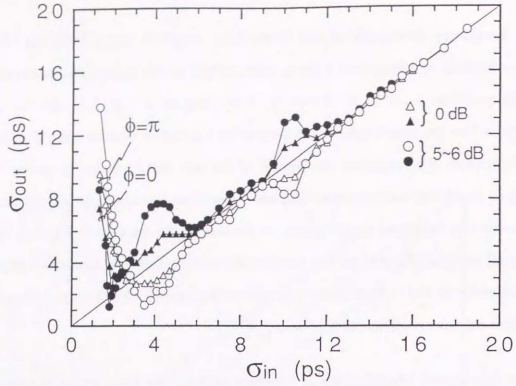

Fig. 5.5 Femtosecond soliton interaction in a 1 km DEDFA. The triangles and circles represent DEDFA optical gains of 0 and 5~6 dB, respectively. The closed (open) triangles and circles correspond to an in phase (out of phase) condition.

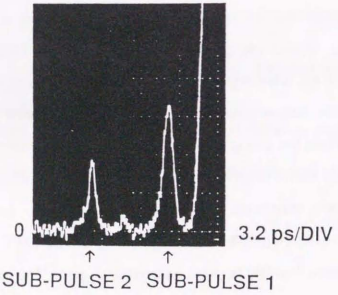

Fig. 5.6 An autocorrelation trace of an input pulse with sub-pulses.

amplitudes. A slight change in the soliton amplitude in the femtosecond region causes a large frequency shift due to the SSFS. Such a small difference in soliton amplitude can easily be caused by the sub-pulses, which are coherently added to or subtracted from the original solitons.

In order to confirm whether or not sub-pulses truly exist after a main pulse, we carefully investigated the input pulses. Figure 5.6 shows the tail of an autocorrelation trace of an input pulse, in which we can clearly see sub-pulses at intervals of about 4 ps (sub-pulse 1) and 10 ps (sub-pulse 2) from the main soliton pulse. These intervals agree with the σ_{in} values for which large differences between the in phase σ_{out} and the out of phase σ_{out} were observed as shown in Fig. 5.5. The full width at half maximum (FWHM) of the traces for sub-pulse 1 and sub-pulse 2 are 1 ps and 0.7 ps, respectively. The intensity of sub-pulse 1 is as small as about 1 % that of the main soliton pulse. These sub-pulses were generated by the surface reflection of the optical components in the femtosecond laser system. It is important to note that, without the sub-pulses, σ_{out} was exactly equal to σ_{in} at around σ_{in}=4 ps and 10 ps. The changes in output pulse separation at σ_{in}=4 ps and 10 ps in the present case are attributed to the existence of sub-pulses 1 and 2 which coherently overlap with one of the two solitons. The σ_{in} range in which σ_{out} changes due to sub-pulse 1 is larger than that for sub-pulse 2, as shown in Fig. 5.5. This is because the pulse width of sub-pulse 1 is larger than that of sub-pulse 2. It should be noted here that the difference between the results shown in Figs. 5.2 and 5.5 for σ_{in} values in the 0~6 ps region is due to the absence of subpulses in the results shown in Fig. 5.2.

In order to analyze the interactions between femtosecond solitons with sub-pulses, we computer-ran equation (5.1). Figure 5.7 shows σ_{out} as a function of σ_{in} when there are 0.7 ps and 0.45 ps-wide sub-pulses at an

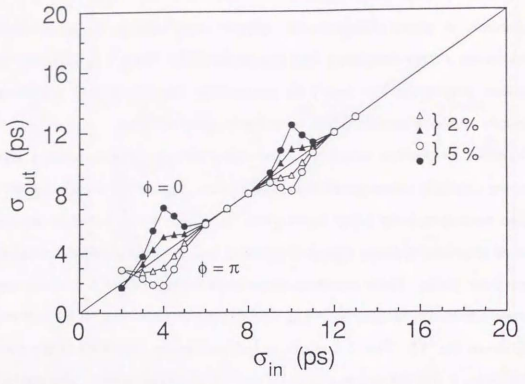

Fig. 5.7 Femtosecond soliton interaction with a 0.7 ps-wide sub-pulse at σ_{in}=4 ps and a 0.45 ps-wide sub-pulse at σ_{in}=10 ps in a lossless transmission line. The triangles and circles represent field intensity ratios of the sub-pulse to the main soliton pulse of 2 and 5 %, respectively. The closed (open) triangles and circles correspond to an in phase (out of phase) condition.

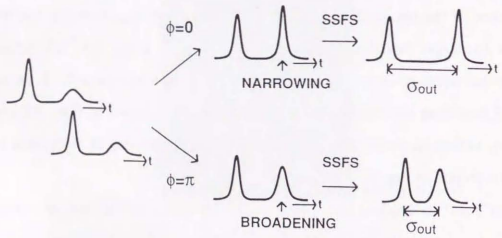

Fig. 5.8 Schematic representation of soliton interaction with small sub-pulses under both in phase (ϕ=0) and out of phase (ϕ=π) conditions.

interval of 4 ps and 10 ps, respectively, from the main soliton pulse. This corresponds to our experimental condition. Thus, the sub-pulse which exists behind the front soliton pulse and the rear soliton pulse overlap at the input end of the DEDFA for σ_{in}=4 ps and 10 ps. The input pulses are N=1 solitons with a pulse width of 450 fs. The fiber length is 1 km which corresponds to about 40 soliton periods. The triangles in Fig. 5.7 show a soliton interaction when the electric field of a sub-pulse is as small as 2 % that of the main soliton pulse. As shown with the closed triangles in this figure, when the rear soliton pulse and the sub-pulse are in phase, σ_{out} increases at around σ_{in}=4 ps and 10 ps. On the other hand, when the rear soliton pulse and the sub-pulse are out of phase, σ_{out} decreases. When there is no sub-pulse, σ_{out} is equal to σ_{in} at around σ_{in}=4 ps and 10 ps. Thus, it is concluded that a very small, coherent sub-pulse causes a strong soliton interaction. It is also shown in Fig. 5.7 that the σ_{in} range in which σ_{out} changes due to a 0.75 ps-wide sub-pulse is larger than that for a 0.45 ps-wide sub-pulse. By increasing the amplitude of the sub-pulse to 5 % that of the soliton pulse, the change in the output pulse separation at around σ_{in}=4 ps increases greatly as shown by the circles in Fig. 5.7. This is because the larger amplitude perturbation due to the sub-pulse causes a larger difference in the frequency shift between two solitons. These numerical calculations of soliton interactions with sub-pulses agree well with the experimental results shown in Fig. 5.5.

It should be noted that a small change in the soliton amplitude in the femtosecond region causes a large frequency shift due to the SSFS. As shown in Fig. 5.8, when the rear soliton pulse and a sub-pulse are in phase and the soliton amplitude is increased coherently, the frequency downshift of the rear soliton pulse is larger than that of the front soliton, resulting in an increase in output pulse separation between the front and rear solitons. On the other

hand, when the rear soliton pulse and a sub-pulse are out of phase and the soliton amplitude is decreased slightly, the frequency downshift of the rear soliton becomes smaller than that of the front soliton and output pulse separation decreases. The closed triangles and circles at around σ_{in}=4 ps and 10 ps in Fig. 5.5 correspond to a condition in which the main (rear) soliton pulse and sub-pulse are in phase. The open triangles and circles correspond to an out of phase condition. The interaction at σ_{in} of less than 2 ps as shown in Fig. 5.5 is an ordinary soliton-soliton interaction without sub-pulses, in which ϕ is the relative phase between the two solitons. It is also important to note that the modification of the soliton interaction by sub-pulses is greatly increased by amplifying the sub-pulse and main (rear) soliton pulse.

5.3.3 Soliton Self-Frequency Shift Accelerated by Femtosecond Soliton Interaction

In this subsection, we show that the SSFS is greatly accelerated through soliton interaction when the input femtosecond soliton pair is in phase. Frequency spectra and autocorrelation traces of the input and output soliton pair are shown in Fig. 5.9, under in phase and out of phase conditions in a 9.4 km DEDFA. The erbium ion doping concentration was 0.5 ppm. The mode field diameter at 1.55 μm was 7.7 μm and the zero dispersion wavelength was 1.49 μm. The soliton period was 20 m, which means that the fiber length was as long as 470 soliton periods. The input pulses were N=0.8 solitons with a width of 410 fs and a wavelength of 1.550 μm. The total pump power was 24 mW (forward; 12 mW, backward; 12 mW) and the gain was about 9 dB. σ_{in} was set at 1.0 ps, which was 2.4 times the input pulse width.

The frequency spectrum and the autocorrelation trace of the output pulse pair under an in phase (ϕ=0) condition are shown in Fig. 5.9(b). The peak

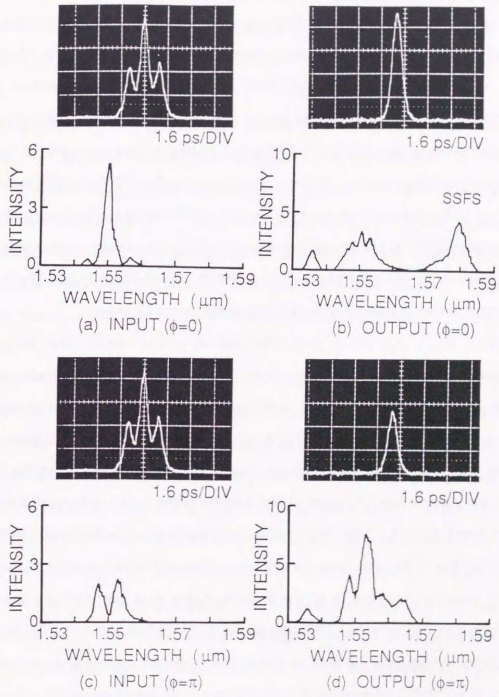

Fig. 5.9 Soliton interaction in a 9.4 km DEDFA with a 0.4 ps soliton. Frequency spectrum and pulse waveform of input (a) and output (b) solitons (in phase). Those of input (c) and output (d) solitons (out of phase).

wavelength of the output pulse shifted to 1.579 μm due to the SSFS, corresponding to a frequency shift of 3.6 THz. The new spectral component at 1.535 μm is an amplified spontaneous emission (ASE). The photograph in Fig. 5.9(b) shows an autocorrelation trace of the output pulse pair. Although there were two output pulses, only the frequency downshifted pulse component with the higher peak power was detected with the autocorrelator. This was because the separation of the two output pulses was greater than the autocorrelator scan range (~50 ps). The output pulse width broadened to 480 fs. This pulse broadening may be due to the increase in the group velocity dispersion (GVD) at the center wavelength of the frequency shifted soliton or the limitation of the gain bandwidth, because the increase in the GVD value requires broader pulses to maintain the same soliton power.

When the input pulse pair was out of phase ($\phi=\pi$), the frequency spectrum and the autocorrelation trace of the output pulse pair changed as shown in Fig. 5.9(d). The peak wavelength of the output pulse changed to 1.553 μm corresponding to a frequency shift of 0.4 THz, which was much smaller than that under the in phase condition. The photograph in Fig. 5.9(d) shows an autocorrelation trace of the output pulse pair. Although there are two output pulses, only one pulse component was detected with the autocorrelator. This was because the separation of the two output pulses was greater than the scan range of the autocorrelator as a result of the repulsive force between the solitons. The output pulse width broadened to 480 fs. This pulse broadening may be due to the initial pulse broadening caused by the excitation of N=0.8 solitons or the limitation of the gain bandwidth.

Here it is important to note that when one of the interferometer arms was blocked, we did not observe the large frequency shift seen in the frequency spectrum of the output pulse pair under a $\phi=0$ condition. Figure

5.10 shows the frequency spectra and the autocorrelation traces of the input and output pulses when one of the interferometer arms was blocked. As shown in Fig. 5.10(b), the peak wavelength of the output pulse changed a little to 1.552 μm and no large SSFS was observed with an output pulse width of 460 fs.

The frequency shift of the output pulses is shown in Fig. 5.11 as a function of the relative phase between two solitons in a 9.4 km DEDFA. As shown in Fig. 5.11, the soliton frequency shift was a periodic function of the relative phase with a period of 2π and was maximized at $\phi=0$ (in phase) and minimized at $\phi=\pi$ (out of phase). It is important to note that the SSFS was negligible when one of the interferometer arms was blocked. Thus, it is found that a collision between femtosecond solitons greatly accelerates the SSFS.

In order to analyze femtosecond soliton interactions in a lossless transmission line, Eq. (5.1) was again computer-run. Figure 5.12 shows waveforms and spectra of output pulse pairs under a $\phi=0$ condition. The input pulses are N=1 solitons with a pulse width of 400 fs. The input pulse separation is set at $3\tau_{in}$, where τ_{in} is the input pulse width. When the input pulse pair is in phase, soliton interaction (collision) occurs at around $Z/Z_{sp}=6$ as shown in Fig. 5.12, where Z_{sp} is the soliton period. When soliton interaction occurs, the output pulse narrows and the spectral width broadens. Pulse narrowing due to the soliton interaction greatly accelerates the SSFS, because the frequency shift is proportional to τ^{-4}. The SSFS is clearly seen in the longer wavelength region. The narrower soliton with a higher intensity at $Z/Z_{sp}=20$ has a longer wavelength carrier, and two solitons propagate with different frequencies. After the interaction, the output pulse separation

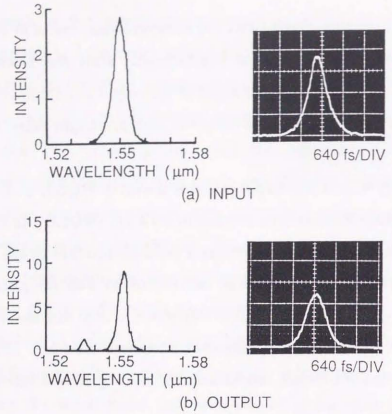

Fig. 5.10 Frequency spectra and autocorrelation traces of input (a) and output (b) solitons when one of the interferometer arms was blocked.

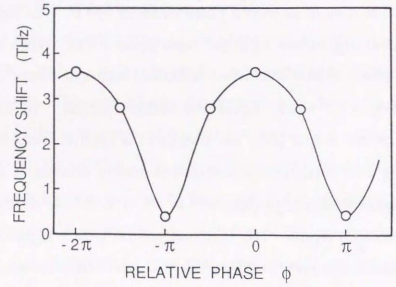

Fig. 5.11 Frequency shift of the output pulses as a function of the relative phase between two solitons.

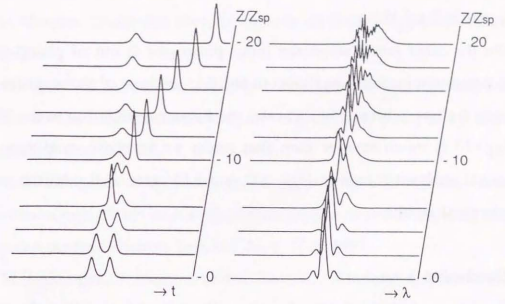

Fig. 5.12 Femtosecond soliton interaction with the SSFS under a $\phi=0$ condition in a lossless transmission line.

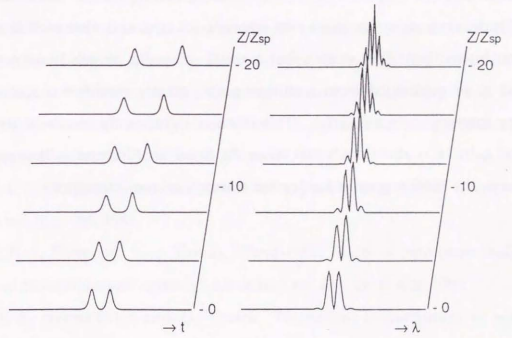

Fig. 5.13 Femtosecond soliton interaction with the SSFS under a $\phi=\pi$ condition in a lossless transmission line.

increases along the fiber because of the different group velocities, as shown at Z/Z_{sp}=20 in Fig. 5.12.

On the other hand, when the input pulse pair is out of phase, output pulse separation increases as shown in Fig. 5.13, because of the repulsive force between the two solitons. In this case, the frequency shift due to the SSFS at Z/Z_{sp}=20 is much smaller than that under an in phase condition. The numerical analyses shown in Figs. 5.12 and 5.13 agree well with the present experimental results.

5.4 Conclusion

Femtosecond soliton interactions have been investigated in a distributed erbium-doped fiber amplifier (DEDFA). In the femtosecond region, a slight difference between the amplitudes of the two solitons causes a significant change in the soliton-soliton interaction as a result of the SSFS. The noninstantaneous response of the nonlinear medium, that is SSFS, causes amplitude asymmetry between two adjacent solitons and also modifies the soliton interaction. It is shown that a small sub-pulse, which is coherently added to or subtracted from a soliton pulse, greatly modifies the soliton-soliton interaction in a DEDFA. This effect is significantly increased by the optical gain. It is also shown that when the input femtosecond soliton pair is in phase, the SSFS is greatly accelerated through soliton interaction.

References

[5.1] D. Marcuse, "Pulse distortion in single-mode fibers," Appl. Opt. vol. 19, p. 1653, 1980.

[5.2] K. Suzuki, Y. Kimura, and M. Nakazawa, "Subpicosecond soliton amplification and transmission using Er^{3+}-doped fibers pumped by InGaAsP laser diodes," Opt. Lett. vol. 14, p. 865, 1989.

[5.3] S. T. Davey, D. J. Williams, D. M. Spirit, and B. J. Ainslie, "Lossless transmission over 10 km of low-dispersion erbium doped fibre using only 15 mW pump power," Electron. Lett. vol. 26, p. 1148, 1990.

[5.4] M. Nakazawa, Y. Kimura, and K. Suzuki, "Ultralong dispersion-shifted erbium-doped fiber amplifier and its application to soliton transmission," IEEE J. Quantum Electron. vol. QE-26, p. 2103, 1990.

[5.5] M. Nakazawa, and K. Kurokawa, "Femtosecond soliton transmission in 18 km-long dispersion-shifted, distributed erbium-doped fibre amplifier," Electron. Lett. vol. 27, p. 1369, 1991.

[5.6] K. Kurokawa and M. Nakazawa, "Femtosecond soliton transmission characteristics in an ultralong erbium-doped fiber amplifier with different pumping configuration," IEEE J. Quantum Electron. vol. QE-28, p. 1922, 1992.

[5.7] V. I. Karpman and V. V. Solov'ev, "A perturbational approach to the two-soliton systems," Physica vol. 3D, p. 487, 1981.

[5.8] J. P. Gordon, "Interaction forces among solitons in optical fibers," Opt. Lett. vol. 8, p. 596, 1983.

[5.9] K. J. Blow and N. J. Doran, "Bandwidth limits of nonlinear (soliton) optical communication systems," Electron. Lett. vol. 19, p. 429, 1983.

[5.10] B. Hermansson and D. Yevick, "Numerical investigation of soliton interaction," Electron. Lett. vol. 19, p. 570, 1983.

[5.11] P. L. Chu and C. Desem, "Optical fiber communication using solitons," 4th International Conference on Integrated Optics and Optical Fiber Communication, IOOC'83, Tokyo, Japan, Tech. Dig., vol. 27-30, p. 52, 1983.

[5.12] E. Shiojiri and Y. Fujii, "Transmission capability of an optical fibre communication system using index nonlinearity," Appl. Opt. vol. 24, p. 358, 1985.

[5.13] F. M. Mitschke and L. F. Mollenauer, "Experimental observation of interaction forces between solitons in optical fibers," Opt. Lett. vol. 12, p. 355, 1987.

[5.14] Y. Kodama and L. Nozaki, "Soliton interaction in optical fibers," Opt. Lett. vol. 12, p. 1038, 1987.

[5.15] F. M. Mitschke and L. F. Mollenauer, "Discovery of the soliton self-frequency shift," Opt. Lett. vol. 11, p. 659, 1986.

[5.16] J. P. Gordon, "Theory of the soliton self-frequency shift," Opt. Lett. vol. 11, p. 662, 1986.

CHAPTER VI. CONCLUSION

The thesis described early research work on the propagation characteristics of a femtosecond optical soliton in an active gain medium, erbium doped optical fiber amplifier (EDFA), including the development of a femtosecond infrared light source. The obtained results are summarized as follows:

(1) We have developed a high peak-power, infrared femtosecond light source. Tunable femtosecond~subpicosecond infrared pulses have been generated in the 1.4-1.6 μm region by mixing a 1.06 μm Nd:YAG laser pulse and a visible subpicosecond pulse from a cavity dumped, synchronously pumped dye laser.

Three kinds of nonlinear crystal, KTP, $LiNbO_3$, and β-BaB_2O_4(BBO) were used for difference frequency generation (DFG). It is found that KTP is the most suitable crystal of the three for femtosecond DFG. Pulses as short as 94 fs with a peak power of 8.4 kW have been obtained with a KTP crystal at a rate of 3.8 MHz. Because of the large value of the group velocity mismatch β and the low threshold of the optical damage, $LiNbO_3$ is less suitable than KTP for DFG with femtosecond pulses. BBO is less suitable than KTP because of the smaller effective nonlinear coefficient d_{eff} and the larger walk-off angle ρ than those for KTP.

(2) We have shown the amplification characteristics of a femtosecond pulse in an EDFA. The gain bandwidth of the EDFA is large enough to amplify a femtosecond pulse. A gain of 9 dB has been obtained in an EDFA for input pulses with a peak power of 30 W, an average power of 30 μW (-15.2 dBm), and a pulse width of 260 fs.

When the input peak power is increased in the soliton power regime, interesting features peculiar to the optical soliton have been observed in the

amplification process of the femtosecond pulses. When the gain is moderate, we have experimentally observed adiabatic narrowing of a femtosecond fundamental soliton at 1.55 μm. By increasing the amplifier gain to nonadiabatic region, pulse compression by as much as a factor 4 has been observed by using 240-fs pulses. This feature is very interesting since the pulse width of the output soliton can be fully controlled by changing the pump power. However, at the same time the frequency of the soliton strongly shifts toward longer wavelength region outside the EDFA gain bandwidth due to a higher-order nonlinear effect, that is, a soliton self-frequency shift (SSFS). Therefore, the SSFS prevents from the efficient amplification of femtosecond soliton pulses by using the EDFA.

(3) Transmission characteristics of a femtosecond soliton have been investigated in a dispersion-shifted, distributed erbium-doped fibre amplifier as long as 18.2 km. Solitons (A=0.7~1.2) with a pulse width of about 450 fs have been transmitted. However, a femtosecond soliton is very weakly trapped in the EDFA gain bandwidth of 1.55 μm and the soliton self-frequency shift inevitably occurs.

It has been found that the transmission characteristics of a femtosecond optical soliton depend strongly on the pumping configurations. With backward pumping, a lossless transmission of 440 fs solitons at 1.55 μm has been realized with a pump power of 16 mW. Here the output pulse width is determined by the spectrum modified by the soliton self-frequency shift. On the other hand, in the forward pumping and the bi-directional pumping configurations, there are two output pulses when the pump power is above 30 mW. One is a frequency-downshifted pulse due to the SSFS and the other corresponds to the original 1.55 μm spectrum. And the autocorrelation signal of the former is much smaller than that of the latter because of the optical loss

outside the gain bandwidth of the DEDFA. A new pulse at 1.55 μm may be generated by the amplification of a non-soliton component at 1.55 μm.

When the pulse width shortens to a femtosecond region a strong SSFS becomes a big problem in the realization of a long-distance transmission of an optical soliton with a DEDFA, as similar to the amplification process of a femtosecond optical soliton in an EDFA.

(4) Femtosecond soliton interactions have been investigated in a DEDFA. In the femtosecond region, a slight difference between the amplitudes of the two solitons causes a significant change in the soliton-soliton interaction as a result of the SSFS. The noninstantaneous response of the nonlinear medium, that is SSFS, causes amplitude asymmetry between two adjacent solitons and also modifies the soliton interaction. It is shown that a small sub-pulse, which is coherently added to or subtracted from a soliton pulse, greatly modifies the soliton-soliton interaction in a DEDFA. This effect is significantly increased by the optical gain. It is also shown that when the input femtosecond soliton pair is in phase, the SSFS is greatly accelerated through soliton interaction.

As summarized above, when the pulse width shortens to a femtosecond region the soliton self-frequency shift strongly occurs in both amplification and transmission processes and should play an important role in the realization of ultrahigh speed optical communication using ultrashort optical soliton with the EDFA. Recently very short pulses with a pulse width of picosecond ~ subpicosecond are used for ultrahigh speed optical transmission experiment with time division multiplexing (TDM) and/or wavelength division multiplexing (WDM) techniques. The present work

opens new research field of propagation of an ultrashort optical nonlinear wave in optical fibers.

LIST OF PUBLISHED PAPERS

[1]. K. Kurokawa, T. Hattori, and T. Kobayasi, "Subpicosecond molecular dynamics studied by degenerate four-wave mixing with incoherent light," Phys. Rev. A. vol. 36 no. 3, pp. 1298-1304, 1987.

[2]. K. Kurokawa, H. Kubota, and M. Nakazawa, "48 fs, 190 kW pulse generation from a cavity dumped, synchronously pumped dye laser," Opt. Commun. vol. 68 no. 4, pp. 287-290, 1988.

[3]. K. Kurokawa and M. Nakazawa, "Femtosecond 1.4-1.6 μm infrared pulse generation at a high repetition rate by difference frequency generation," Appl. Phys. Lett. vol. 55 no. 1, pp. 7-9, 1989.

[4]. K. Kurokawa, H. Kubota, and M. Nakazawa, "Generation of 72-fs pulse from a cavity dumped, synchronously pumped dye laser with a single jet," Opt. Commun. vol. 73 no. 4, pp. 319-321, 1989.

[5]. K. kurokawa and M. Nakazawa, and T. A. Caughey, "Near infrared ultrashort pulse generation with $LiNbO_3$ by difference frequency generation," Opt. Commun. vol. 75 no. 5,6, pp. 413-418, 1990.

[6]. K. Kurokawa and M. Nakazawa, "Wavelength-dependent amplification characteristics of femtosecond erbium-doped optical fiber amplifiers," Appl. Phys. Lett. vol. 58 no. 25, pp. 2871-2873, 1991.

[7]. K. Kurokawa and M. Nakazawa, "Femtosecond soliton transmission in an 18 km-long erbium-doped fibre amplifier with different pumping configurations," Electron. Lett. vol. 27 no. 19, pp. 1765-1766, 1991.

[8]. K. Kurokawa and M. Nakazawa, "Femtosecond soliton transmission characteristics in an ultralong erbium-doped fiber amplifier with different pumping configurations," IEEE J. of Quantum Electron. vol. 28 no. 9, pp. 1922-1929, 1992.

[9]. K. Kurokawa, H. Kubota, and M. Nakazawa, "Soliton self-frequency shift accelerated by femtosecond soliton interaction," Electron. Lett. vol. 28 no. 22, pp. 2052-2053, 1992.

[10]. K. Kurokawa, H. Kubota, and M. Nakazawa, "Significant modification of femtosecond soliton interaction in gain medium by small subpulse," Electron. Lett. vol. 28 no. 25, pp. 2334-2335, 1992.

[11]. K. Kurokawa, H. Kubota, and M. Nakazawa, "Femtosecond soliton interactions in a distributed erbium-doped fiber amplifier," IEEE J. of Quantum Electron. vol. 30 no. 9, pp. 2220-2226, 1994.

Co-authored papers

[1]. T. Kobayashi, H. Ohtani, and K. Kurokawa, "Picosecond time-resolved absorption and gain spectroscopy of a giant dipole molecule, 4-Diethylamino-4'-nitrostilbene, in solution and in polymer film," Chem. Phys. Lett. vol. 121 no. 4,5, pp. 356-360, 1985.

[2]. T. Kobayashi, T. Hattori, A. Terasaki, and K. Kurokawa, "Femtosecond relaxation processes in nonlinear materials studied with incoherent light," Rev. Phys. Appl. vol. 22, pp. 1773-1785, 1987.

[3]. T. Kobayashi, A. Terasaki, T. Hattori, and K. Kurokawa, "The application of incoherent light for the study of femtosecond-picosecond relaxation in condensed phase," Appl. Phys. B, vol. 47, pp. 107-125, 1988.

[4]. H. Kubota, K. Kurokawa, and M. Nakazawa, "29-fsec pulse generation from a linear-cavity synchronously pumped dye laser," Opt. Lett. vol. 13 no. 9, pp. 749-751, 1988.

[5]. M. Nakazawa, K. Kurokawa, H. Kubota, K. Suzuki, and Y. Kimura, "Femtosecond erbium-doped optical fiber amplifier," Appl. Phys. Lett. vol. 57 no. 7, pp. 653-655, 1990.

[6]. M. Nakazawa, K. Kurokawa, H. Kubota, and E. Yamada, "Observation of the trapping of an optical soliton by adiabatic gain narrowing and its escape," Phys. Rev. Lett. vol. 65 no. 15, pp. 1881-1884, 1990.

[7]. M. Nakazawa, H. Kubota, K. Kurokawa, and E. Yamada, "Femtosecond optical soliton transmission over long distances using adiabatic trapping and soliton standardization," J. Opt. Soc. Am. B vol. 8 no. 9, pp. 1811-1817, 1991.

[8]. M. Nakazawa and K. Kurokawa, "Femtosecond soliton transmission in an 18 km-long dispersion-shifted, distributed erbium-doped fibre amplifier," Electron. Lett. vol. 27 no. 15, pp. 1369-1370, 1991.

[9]. M. Nakazawa, Y. Kimura, K. Kurokawa, and K. Suzuki, "Self-induced transparency solitons in an erbium-doped fiber waveguide," Phys. Rev. A. vol. 45 no. 1, pp. 23-26, 1992.

[10]. T. Sugawa, K. Kurokawa, H. Kubota, and M. Nakazawa, "Soliton self-frequency shift in orthogonally polarized femtosecond solitons," Electron. Lett. vol. 30 no. 23, pp. 1963-1964, 1994.

[11]. T. Sugawa, K. Kurokawa, H. Kubota, and M. Nakazawa, "Polarization dependence of soliton interactions in femtosecond soliton transmission," IEICE Transactions on Electronics, vol. E78-C no. 1, pp. 28-37, 1995.

International Conference

[1]. M. Nakazawa, H. Kubota, and K. Kurokawa, "Generation of 29-Femtosecond Pulses from a Synchronously Pumped Dye Laser and Its Cavity-Dumping Technique," Technical Digest in Sixth International Conference on Ultrafast Phenomena, TuC3, pp. 32-33, Kyoto, Japan, 1988.

[2]. K. Kurokawa and M. Nakazawa, "Femtosecond Pulse Generation in the 1300~1600 nm Region and Application to Optical Communication (Invited Talk)," in Conference Proceedings of 16th European Conference on Optical Communication, Vol. 2, MoB3.1, pp. 705-712, Amsterdam, The Netherlands, 1990.

[3]. H. Kubota, M. Nakazawa, and K. Kurokawa, "Femtosecond optical pulse transmission over long distances using adiabatic soliton trapping and soliton standardization," Technical Digest in Optical Fiber Communication, Vol. 4, TuK2, p. 39, San Diego, USA, 1991.

[4]. M. Nakazawa, Y. Kimura, K. Suzuki, K. Kurokawa, and H. Kubota, "Self-induced transparency soliton propagation in an erbium-doped optical fiber waveguide," Technical Digest in OSA Annual Meeting, Vol. 17, PD11, p. 264, San Jose, USA, 1991.

[5]. K. Kurokawa, H. Kubota, and M. Nakazawa, "Femtosecond soliton interactions in a distributed Erbium-doped fibre amplifier," in Conference Proceedings of 18th European Conference on Optical Communication, Vol. 1, TuA6.3, pp. 197-200, Berlin, Germany, 1992.

[6]. K. Kurokawa, H. Kubota, and M. Nakazawa, "Femtosecond Soliton Interaction with Adiabatic Soliton Narrowing in a Distributed Erbium Doped Fiber Amplifier," Technical Digest in Optical Amplifiers and Their Applications, Vol. 14, TuB4, pp. 282-285, Yokohama, Japan, 1993.

[7]. T. Sugawa, K. Kurokawa, H. Kubota, and M. Nakazawa, "Polarization dependence of soliton interactions and soliton self-frequency shift in a femtosecond soliton transmission," Technical Digest in Optical Fiber Communication, Vol. 8, FB1, pp. 301-302, San Diego, USA, 1995.